

Laser-assisted growth of carbon nanotubes

Citation for published version (APA):

Burgt, van de, Y. B. (2014). *Laser-assisted growth of carbon nanotubes*. [Phd Thesis 1 (Research TU/e / Graduation TU/e), Mechanical Engineering]. Technische Universiteit Eindhoven.
<https://doi.org/10.6100/IR772901>

DOI:

[10.6100/IR772901](https://doi.org/10.6100/IR772901)

Document status and date:

Published: 01/01/2014

Document Version:

Publisher's PDF, also known as Version of Record (includes final page, issue and volume numbers)

Please check the document version of this publication:

- A submitted manuscript is the version of the article upon submission and before peer-review. There can be important differences between the submitted version and the official published version of record. People interested in the research are advised to contact the author for the final version of the publication, or visit the DOI to the publisher's website.
- The final author version and the galley proof are versions of the publication after peer review.
- The final published version features the final layout of the paper including the volume, issue and page numbers.

[Link to publication](#)

General rights

Copyright and moral rights for the publications made accessible in the public portal are retained by the authors and/or other copyright owners and it is a condition of accessing publications that users recognise and abide by the legal requirements associated with these rights.

- Users may download and print one copy of any publication from the public portal for the purpose of private study or research.
- You may not further distribute the material or use it for any profit-making activity or commercial gain
- You may freely distribute the URL identifying the publication in the public portal.

If the publication is distributed under the terms of Article 25fa of the Dutch Copyright Act, indicated by the "Taverne" license above, please follow below link for the End User Agreement:

www.tue.nl/taverne

Take down policy

If you believe that this document breaches copyright please contact us at:

openaccess@tue.nl

providing details and we will investigate your claim.

Laser-assisted growth of carbon nanotubes

PROEFSCHRIFT

ter verkrijging van de graad van doctor aan de
Technische Universiteit Eindhoven, op gezag van de
rector magnificus prof.dr.ir. C.J. van Duijn, voor een
commissie aangewezen door het College voor
Promoties, in het openbaar te verdedigen
op maandag 31 maart 2014 om 16:00 uur

door

Yoeri Bertin van de Burgt

geboren te Huisseling

Dit proefschrift is goedgekeurd door de promotiecommissie:

voorzitter: prof.dr. L.P.H. de Goey
1^e promotor: prof.dr.ir. J.M.J. den Toonder
2^e promotor: prof.dr. A.H. Dietzel (Technische Universität Braunschweig)
copromotor: dr. Y.J. Bellouard
leden: dr. A. Salleo (Stanford University)
prof.dr. E.P.A.M. Bakkers (Technische Universiteit Delft)
prof.dr.ir. A.A. van Steenhoven
adviseur: dr. R. Mandamparambil (Holst Centre - TNO)

Laser-assisted growth of carbon nanotubes

Yoeri van de Burgt

Laser-assisted growth of carbon nanotubes
Copyright © 2014 by Yoeri van de Burgt
Technische Universiteit Eindhoven

A catalogue record is available from the Eindhoven University of Technology Library
ISBN: 978-94-6108-628-0

Printed by: Gildeprint Drukkerijen - The Netherlands
Cover design: Yoeri van de Burgt and Berry van Uden

This research has been financially supported through a research grant offered by a 3TU contract with TNO Holst Centre.

TU/e Technische Universiteit
Eindhoven
University of Technology



Contents

Summary	vii
1 Introduction to laser-assisted growth of carbon nanotubes	1
1.1 A brief introduction on carbon nanotubes.	2
1.2 Parameters influencing carbon nanotube growth by localized laser heating. . .	9
1.3 Process control.	17
1.4 Outline and objectives.	27
2 Closed-loop controlled laser-assisted carbon nanotube growth	29
2.1 Introduction.	30
2.2 Experimental setup.	30
2.3 Open-loop growth to identify characteristic regimes.	31
2.4 Closed-loop control	36
2.5 Thermal modeling	38
2.6 Catalyst	42
2.7 Results of temperature closed-loop control	45
2.8 Catalyst activation control	50
2.9 Summary	50
3 Miniaturized reaction-chamber for optimized carbon nanotube growth	53
3.1 Introduction.	54
3.2 Design and setup.	54
3.3 Thermal modeling	56
3.4 Results.	58
3.5 Summary	63
4 Growth kinetics	65
4.1 Introduction.	66
4.2 Experimental setup for measuring growth kinetics.	66
4.3 Growth kinetics.	68
4.4 Results.	73
4.5 Summary	86

5 Application perspectives	89
5.1 Introduction	90
5.2 Transfer of carbon nanotubes into polymers	90
5.3 Growth in a narrow enclosure.	91
5.4 Writing lines of carbon nanotubes	91
5.5 <i>In situ</i> carbon nanotube growth inside partially sealed enclosures	92
5.6 Summary and outlook	97
6 Conclusions and Outlook	99
6.1 Conclusions	100
6.2 Outlook	101
Bibliography	103
List of publications	119
Samenvatting	121
Dankwoord / Acknowledgements	123
Curriculum vitae	127

Summary

Carbon nanotubes are nano-sized tubular allotropes of carbon and have a technological potential in many applications such as field emitters, field effect transistors, filters, interconnects, sensors, displays, solar cell technology and flexible electronics. Among the various production methods, chemical vapor deposition (CVD) growth of carbon nanotubes (CNTs) is nowadays regarded as one of the most promising for CNT growth. This process allows a high degree of control over the resulting growth and morphology by tailoring the catalyst that adsorbs and dissociates the carbonaceous gas.

For several specific applications, localized growth of carbon nanotube structures and in particular laser-assisted CVD (LACVD) has recently emerged as a promising technique for growing CNTs on selected places and sensitive substrates. Using a laser to locally heat the substrate offers a fast, highly versatile process compatible with a broader range of substrates that can have various shapes or temperature-sensitive elements already attached to them. However, for laser-assisted CVD (LACVD) growth of CNTs, detailed process information, such as temperature evolution and process monitoring over time are lacking, due to the nature of the localized process, and requires solutions for better control and optimization.

In this thesis, the investigation and optimization of a laser-assisted chemical vapor deposition method for carbon nanotube growth is reported. A closed-loop control mechanism is developed to precisely monitor and control the laser-assisted chemical vapor deposition process. Several optical sensors are used to monitor and collect *in situ* information about the growth. These signals are used in the feedback control and as a first approximation of growth kinetics.

For more precise control of gas flow conditions and composition, essential for studying growth kinetics, a miniaturized reactor chamber has been designed. This chamber ensures a precise control of the gas flow and composition at the laser-growth site by producing a laminar flow of process gases over the substrate.

To further optimize the process, carbon nanotube growth kinetics is investigated. This allows for the determination of activation energy as a function of experimental parameters such as partial pressures and flow rates. A model has been developed, introducing four different regimes that are linked to the quality and structure of carbon nanotube growth. For these regimes, different activation energies were found, ranging from 0.3 to 0.8 eV.

Finally, as a proof of the versatility of the process several potential applications are demonstrated. A forest of aligned carbon nanotubes is transferred into a polymeric layer by simple spin-coating and release techniques. This could potentially be used as interconnects in flexible electronics. As a second illustration, the localized growth of carbon nanotube structures is performed inside a sealed glass micro-channel with potential applications in integrated sensors.

The growth of a line of nanotubes was performed as well, showing the ability to make complex structures of aligned nanotubes without the need for pre-patterning the surface. Lastly, a demonstration of growth inside a narrow enclosure confirms the ability to grow nanotube structures in the vicinity of other components or devices.

Overall, this thesis contributes not only to the understanding and optimization of LACVD for CNT growth, but also provides new insights on CNT growth kinetics in general as well as their potential applications.

Chapter 1 |

Introduction to laser-assisted growth of carbon nanotubes

Laser-assisted chemical vapor deposition (LACVD) is an attractive mask-less process for locally growing carbon nanotubes at selected places on substrates that may contain temperature-sensitive components. This chapter gives a comprehensive overview of the reported research with respect to laser-assisted CVD. Advantages and disadvantages of local growth using laser sources are discussed, with a focus on structural quality and properties such as length, position, alignment and process controllability. After a brief introduction, this chapter is divided into three parts. The first part deals with the influence that the three main parameters for nanotube growth - gas, catalyst and thermal energy - have on the growth of carbon nanotubes by laser-assisted synthesis. The second part describes various approaches to control different aspects of local nanotube growth using a laser-assisted growth method. This literature review covers the state-of-the-art of the technique up until present. In other words, the work described in this thesis is done in parallel to some results described in this chapter. Finally, the objectives of this thesis are outlined.

Part of this chapter has been submitted for publication in

Y. van de Burgt, *Laser-assisted growth of carbon nanotubes - a review*, submitted (2014).^[1]

1.1 A brief introduction on carbon nanotubes

The element carbon that constitutes carbon nanotubes (CNTs) is abundantly present on earth and is crucial for all organic life. Carbon owes its special properties and its ability to bond to its electronic configuration. It can "hybridize" one electron from the fully filled 2s shell, promoting it to the 2p shell. This results in the ability to form two different types of bonds, the σ -bond and the π -bond allowing a great variety of chemical structures and bonds.

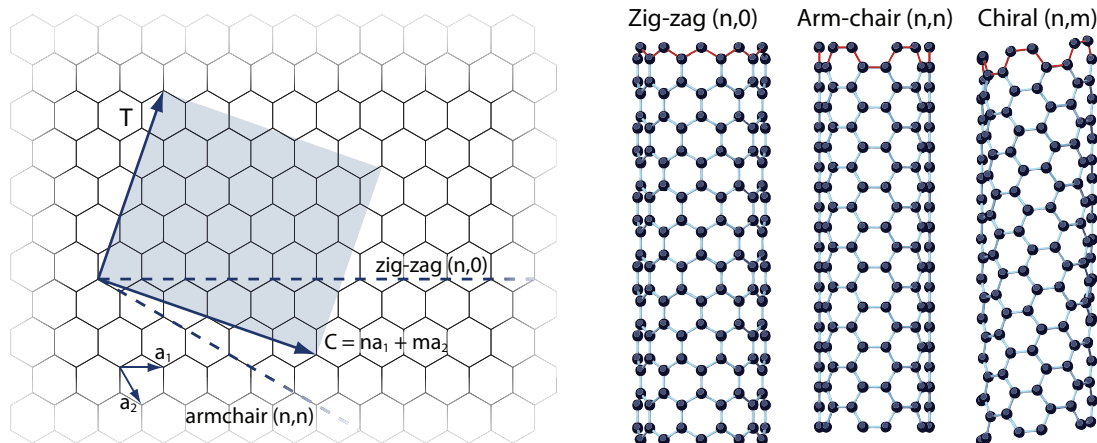
Carbon nanotubes are nano-sized tubular carbon allotropes and can best be viewed as "rolled-up" sheets of graphene, single layer sp^2 hybridized carbon. Generally, two types of CNTs are considered, single-walled CNTs and multi-walled CNTs, where the latter consists of two or more concentric tubes. CNTs can either be metallic or semi-conducting depending on their crystallographic structure. The structure is determined by the chirality of the CNTs, which depends on the way the graphene sheet is rolled up. This is schematically shown in Figure 1.1 where the chirality is determined by a combined vector $C = na_1 + ma_2$. Here a_1 and a_2 are the lattice parameters shown in Figure 1.1 and n and m are integers.

As shown in Table 1.1, the chirality vector C determines the electronic properties.

Table 1.1: Electronic properties of carbon nanotubes

Type	Property
Arm-chair	metallic
Zig-zag	metallic if $n = 3j$ semi-conducting if $n \neq 3j$
Chiral	metallic if $n - m = 3j$ semi-conducting if $n - m \neq 3j$

The hybridization necessary to form the planar bonds in carbon nanotubes is schematically shown in Figure 1.2.



(c) Schematic representation of the chirality vector on a graphene sheet .

(d) Schematic representation of three different types of single-walled carbon nanotubes

Figure 1.1: Chirality of carbon nanotubes.

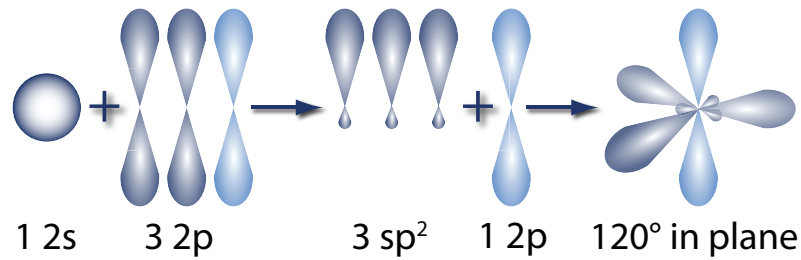


Figure 1.2: Schematic representation of sp^2 hybridized orbitals.

Because of this particular crystallographic structure, CNTs can exhibit extraordinary thermal, electronic and mechanical properties,^[8–11] of which a few are listed in Table 1.2.

Table 1.2: Properties of carbon nanotubes

Morphological	Electronic
Nanometer size	Semiconducting or metallic
High aspect ratio (up to 10^7)	Ballistic conductor
High specific surface area	High current density ($10^9\ \text{A/cm}^2$)
Hollow	
Thermal	Mechanical
High thermal conductivity ($> 3000\ \text{W/mK}$)	Flexible (SWNT) or (relatively) stiff (MWNT)
	High Young's Modulus ($\sim 1\ \text{TPa}$)
	High tensile strength ($\sim 150\ \text{GPa}$)

Those excellent electronic and mechanical properties make them ideal candidates for a wide variety of applications^[12, 13] such as field effect transistors and logic operators,^[14–17] field emitters,^[18–20] displays,^[21] sensors,^[22, 23] flexible electronics,^[24] filters,^[25–27] interconnects,^[28] scanning probe microscopy tips,^[29] solar cell technology,^[30] and computers.^[31]

A prerequisite for most of these applications is the ability to control the CNT crystallographic structure and length. Often this means that aligned CNTs must be grown with specific properties tailored to the particular application. Furthermore, the ability to grow CNT structures locally can be advantageous. For instance, local grown CNTs can act as transistors, field emitters, sensors, and interconnects.

The synthesis of CNTs is highly dependent on the process parameters such as temperature, process gases, potential catalyst, substrate and time. The nature of the localized process makes it difficult to control some of the process parameters, most importantly temperature, in direct-growth processes. In order to obtain specific localized nanotube structures the process must be controlled. This thesis focuses on a specific method for local growth of CNTs, laser-assisted chemical vapor deposition (LACVD).

Although many groups have published research regarding process control and optimization, temperature uniformity, *in situ* growth measurements, fast temperature response etc. in LACVD for CNT growth, an overview of all the different parameters influencing the synthesis and control of this method is still lacking. Many process parameters are available which makes it difficult to compare results. In this chapter, the aim is to fill this gap by providing a comprehensive overview that combines the results of previous papers in a systematic manner.

The main problems with process control and disadvantages of the technique are used as a starting point, where the solutions published are summarized and put into a logical order.

First a brief history is given with respect to general carbon nanotube growth methods that were developed initially. From here, with the focus of this chapter on controlled growth, the different chemical vapor deposition techniques are discussed and their main (dis-)advantages mentioned. Combinations of several techniques are presented, trying to use and combine advantages of the techniques. Other methods for local growth of CNTs are presented and laser-assisted CVD in general is explained.

The remaining part of the chapter is divided into a literature review and the outline of this dissertation. The first part summarizes the unique results regarding the structure, quality and type of CNTs specific for laser growth, with respect to the three main elements of CNT growth by (laser-assisted) CVD: Catalyst and substrate, process gases and thermal energy. The second part treats the research and solutions published with respect to enhancing the control over the process. An overview of attempts and successes to control specific properties, geometry, location and quality as well as techniques used to *in situ* monitor the growth are presented. Next, a brief overview of applications of CNTs specifically fabricated using laser-assisted CVD is given. Finally, the motivation and outline for this thesis are presented. Note that some of the results presented in this chapter were done in parallel to our own work as the literature review covers work until present day.

1.1.1 Chemical vapor deposition

Chemical vapor deposition is essentially a thin film deposition technique. The method relies on chemical reaction at the surface which results in crystal growth of the pre-cursor gas. In Figure 1.3 an example is schematically shown which shows the deposition of SiO₂. A heated substrate initiates the chemical reaction $\text{SiH}_4 + \text{O}_2 \rightarrow \text{SiO}_2 + \text{H}_2$ which results in the controlled deposition of a thin layer of SiO₂.

1.1.2 Methods of carbon nanotube production

Before Iijima's pioneering work in 1991,^[32] it was already known since the late 1950's that carbon filaments or fibers could be catalytically grown using a chemical vapor deposition method (CVD).^[33–35] Already in 1976 Oberlin *et al.* proposed a method for the catalytic decomposition of benzene on iron filaments.^[36] However, the first reported research declaring the growth of CNTs, did not use CVD but instead involved an arc-discharge method.^[32] This process comprises a high current between two graphite electrodes. The CNTs were found in the soot of the graphite electrode and yielded both multi-wall^[32](MWNTs) as well as single-wall CNTs (SWNTs) in a follow-up study.^[37] The disadvantage of this method is that the CNTs are arbitrarily ordered and not aligned, making the method less suitable for many applications that require a certain structure and/or position on a substrate. Also, the temperatures involved in this process are very high, typically in the order of 3000 - 4000°C.

Following up on this discovery, a group at Rice University used their laser evaporation method, originally designed to produce metallofullerenes, to successfully grow MWNTs in 1995.^[38] Later that year, the same group added metallic nano-particles to produce single-wall CNTs.^[39]

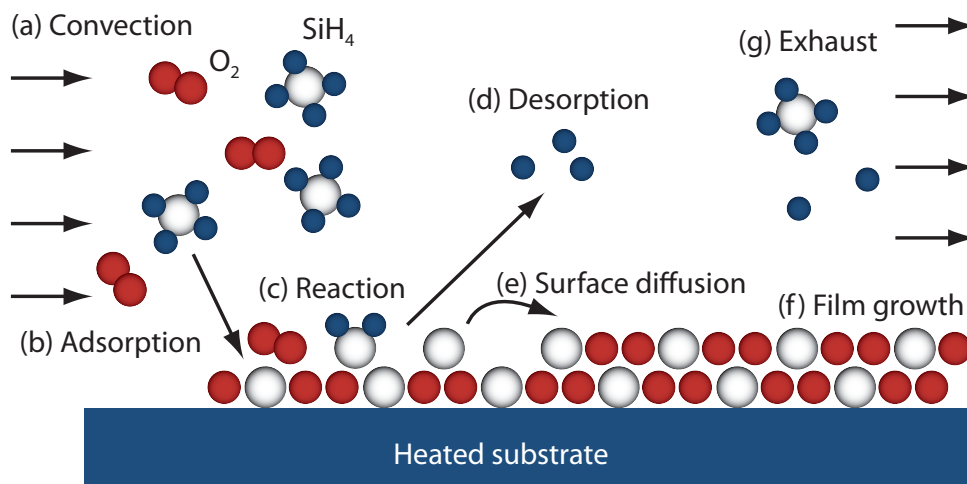


Figure 1.3: Schematic example of chemical vapor deposition of SiO₂ from SiH₄ and O₂. (a) convection drives the precursor gas to the heated substrate. (b) Adsorption of the precursor molecules to the substrate. (c) Reaction of the precursor (d) Desorption of the unused molecules. (e) Surface diffusion to position with minimal Gibbs Free Energy. (f) Crystal film growth.

The laser evaporation method is a relatively expensive method but has the advantage that high quality^[40] SWNTs can easily be grown by controlling the reaction temperature.

Chemical vapor deposition for CNT growth

Producing carbon nanotubes by the CVD method is now adopted as the most widely used process. This method comprises a pressure controlled chamber where a hydrocarbon gas is catalytically decomposed on a metal catalyst at a temperature of about 500 - 1200°C. Ultimately, the growth of CNTs by CVD requires three main elements, namely energy, mostly in the form of an elevated temperature, a carbon feedstock gas, and a catalyst.^[41,42] The influence of all three components has been studied widely. The first report of CNTs grown by the CVD method was already in 1993.^[43] In 1996 Li *et al.* developed a method to grow aligned CNTs using iron nanoparticles as catalyst.^[44] The popularity of CVD over other methods is mainly because the technique uses relatively low synthesis temperatures, compared to the laser ablation and arc-discharge techniques. Because the diameter and, to some extent, the chirality of the nanotubes are dependent on the catalyst diameter or film thickness,^[45-49] the properties of the growth product are highly controllable. Also the ability to grow aligned CNTs is favorable since many applications such as Field Effect Transistors and interconnect applications require alignment of the grown CNTs. Optimizing the advantages of the technique, a number of other CVD techniques for the growth of CNTs, such as plasma-enhanced CVD,^[50,51] aerosol-assisted CVD^[52] and fluidized-bed CVD,^[53,54] were developed in the years thereafter.

Combinations of different growth techniques were developed as well. For instance, Kanzow *et al.* developed a method which combined the laser vaporization method with CVD to grow MWNTs.^[55] The laser was used for producing the catalytic nano-particles whereas the substrate was heated as in conventional CVD. Grobert *et al.* used a similar method, where the laser was used only to deposit a thin metal catalyst film and aligned carbon nanotube bundles were grown from solid organic precursors.^[56] The group of Rummeli and Loffler developed

both a method comprising a laser-assisted CVD with solid carbon as feedstock rather than a gas^[57] as well as a laser ablation process combined with CVD.^[58]

Another possible advantage of a combined CVD process was discovered by Maehashi *et al.*^[59] They developed a method to remove particular CNTs through selective absorption of the exciting laser wavelength only by specific nanotubes after growing by thermal CVD. Similar methods were reported later, by using a Free Electron Laser during growth to control the chirality of the grown CNTs^[60] and laser induced selective removal of metallic nanotubes.^[61]

Although CVD is the most widely used method to grow CNTs, the technique also has a number of limitations. Firstly, the process requires a catalyst which generally remains in either the top or the root of the nanotube. This reduced purity can be a problem with respect to the properties of the CNT as well as specific applications. Second, the relatively low synthesis temperature decreases the structural quality of CNTs and results in a lower degree of graphitization. Nonetheless, CVD is still considered the most promising method to grow controlled nanotube structures for many applications and it has also been suggested that SWNTs grown by the CVD method have less inferior properties than MWNTs.

Although not sufficient for optimal structural properties of the CNTs, the process temperatures are still relatively high, typically above 500°C.^[62] In both a hot-wall reactor as well as a cold-wall reactor the complete substrate is therefore heated to these high temperatures, which makes it impossible to apply the technique to substrates and/or features that cannot withstand these temperatures. This can be problematic when the CNTs are to be implemented in a manufacturing line or product that has temperature sensitive features. A transfer step is then necessary, introducing more complexity and higher costs to the production line. Local CNT growth with localized heating would be a solution to this problem.

1.1.3 Methods of local growth of carbon nanotubes

Local growth of CNTs can be obtained by the localization of one of the three main components required for CNT synthesis: catalyst, feedstock gas and thermal energy.

The catalyst can be localized by depositing it locally,^[63] or by creating a pattern through removing part of the catalyst layer. Usually this is done by an extra and expensive lithographic step.^[19, 64–66] Localization of the carbon feedstock gas has been demonstrated^[67] but this is a process difficult to control.

The most promising method for localization of the CNT growth is to confine the required thermal energy to the area where the growth has to take place. A number of researchers have used micro-resistive heaters^[68–72] to induce the heat locally. Some groups succeeded in growing local CNT structures on CMOS-compatible metal electrodes^[66] and heaters.^[71, 72] Sosnowchik *et al.* used micro-induction to induce locally the thermal energy necessary for the CNT synthesis.^[73] A comprehensive overview of these and other techniques to localize heat for the growth of local nanotube structures is given in a review paper by Sosnowchik *et al.*^[74]

This thesis focusses on locally induced heat by a laser source. That means that CNT structures are grown with a chemical vapor deposition process, but only at locations where the laser provides the necessary thermal energy to reach the CNT synthesis temperature. Using a laser as the heat source has the advantage that it is much more flexible than the approaches mentioned above, since the laser can be focused virtually anywhere on the substrate. Also this

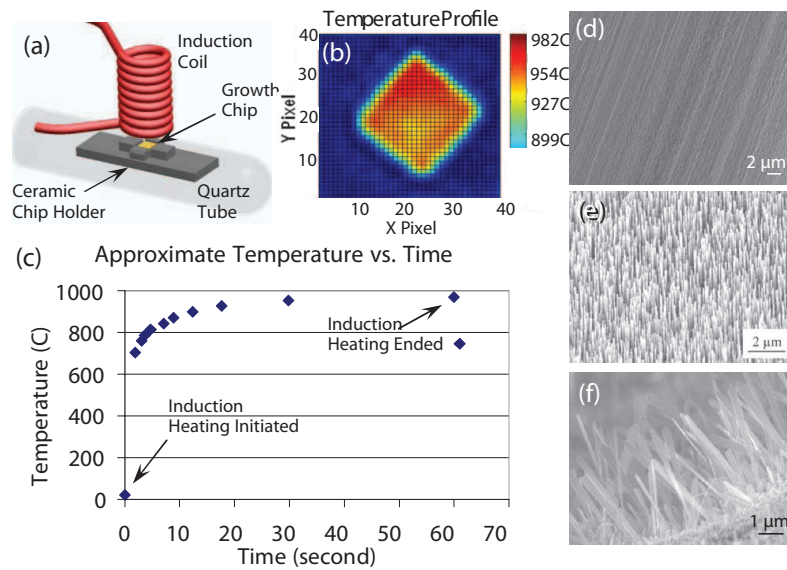


Figure 1.4: Experimental setup for CNT synthesis. (a) Schematic overview of the CNT synthesis chamber, chip holder, and induction heating coil. (b) Thermal profile of inductively heated silicon chip. (c) Estimated temperature profile for a one-minute test. Synthesis has been demonstrated for (d) CNTs, (e) zinc oxide nanowires, and (f) titanium dioxide nanoswords. Reprinted with permission from.^[74] Copyright 2010, AIP Publishing LLC

approach does not require the difficult fabrication and integration of micro-heaters near the growth side. The downside of this technique is the difficult process controllability. Table 1.3 lists several different properties, advantages and disadvantages and process parameters of LACVD compared to conventional thermal CVD.

Considering the three main requirements for CNT growth: catalyst and substrate, process gases and thermal energy, the physics of laser-assisted CNT synthesis is different from conventional growth methods. For instance, catalyst reduction and structuring were found to be able to be created *in situ* without a pre-treatment step in an inert environment. The synthesis gas can be influenced by the laser wavelength and the temperature created on the substrate by the Gaussian laser beam clearly has a very different profile than the flat and uniform temperature profile of a conventional hot-wall CVD apparatus. These and other parameters influencing growth are discussed in section 1.2. The control of the CNT synthesis using LACVD thus requires a different approach. The combination of non-contact local laser heating with fast temperature response and a non-uniform temperature distribution resulted in a variety of solutions to enhance controllability over the process. The enhanced versatility of the process over conventional growth methods, i.e. growing on small structures and writing lines and patterns or single tubes across a certain geometry, resulted in some creative and unique opportunities. This is discussed in section 1.3 with focus on process control. To understand the physics of the process, first the laser-assisted CVD process in general is briefly discussed.

1.1.4 General laser-assisted CVD

Laser-assisted or laser-induced CVD for the decomposition of a certain precursor can be divided into two categories: photochemical-, or -photothermal LACVD.^[75] Both processes are

Table 1.3: Comparison of different properties and process parameters between laser-assisted CVD and conventional CVD for carbon nanotube growth.

LACVD	CVD
Localized growth	Complete substrate growth
<ul style="list-style-type: none"> – Temperature sensitive components / substrates – Versatile process – Writing patterns – Direction control 	<ul style="list-style-type: none"> – High quantity growth of CNTs – Necessity for pre-patterning
Fast heating / temperature response	Low heating rate
<ul style="list-style-type: none"> – Catalyst structuring and activation <i>in situ</i> 	<ul style="list-style-type: none"> – Catalyst pre-patterning step
Direct, <i>in situ</i> measurement of growth (type, length, and/or quality)	Indirect <i>in situ</i> measurement of growth (type, length, and/or quality)
Non-uniform temperature distribution	Uniform temperature distribution (hot wall)
No direct control of temperature	Temperature set
Small amount of CNTs	Large amount of CNTs
<ul style="list-style-type: none"> – Fast response to changes in environment 	<ul style="list-style-type: none"> – High inertial environment

schematically depicted in Figure 1.5. The first process, photochemical (or photolytic) LACVD is based on the decomposition of a precursor gas by selective excitation and breaking of the molecular bonds, typically with lasers in the visible or UV range, such as gas or excimer lasers. The result is that the decomposition takes place in the total laser-gas interaction volume. Generally, this process is used for thin film deposition at relatively low temperatures making the process ideal for the growth on temperature sensitive materials.^[76] Photochemical LACVD has also been proposed for the production of microstructures^[77] but the results did not yield well-defined deposits as a result of diffusion of the excited molecules.^[78] Photolytic deposition of metal-carbonyls (such as Fe(CO)₅) is a more widely used process for the deposition of thin metal films, with laser radiation wavelength typically below 350 nm. Other examples are the deposition of thin CrO₂ layers with UV lasers, requiring low deposition temperatures due to its metastable state and boron carbide films, using a CO₂ laser.^[76]

The second process, photothermal (or pyrolytic) LACVD is based on the thermal activation of the precursor by the laser beam. The process was developed in 1972 and among the first reports of this technique were the deposition of silicon by an infrared CO₂ laser^[76] and the deposition of carbon using the visible radiation of an Argon ion laser.^[79] Pyrolytic LACVD often requires high temperatures but enables the deposition of halogen compounds, hydrocarbons and silanes.^[75] This process solely uses the laser for heating the substrate on which the precursor material is then deposited. The material is only deposited where the temperature is high enough. Since laser beams generally provide a Gaussian distribution of irradiance on the focus spot, the feature size of the deposit can be smaller than the spot-size of the focused laser beam as long as the required temperature is only reached in a certain part of the center of the spot.^[80] To obtain the smallest structural features, usually excimer lasers with Argon (193 nm) or Krypton (222 nm or 248 nm) are used due to their short wavelengths. Some

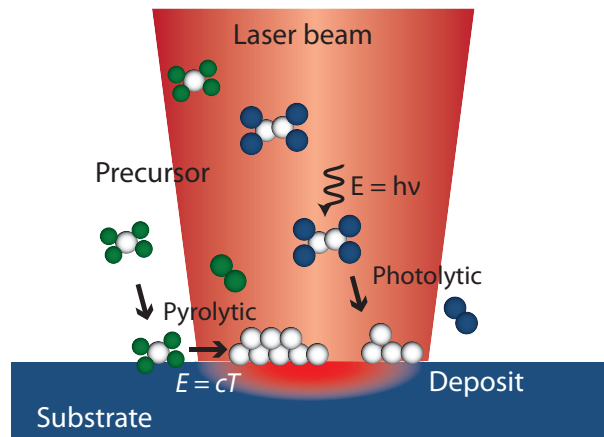


Figure 1.5: Schematic for both laser-assisted chemical vapor deposition techniques: pyrolytic and photolytic.

LACVD processes consist of a combination of both of the previous processes where one of the two can dominate the deposition rate over the other. This combined process is called photophysical LACVD.

1.2 Parameters influencing carbon nanotube growth by localized laser heating

When comparing laser-assisted synthesis of CNTs with a conventional CVD growth method, the main difference is the localized heat provided onto the substrate. However, with this core difference other aspects of the process are influenced as well. Actually, all three main elements of the growth process are changed to a certain degree opening up new opportunities and remarkable results as well as imposing several problems. When comparing LACVD with other techniques, the resulting growth is assessed on structural and morphological quality of the carbon nanotubes. Raman spectroscopy is generally used to quantitatively assess the quality of the CNTs.^[81, 82] At the same time, the type of nanotubes (single-walled or multi-walled), alignment and growth direction can be viewed as a specific qualitative comparison between the different growth techniques.

The first reported research^[83] on laser-assisted CNT growth showed the possibility of growing local CNT structures using a laser as the heat source. These reports also gave a first impression of the changed influence of process parameters on the resulting growth. Catalyst formation on the substrate, influence of gas and gas flows and temperature distribution are among the parameters that are fundamentally changed. Also the laser source used in the process, its wavelength, irradiance and whether it is a continuous-wave (CW) or pulsed laser, can have a noticeable effect on the resulting growth. In Figure 1.6 a general schematic of laser-assisted growth for carbon nanotubes is given, demonstrating several variations. The laser source, providing the thermal energy necessary for CNT synthesis, can either be directed onto the substrate from the top side or the bottom side. The substrate is usually placed on a stage and can contain the catalyst, although catalyst precursors delivered through gas phase are possible as well. Several sensors, such as a pyrometer or *in situ* Raman spectroscopy can be used to

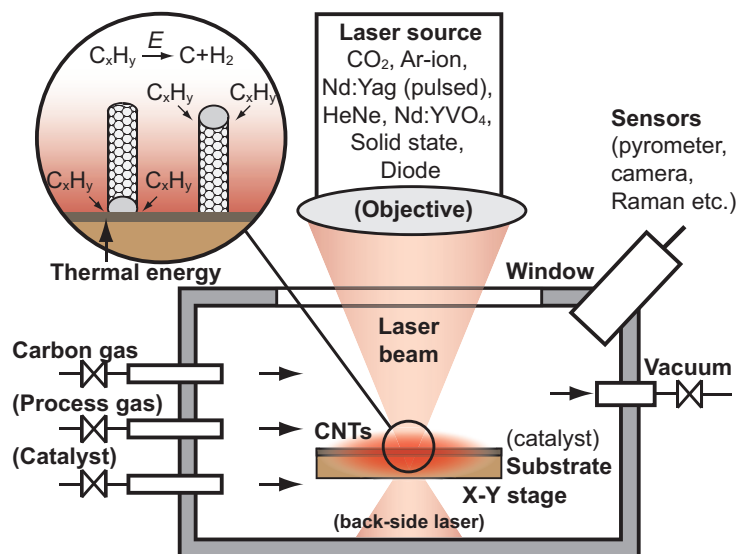


Figure 1.6: General schematic for a laser-assisted chemical vapor deposition setup including the laser source, gas input, substrate and catalyst, stage and sensors. Between brackets some variations or options are shown. The inset shows the two variations of CNT growth, base-growth (left) and tip-growth (right).

monitor the process. The inset of the figure shows the two growth methods, common for CVD growth, base-growth and tip-growth.

In what follows, the influence that the three main elements for nanotube growth, - catalyst and substrate, gas, and thermal energy - have on the growth of carbon nanotubes by laser-assisted synthesis is described.

1.2.1 Catalyst and substrate

The laser heating allowed for a different method of catalyst deposition and preparation. In conventional CVD it is common to have a catalyst preparation step, prior to the growth, which can take up to tens of minutes. In this step the temperature is gradually ramped to the desired growth temperature in an inert gas, usually Nitrogen. In laser-assisted CVD this step can be much faster and even done *in situ*. Alexandrescu *et al.* were the first to report on this.^[83] A CO₂ laser with a maximum power of 100 W was directed onto a silicon substrate. The catalyst precursor that was used was iron-pentacarbonyl gas, Fe(CO)₅, which was formed *in situ* on the substrate as iron nano-particles, by heating the substrate as well as the gas (photophysical heating). The authors reported straight, curved and branched multi-wall as well as single-wall CNTs and evidently showed the possibility of growing different types of CNTs using this method. By depositing and forming the catalyst directly from the gas state onto the substrate, they also proved the possibility of a fast *in situ* catalyst preparation step. Following their first report, the same authors then optimized the process by reducing the supply of catalyst and feedstock gas and investigated the separation of the catalyst deposition process from the CNT growth process.^[84] Both the co-deposition process as well as the two-step process resulted in high quality CNTs but only with the co-deposition process a dense aligned MWNT film was obtained, see Figure 1.7. Further, the nanotube diameters that were obtained by the co-deposition process were found to be considerably smaller than those obtained by the two-step

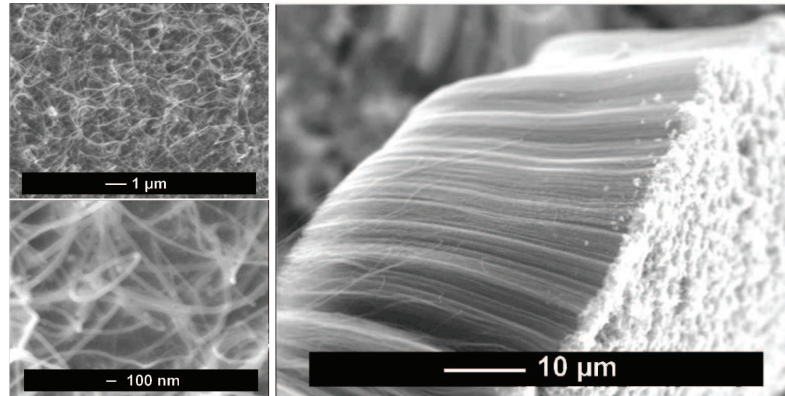


Figure 1.7: SEM images of a carbon nanotube film synthesized in a two-step experiment (left) and SEM image of a densely packed aligned MWNT film. Reprinted with permission from.^[84] Copyright 2002, American Vacuum Society.

process which was attributed to smaller catalyst nano-particles in the case of co-deposition.^[84] This was explained by the fact that nanotube nucleation starts when the nano-particles reach a critical diameter instead of the nano-particles having their diameters determined by the duration of the preparation step.

Apart from the catalyst, the substrate and sub-catalyst layer beneath the catalyst also influence the resulting growth. This is a result of the change in surface energy and wetting properties of the catalyst^[85] as well as the different heat distribution through the sub-catalyst layer and substrate.^[86, 87] On top of that, transparency of the substrate for certain wavelengths is another property that significantly influences the growth method that can be used. The most commonly used substrate is silicon, although fused silica,^[86–88] graphite and grafoil^[89] and porous Al_2O_3 membranes^[90, 91] were also used in combination with laser-assisted growth. Shi *et al.* synthesized suspended multi-wall (650°C) as well as single-wall (770°C) nanotubes on inverse opal templates of silicon covered with a NiFe catalyst.^[92]

By using a substrate transparent for the laser wavelength, Chen *et al.* were able to grow nanotubes from the backside of the substrate.^[86] However, the problem arose of how to efficiently heat up the very thin catalyst layer. As a solution, Chen *et al.* proposed using a light absorbing layer to support the catalyst. Their laser-assisted CVD process used a low power diode laser operating at 808 nm as the heat source. The glass substrate used was transparent to the laser wavelength and a layer of either carbon black, or commercial graphite inner coating was used to absorb the laser light. Chen *et al.* succeeded in growing arrays of well-aligned multi-wall CNTs. Park *et al.* used a quartz substrate in combination with a focused green (frequency-doubled) Nd:YVO₄ laser and used a combination of chromium and an aluminum buffer layer to absorb the laser light.^[87]

The sub-catalyst layer co-determines the properties of the catalyst particles.^[85] Oxides such as alumina (Al_2O_3) or silicon-oxide (SiO_2) are the most commonly used sub-catalyst layers and they both prevent strong wetting of the metal catalyst ensuring the proper catalyst morphology while enhancing charge transport through catalyst and support.^[41] The presence of the sub-catalyst layer also narrows the size distribution of the catalyst.^[62] The complex interactions that play a role in these mechanisms are not yet completely understood and as such also the role of local photo-physical heating by laser irradiance is not clear. The influence of the laser-

induced photons on the reactions, as well as the induced temperature gradient on temperature sensitive chemical reactions might not be neglected. At the same time, a reduction of these stable oxides by thermal energy under hydrogen atmosphere is not expected.^[85]

1.2.2 Gas

Gas supply plays a significant role in the nanotube formation process. The binding energy of the carbon-containing gas typically determines the absorption rate of the gas on the catalyst and therefore indirectly influences the growth rate. Hydrogen, ammonia and inert carrier gases influence the growth as well, by co-determining chemical and thermodynamic process parameters.^[62] On top of that, the precursor gases can influence the catalyst reduction and re-structuring,^[93] effectively determining the CNT growth.

For some laser-assisted CVD growth the photo-chemical heating of gases should also be considered. Ethylene has a resonant absorption at the CO₂ laser wavelength of 10.6 μm. This effect was used to co-heat iron-pentacarbonyl gas, Fe(CO)₅ and decompose this catalyst on the substrate^[83] although follow-up research has shown that the mere thermal heating of the substrate provides sufficient energy for iron catalyst nano-particles to form. In contrast, in thermal CVD, particularly at low temperatures, it is suggested that the pre-heating of the process gases can be useful to improve and enhance the growth process.^[94,95]

A few studies have been done linking the CNT quality to gas concentration for laser-assisted growth. Rohmund *et al.* reported that high quality CNTs were only obtained when a significantly reduced acetylene concentration was used in the co-deposition process, with respect to their two-step process.^[84] The result was a high quality dense MWNT film and this was explained by a decreased growth rate. A lower carbon supply rate results in a lower growth rate and thus a lower defect formation at the same temperature.

Conversely, Bondi *et al.* reported on more and denser tubes with increasing acetylene concentration.^[89] However, the growth took place in a statically filled chamber with no flow. The authors argued that a sufficiently large reaction-chamber ensured that the feedstock gas was not consumed during the experiment since the laser heating only resulted in a small amount of CNT growth. However, the authors did not measure the quality of the nanotubes, only the amount and the density.

Morjan *et al.* investigated the influence of acetylene and ethylene precursor gas on LACVD growth. The authors reported that their experiments did not lead to any CNT growth by only using ethylene as a feedstock gas which was consistent with their previous work.^[84,96] The higher bonding energy of ethylene with respect to acetylene was given as an explanation,^[97] implying that the activation energy of the process is much higher, requiring higher temperatures to initiate growth. Consistent with thermal chemical vapor deposition,^[98] an increase in ethylene concentration in laser-assisted CVD was found to increase the mean CNT diameter and the diameter size distribution to become broader,^[97] see Figure 1.8. At high temperatures, ethylene gas can decompose thermally resulting in more amorphous carbon deposition. This effect is larger when the ethylene gas is directly heated in the gas phase by the laser as well, which can explain the lower quality and larger diameter CNTs at higher ethylene concentration.^[96,97]

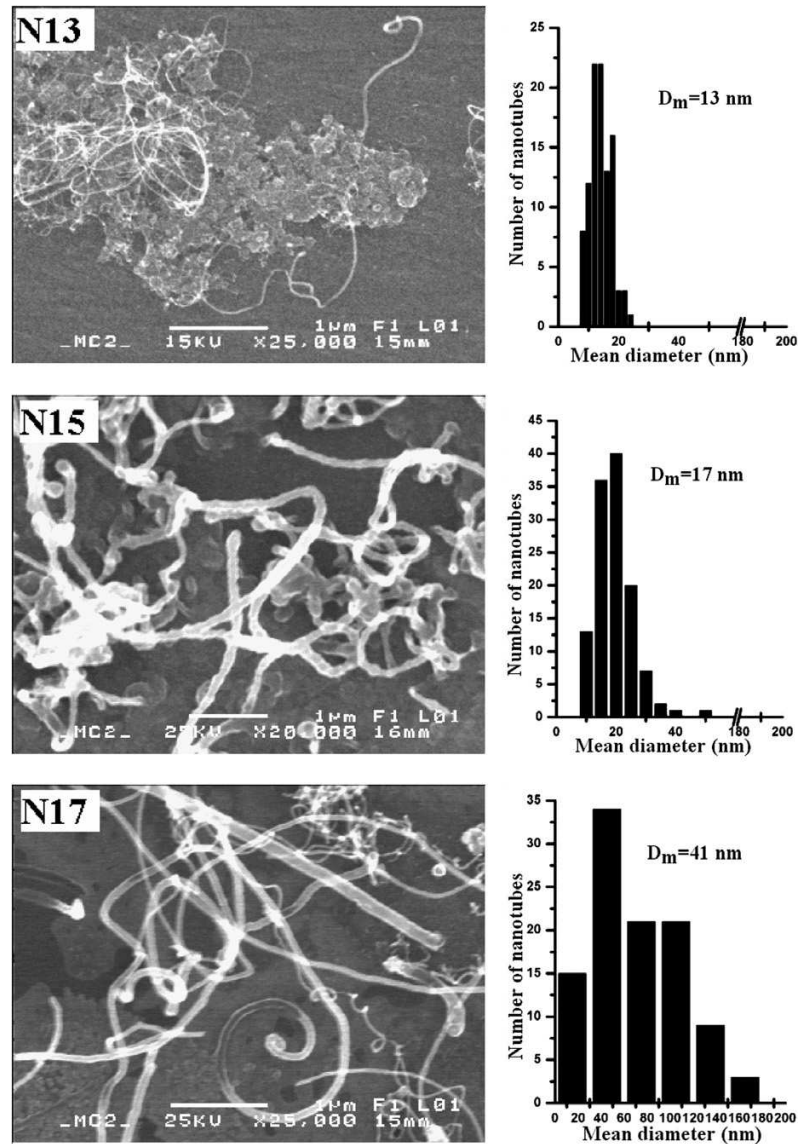


Figure 1.8: SEM images of as-grown CNT films with increasing ethylene flow rates (up to bottom direction) and their respective diameter distributions (on the right side of each image). Reprinted from^[97] with permission from Elsevier.

Some addition of ammonia-gas is commonly used to improve the growth by ensuring the presence of nucleation sites on the catalyst^[96] and preventing the formation of amorphous carbon.^[65] It can also be used to reduce the oxidized catalyst and remove amorphous carbon. However, in combination with laser-assisted growth, too high concentrations of ammonia were found to decrease the quality of the CNTs.^[96] This was likely a result of the low absorption of ammonia gas at the laser wavelength causing cooling effects.

Very high temperature gradients around the laser hot spot can also introduce local turbulences in the local gas supply. Particularly if the growth takes place in a chamber with steady-state pressure and gases, without a forced flow of process gases, turbulence or uncontrolled convection and local undersupply of carbon precursor might become a problem. However to date no systematic studies exist supporting this statement. Sufficient carbon feedstock supply to the hot spot is necessary to ensure stable growth, although Bondi *et al.* argued that in the

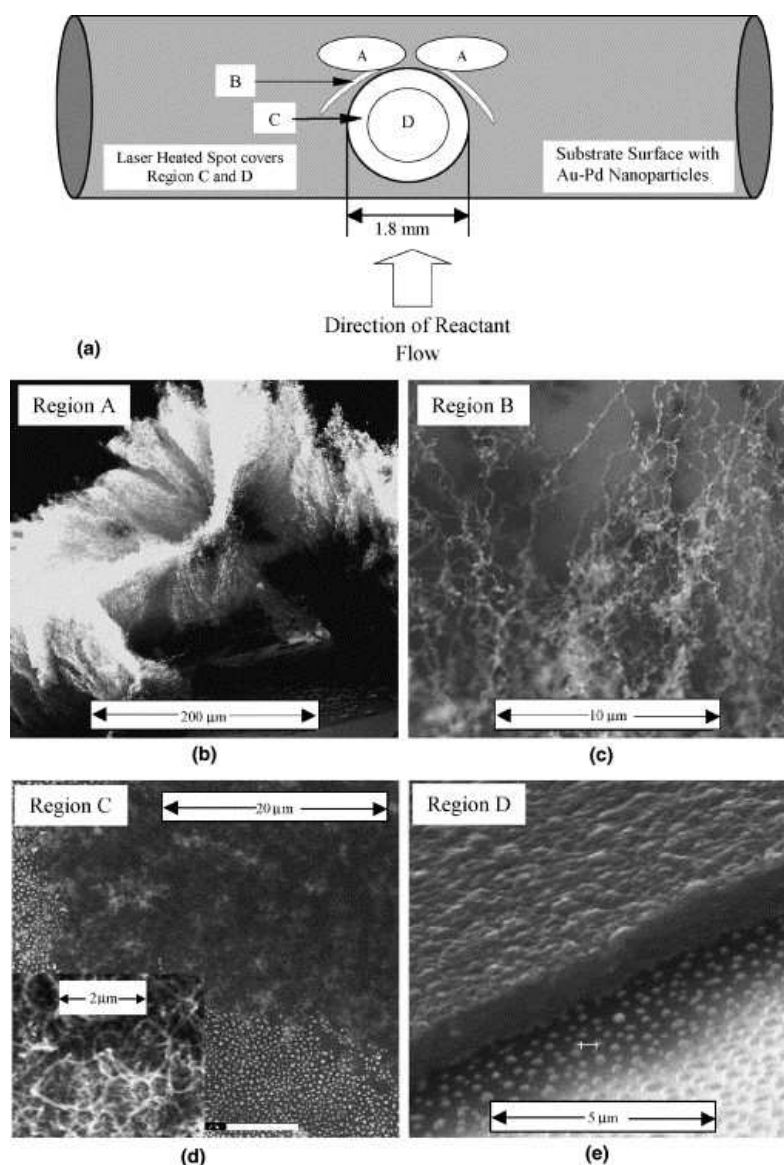


Figure 1.9: (a) Schematic of the different carbon growth regions observed on the substrate after laser heating. SEM image of (b) dense packed carbon nanotube material, (c) scattered carbon nanotubes, (d) a region covered with a thin layer of ultra-dense carbon nanotubes and (e) a thin layer of pyrolytic carbon covering the substrate and catalyst particles. Reprinted from^[99] with permission from Elsevier.

case of laser-assisted growth in a static chamber, the consumption of acetylene gas is so small that no noticeable depletion is occurring.^[89]

A specific example of exploiting the localized nature of laser-assisted growth combined with local gas control is given by the open-air apparatus of Kwok *et al.*^[99] Their approach was to separate the process gasses from the surrounding by generating different flows around the substrate. With this method the authors were able to grow MWNTs on a quartz substrate in a controlled manner without the need for a vacuum chamber. A Schematic and results are shown in Figure 1.9.

As a final note, high flow rates directed onto the heated surface could also lead to temperature drops as a result of additional cooling effects. This effect is largest with high thermally

conducting gases such as hydrogen and helium and was found to significantly affect process conditions in a thermal CVD setup.^[100] Therefore it is likely that this effect will be larger with smaller heated surfaces, as is the case with laser-assisted growth. To overcome this problem, temperature control can be implemented which will be discussed in subsection 1.3.1.

1.2.3 Thermal energy

One of the main advantages of using a laser as the heat source is that very high heating rates are achieved and the catalyst activation process is much faster. The whole process is therefore much faster. This is a direct result of the local concentrated photo-physical heating of the substrate. Using a CO₂ laser in combination with ethylene gas, this can even be further enhanced by exploiting the laser absorption at the substrate-gas interface.^[97]

On the other hand, lasers have the disadvantage of introducing a non-uniform temperature distribution over the heated spot. This effect can be stronger for more tightly focused spots, due to the thermal conduction over the substrate. This is caused by the Gaussian distribution of the laser beam and often requires solutions to the heat dissipation over and through the substrate. The grown CNTs can therefore differ in type, quality and amount throughout the laser-affected zone. This was first shown by Fujiwara *et al.*^[101] The authors used an Ar-ion laser focused to a spot with a diameter of 5 - 40 μm as the heat source. Similar to the laser intensity profile, the resulting temperature profile had a Gaussian distribution as well. The corresponding growth resulted in the absence of CNTs in the center of the laser spot, where the temperature was too high, and SWNTs around the edges of the spot. By reducing the power of the laser beam the authors succeeded in achieving growth over the complete focused laser spot. However, as expected, there was a variance in nanotube size, quality and type over the radius of the spot.

Kasuya *et al.* proposed a solution to the problem of the non-homogeneous temperature distribution.^[102] Their solution also tackled the problem of the heat dissipation through the highly thermally conductive silicon substrate that is often used. Because of the conductive silicon, a focused beam can result in a very flat temperature distribution much larger than the spot-size. To overcome these problems the group proposed to use a substrate with an "energy confining layer".^[102] This layer consists of a 100 nm thick chromium layer to absorb the Nd:YAG laser source and a heat insulation layer of SiO₂ with a thickness of 1.5 μm, see Figure 1.10. Using this layer, they successfully confined the heat into the area of laser irradiation which resulted in a rapid, 1 second, localized synthesis of SWNTs.

Similarly, in the research of Park *et al.* the chromium layer between the transparent quartz substrate and nickel catalyst acted as the light and heat absorbing layer while the aluminum buffer layer contributed to the uniformity of the growth, as shown in Figure 1.11.^[87] By using iron as a catalyst Park *et al.* also succeeded in growing MWNT pillars^[103] and by using a modified catalyst deposition process high density SWNTs were grown as well.^[104]

Another solution to the problem of non-uniform temperature distribution could be to use beam-shaping or profiling. This technique has been successfully demonstrated in laser curing^[105] and requires the inverse of the temperature distribution as an input in the beam profiler. A few examples are flat-top laser beams or donut shaped intensity profiles. To date, *no research* with laser-assisted growth of CNTs with these beam profiles has been presented.

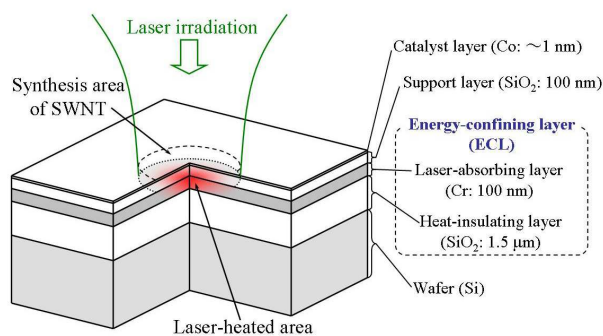


Figure 1.10: Schematic of the laser-assisted CVD synthesis of SWNTs on a multilayer substrate with the Energy Confining Layer as proposed by Kasuya *et al.*^[102] Copyright 2007 The Japan Society of Applied Physics.

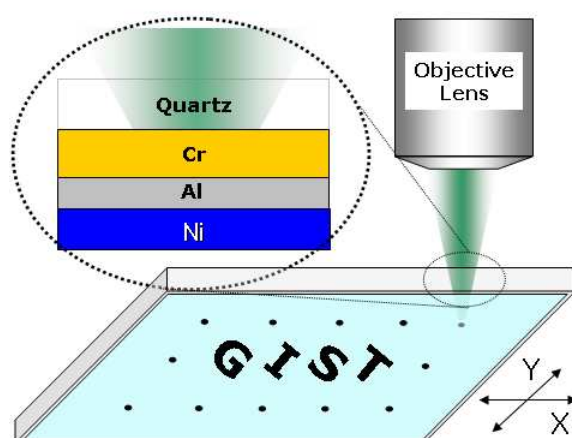


Figure 1.11: Illustration of the direct laser writing of CNTs using the proposed LCVD method on multiple catalyst (Ni/Al/Cr) layers. Reprinted from^[87] with permission from Elsevier.

From a global point of view, thermal energy can be provided by any type of heat source. However, different energy sources can also influence the kinetics of the heating process differently. In fact, the laser type and wavelength could influence the resulting growth. Apart from the most commonly used CO₂ lasers, a wide variety of different laser sources have been reported to grow CNT structures, such as Ar-ion lasers,^[90, 91, 101, 106] Nd:Yag lasers,^[102, 107] diode lasers,^[2, 3, 6, 86, 108] Nd:YVO₄ lasers^[87, 103, 104] and a solid state laser.^[88] These reported laser sources all are continuous-wave (CW) lasers where the beam irradiates the substrate continuously for a certain duration. In 2008 Liu *et al.* reported for the first time CNT growth using a high-power pulsed-laser source instead of the conventional continues-wave lasers.^[109] The reason for doing so was to be able to investigate kinetics of nucleation and growth of CNTs. Using a pulsed Nd:YAG laser, Liu *et al.* grew exclusively SWNTs with estimated growth rates between 10 and 100 μm/s and a minimum nucleation time of 0.1 seconds. Similarly, Uchida *et al.* used a pulsed Nd:YAG laser to grow SWNTs as well but combined this with resistive heating of the substrate.^[110]

A special case arises when a laser is used with a frequency equal to the resonance frequency of the catalyst nano-particles. The surface plasmon resonance effect of metal nanoparticles is the basis for the plasmon-assisted CVD process.^[111] The laser-light is efficiently converted

into heat inside the particles. In the research of Cao *et al.*^[112] and Hung *et al.*^[113] a low-power 532 nm CW-laser is used to locally induce the surface plasmon reaction on nano-particles. As a result, these particles are quickly heated to an elevated temperature, allowing the synthesis of CNTs on nickel^[112] and gold particles.^[113] Formally, the method described does not fit the laser-assisted CVD methods; nevertheless it can be argued that it is in fact a CVD process using a low-power focused laser to stimulate the growth of CNTs. Actually, using this method it has been demonstrated that local growth occurred only there, where the laser beam was focused and a metal nano-particle was present, with even better confined heat distribution than in other laser-assisted CVD processes. As a result the growth of CNTs on an SU-8 polymer substrate was demonstrated.^[113]

1.2.4 Summary of parameters influencing carbon nanotube growth

Laser-assisted heating significantly influences the process parameters in CNT growth. The rapid heating allows for a fast *in situ* preparation and deposition of the catalyst without the need for a pre-treatment in an inert environment, while the substrate characteristics result in a number of interesting applications such as direct local growth initiated from the bottom. Although focused laser spots tend to induce a widened and non-uniform temperature distribution, a number of solutions were proposed involving different, less thermally conductive, substrates and energy confining layers. However, the resulting CNT growth might still vary over the radius of the heated area, and beam profiling could limit these effects.

The process gases and their partial pressure and flow rates significantly influence the growth, morphology and structural quality of CNTs. Similarly to thermal CVD, this is a result of the binding energies that determine dissociation and absorption rates. For laser-assisted growth however, ethylene and ammonia gas can be influenced by co-heating of the gas phase as a result of the CO₂ wavelength absorbance of these gases, although it seems that the co-heating has no or a negative influence on the growth. The general influence of gas on growth kinetics in combination with laser-assisted growth has not been investigated widely and systematic studies are missing.

Also the type of laser that is used directly affects the resulting growth, as the co-heating of ethylene with a CO₂ laser demonstrates. Numerous different lasers have been used where the power and wavelength generally are most important to the resulting growth. A pulsed-laser source opens up special possibilities including growth kinetics investigations.

1.3 Process control

This section deals with the different control aspects of the LACVD growth. Using a laser as the localized heat source introduces difficulties with respect to process control but at the same time opens up different opportunities with respect to controlling, measuring and monitoring the CNT growth process *in situ*. Because of the small area that is heated, the laser provides an almost instantaneous temperature response, making it much faster and more flexible in controlling the process than a global heating process. The laser source itself can also provide information on the process by for instance monitoring the reflection or a scattered Raman signal. However, the Gaussian distribution of the laser beam results in a non-uniform

temperature distribution over the laser spot and surrounding, and control over the growth temperature is therefore not straightforward.

1.3.1 Temperature control

Temperature control is crucial to the control of the carbon nanotube growth. In conventional CVD systems the temperature control is relatively straightforward. The process consist of either a tube furnace heating both the furnace and substrate, or a resistive or induction heater just below the substrate, heating only the substrate.^[114] With laser-assisted CVD the control of temperature is much less straightforward. Generally, not the complete substrate is heated so using a thermocouple or conducting another physical measurement of temperature within the laser affected zone is not possible. However, if the locally heated area is large and sufficiently uniform^{[83][84][97]} or if the thermocouple is close enough,^[108] a first approximation of the growth temperature can be obtained.

Pyrometer controlled temperature

A better option is to use an optical pyrometer to measure the temperature within the laser spot directly^[84, 90, 92, 97, 99, 107, 109, 115–117] if the laser-affected zone is large and uniform enough. Uniformity is necessary because the relatively small center of the laser spot should not have a temperature much higher than the overall spot temperature, since that would lead to biased temperature estimation. A number of different pyrometers are available, measuring in a range from 0 - 3000 °C and a spot diameter of 2 mm and larger. Liu *et al.* used a pyrometer in combination with a pulsed Nd:YAG laser source to investigate nanotube nucleation and growth.^[109] The 2 ms temporal and 2 mm spatial resolution of the two-color pyrometer enabled them to investigate the effect on sample temperature of a 50 ms pulse. The calculated ramping rate was $\sim 3.3 \times 10^4$ °C/s, as the sample was heated to 900 °C in 25 ms. The pyrometer is generally used to maintain a certain temperature in the laser spot at the surface but can also be used as feedback to dynamically change the temperature in time. This was demonstrated by Mahjouri-Samani *et al.* by showing the ability to control and dynamically change the local temperature during growth.^[117]

In situ Raman spectroscopy for temperature control

For a more precise control of temperature, an *in situ* Raman spectroscopy signal can also be used. This enables the direct measurement of the temperature of the substrate in the laser spot by measuring the Raman shift of the silicon substrate.^[118] The spatial resolution is thus determined by the optics and ability to focus the Raman excitation laser while the temporal resolution is depending on the intensity of the Raman intensity. It has also been reported that Raman shift, peak width, and intensity of the radial breathing mode (RBM) are a function of temperature.^[119] Using these methods Hung *et al.*^[113] and Chiasi *et al.*^[106] were able to determine *in situ* the temperature during CNT growth by laser irradiation. This is graphically shown in Figure 1.12. Bock *et al.* used the *in situ* Raman signal for a first approximation of the temperature.^[88] A downside of this technique is the difficult implementation of the Raman

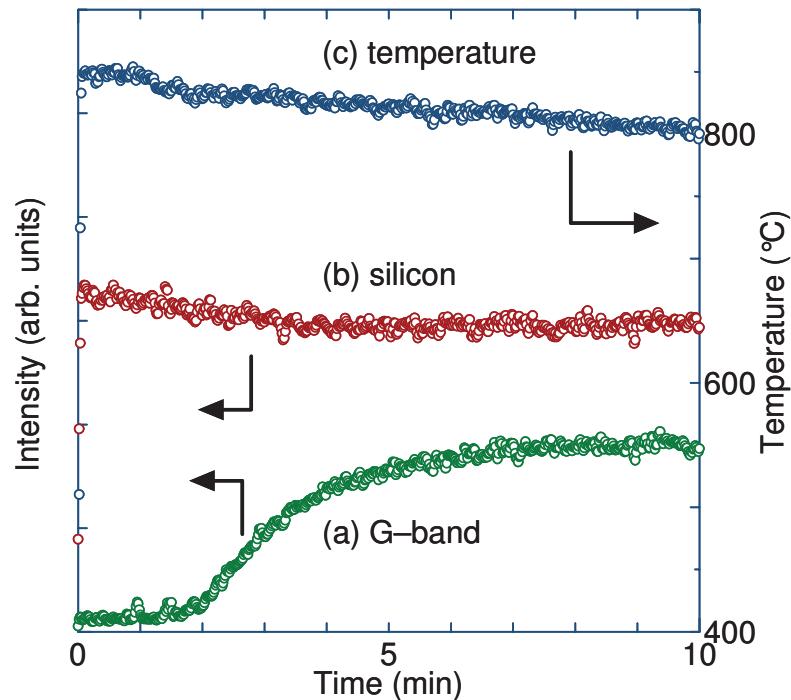


Figure 1.12: Time variation of the silicon and the G-band peak intensities during the entire laser heating CVD process. While the silicon peak intensity (b) was almost constant, the intensity of the G-band (a) appeared after the supply of ethanol gas (at 1 min) and increased with time. Published under a CC BY-NC-SA license by IOP Publishing Ltd.^[106]

laser source in a growth setup. The high costs of the Raman laser source and setup are also contributing to the fact that not much research has been published with this technique yet.

Modeling of temperature

Next to the possibility of a direct measurement of temperature, using *in situ* Raman or applicable pyrometer, another approach to investigate temperatures involved in the process is to use finite element method modeling (FEM) to calculate the corresponding temperatures. This was first demonstrated by Bondi *et al.* who used a combination of computational fluid dynamics and finite difference modeling to implement the different heat transport mechanisms and convective fluid flow around the heated zone.^[89] The model also had the ability to include a scanning laser beam. A thermal camera was used to validate the model by comparing temperatures within the range of that camera. Kasuya *et al.* used a model without temperature dependent properties of the materials to investigate the temperature around the laser spot and as a function of time.^[102] In their case the results should be interpreted qualitatively and mainly provide a first approximation of the rise time for the temperature and the spatial distribution of temperature around the laser heated spot. Neglecting convection and radiation effects, Cao *et al.* used thermal modeling to describe their plasmon resonance process calculating the local temperature around a nano-particle.^[112] The model included a frequency-dependent absorbed fraction of the laser power, which was highest at the surface plasmon resonance.

1.3.2 Carbon nanotube diameter control

Since the beginning of CNT research, controlled synthesis has been widely investigated and many attempts to optimize the growth have been made. Specifically chirality- and diameter-control is of great importance to be able to fully utilize the exceptional properties of CNTs in electronics and related fields.^[120] The CVD process opened up more control of growth direction, alignment, location and properties of the nanotubes, using a controllable metal catalyst as the basis for the growth. Ultimately, the research on CVD for CNT growth led to the well-known relation between catalyst particle size and diameter of the carbon nanotube.^[45–47] Even a direct relation between deposited catalyst precursor metal film thickness and nanotube diameter has been reported.^[48,49] Catalyst and morphology thus are an important control parameter in the controlled growth of nanotubes.

Numerous different catalysts have been studied but nickel, iron, cobalt and their alloys or compounds appear to be at the basis of most CNT growth. Laser-assisted CVD research shows a wide variety of catalysts as well. The early reports used iron-pentacarbonyl gas $\text{Fe}(\text{CO})_5$ as catalyst precursor^[83, 84, 89, 96, 97] but iron has been reported most.^[2, 3, 6, 88, 103, 104, 108, 109, 116] The control of catalyst morphology allows for a better control of the process, although there has not been a significant advantage of laser-assisted CVD over other CVD methods with respect to catalyst morphology control. In fact, the non-uniform temperature distribution most likely results in non-uniform size distribution of the formed nano-particles and consequently a larger variety of CNT diameter and chirality. However, the quick temperature response to variations of the laser intensity allowed Mahjouri-Samani *et al.* to modulate the SWNT diameter during growth.^[117] The resulting SWNT with changing diameter is shown in Figure 1.13. Also, the rapid temperature rise characteristic to laser heating could provide an advantage as research on the formation of nano-particles using laser ablation techniques suggests.^[121] Some groups have exploited laser-assisted growth combined with catalyst size control to better control the nanotube diameter distribution. For instance, Kwok *et al.* used gold-palladium nano-particles that were created in a separate process requiring a preparation step in nitrogen gas.^[99] This enabled them to have greater control over the diameter distribution of the nano-particles. As expected, they were able to show a relation between the size of the nano-particles and the nanotube diameter under constant laser radiation. Also Morjan *et al.* investigated CNT diameter with respect to process parameters. Well-defined iron-carbon composite nanoparticles with a narrow particle distribution were used as catalyst for the laser-assisted growth. The catalysts were produced by a pyrolysis of acetylene, ethylene and iron-pentacarbonyl gas.^[122] Using pre-created catalyst nanoparticles with a narrow diameter distribution allowed for a greater control over the resulting nanotube diameters.^[96, 97] As an explanation for the observed widening of the nanotube diameter distribution, the tendency for the nano-particles to cluster has been proposed. This tendency occurs when the substrate and catalyst have a higher temperature resulting in larger particles.^[97] The temperature rises with higher laser energy but can also be influenced by other process parameters. Bondi *et al.* also found a relation between nanotube diameter and process parameters, although they used a gas phase catalyst, iron-pentacarbonyl.^[89] The authors found that a reduction of catalyst precursor gas pressure resulted in more growth and smaller diameters.

A more effective heating of substrate and catalyst has also been proven to positively affect the control over diameter distribution. Longtin *et al.* succeeded in having a greater control over the diameter distribution by directly heating a laser-annealed nickel catalyst layer, electro-

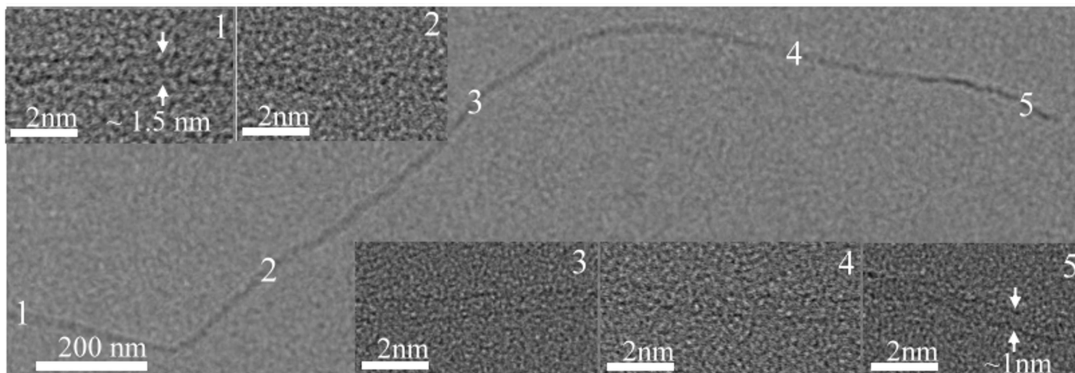


Figure 1.13: TEM image of a 2 μm long SWNT grown with a descending temperature profile. The close up views, (1-5), corresponding to the labeled areas of the tube, show about 0.5 nm variation in the diameter from one end to the other. IOP Publishing. Reproduced by permission of IOP Publishing. All rights reserved.^[117]

chemically deposited within the pores of a porous Al_2O_3 membrane.^[90]

1.3.3 Localization and direction of carbon nanotube growth

One of the major reasons for the popularity of CVD over other CNT growth techniques is the high controllability over properties, alignment and growth direction of the resulting CNTs. Yet, control over specific position and direction sometimes proves to be challenging, especially when integrating the process with other processes and (temperature-) sensitive materials. The unique nature of laser-assisted CVD growth has been found to show some interesting solutions to enhance the controllability of the specific position and direction of the grown CNT structures.

Local aligned growth

Numerous applications require specific alignment of the CNT structures. Particularly vertically aligned CNT structures are preferred. Rohmund *et al.* were the first to demonstrate aligned CNTs using LACVD.^[84] They showed films of vertically aligned multi-walled carbon nanotubes of extremely high packing density. In 2008, Haluska *et al.* grew vertically aligned single-walled and multi-walled carbon nanotube forests^[108] at this university. Bock *et al.* reported on radially aligned multi-walled CNT structures.^[88] Also large mats of aligned carbon nanofibers were reported.^[90, 91]

However, laser-assisted CVD opened up the possibility to grow local aligned CNT structures, with a structural size in the order of the laser spot-size. Chen *et al.* were the first to show local aligned CNT structures.^[86] The authors reported on well-aligned multi-walled carbon nanotube arrays on glass, using a back side laser illumination in combination with a carbon black layer. Park *et al.* also used back side laser illumination to grow vertically aligned pillars of MWNTs.^[103] The pillars were roughly 4 μm in diameter and grew with 1 $\mu\text{m}/\text{s}$ to a height of around 60 μm , see Figure 1.14

Apart from local vertically aligned growth it can also be useful to align the CNTs in any other arbitrary direction. It has been known for some time that an electric field can align the CNT

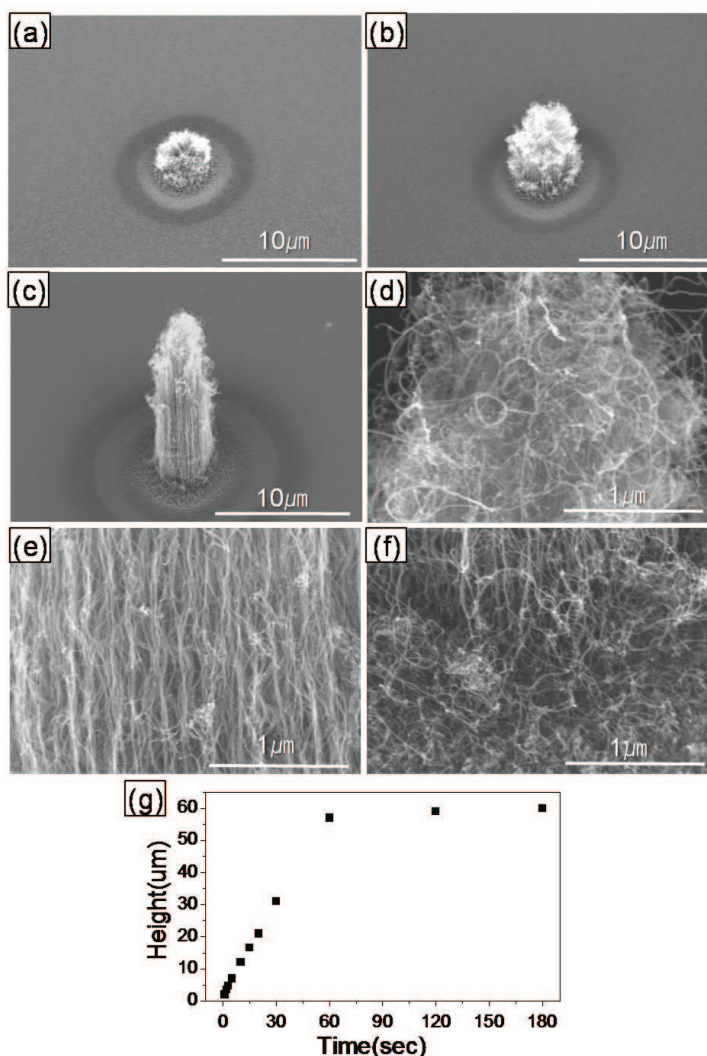


Figure 1.14: SEM images of position-controlled CNTs produced using LACVD with growth times of (a) 1 s, (b) 3 s and (c) 15 s. The magnified images show the (d) top, (e) middle and (f) bottom of the vertically-aligned CNT pillar in (c). (g) Variation of the height of vertically-aligned CNT pillars with respect to irradiation time. Reproduced by permission of IOP Publishing. All rights reserved.^[103]

growth along the field lines.^[123,124] However, applying an electric field over the growth area is not easy. Other groups have shown that also a flow of process gasses could be used to align the nanotube growth in the direction of the flow.^[97,125,126]

To combine the localized laser-assisted growth process with direction control would even further enhance the possibilities for future nanotube-based electronic devices. The control of alignment and direction of CNT growth using LACVD was first demonstrated by Bondi *et al.* They used an electric field in combination with H₂ gas flow to align the tubes in a certain direction.^[89]

The group of Yongfeng Lu investigated the ability to grow suspended aligned CNTs over a variety of structures and geometries. By exploiting the ability of the laser to heat suspended structures, smaller than the laser spot-size, they were able to grow (single) CNTs bridging electrodes or other suspended geometries.^[92,107,116,117] They reported on SWNTs bridging two Mo electrodes using an unfocused as well as a focused CO₂ laser in combination with an

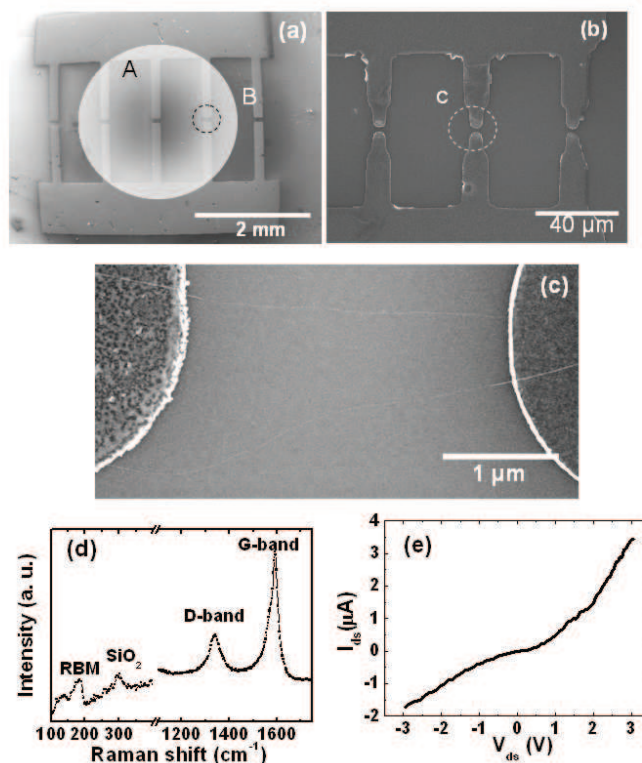


Figure 1.15: SEM micrograph of patterned Mo electrodes. Circle "A" is the typical unfocused 2 mm CO₂ laser beam irradiated on the substrate, while circle "B" is the typical focused laser beam with beam size of 340 μm using a 10 cm ZnSe lens. (b) Magnified electrode pairs inside circle B shown in (a). (c) SEM micrograph of two SWNTs bridging the electrodes inside circle "C" shown in (b). (d) Raman spectroscopy of SWNTs shown in (c). (e) I-V curve of the SWNTs shown in (c). Reprinted with permission from.^[107] Copyright 2006, AIP Publishing LLC

electrical field.^[107] The field applied was varied between 1 - 1.5 Vμm⁻¹. An Ampere meter was used to monitor the completion of the bridging, when a current flow was observed. This typically took around 20 - 30 seconds. The result is shown in Figure 1.15. Following up on this, the group also reported on the local growth of semi-conducting SWNTs bridging two Ruthenium electrodes, using optical near-field effects in the laser-assisted CVD process.^[116] A DC voltage of 1 Vμm⁻¹ assisted the self-aligned growth. The growth took place at 550°C, considerably lower than commonly reported for LACVD. A recent review article provides a comprehensive overview of the techniques developed and used in their lab regarding laser-assisted growth techniques.^[127]

Using a focused CO₂ laser Ruan *et al.* grew forests of CNTs directly on small suspended structures.^[128] They succeeded in growing tens of nanometers thick MWNTs on suspended silicon micro-structures smaller than the laser spot-size using iron as catalyst. Due to the low thermal mass and heat dissipation of these small structures the authors only required a low power CO₂ laser source.

The plasmon resonance process described by Hung *et al.* was used to create a method to control the growth and direction of suspended carbon nanotubes moving the laser in three dimensions.^[113] It is believed that the large temperature gradient generated in the vicinity of the laser spot was responsible for the direction controlled growth.

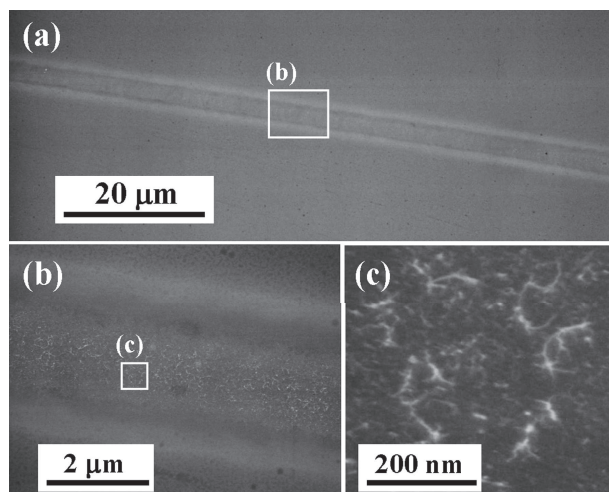


Figure 1.16: SEM images of line-patterned synthesis of SWNTs by scanning of laser-irradiation spot: (a) entire region, (b) enhanced area, and (c) highly magnified image of enhanced area. Reprinted with permission from reference.^[102] Copyright 2007 The Japan Society of Applied Physics.

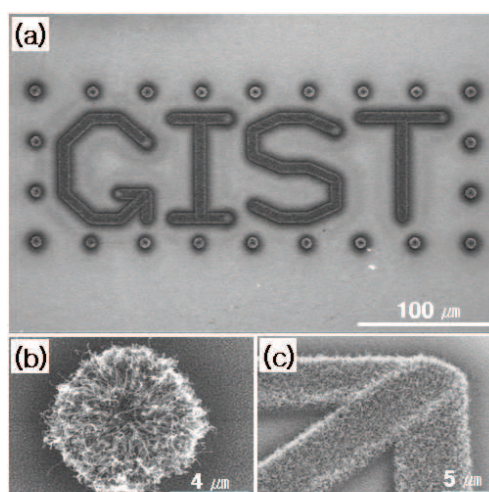


Figure 1.17: Scanning electron microscope images of the CNTs: (a) dot and line patterns, (b) magnified view of a dot pattern, (c) magnified views of cross lines. Reprinted from^[87] with permission from Elsevier.

Writing lines and patterns

Another advantage of using a laser as the localized heat source over other local heat sources such as micro resistive heaters is the flexibility to heat any part of the substrate desired and to move the substrate with respect to the laser spot while growing. Bondi *et al.* were the first to use this advantage and were able to write dot and line patterns of CNTs with a width of 200 μm using a focused CO_2 laser.^[89] Their approach was to scan multiple times with a high speed rather than one scan at low speed. It appeared this method resulted in less unwanted and uncontrolled growth at the laser spot. However, the influence of the laser beam on already grown CNTs was not yet investigated.

Combined with their energy confining layer, Kasuya *et al.* were able to write thin 2 μm wide SWNT lines with a writing speed of 1 $\mu\text{m}/\text{s}$ using their focused Nd:YAG laser.^[102] In Figure 1.16 SEM pictures of the resulting growth are presented. Park *et al.* succeeded in writing dense multi-walled dot and line CNT patterns below 10 μm in size.^[87] Their resulting patterns are depicted in Figure 1.17. The energy absorbing layer that was used proved to be critical in their results as well. It ensured the uniformity of growth, reducing the sensitivity of the catalyst layer to local temperature variations.

1.3.4 *In situ* process monitoring

To study dynamics of nanotube growth, *in situ* and real-time information from the growth process is essential. In thermal CVD nanotube growth several techniques, such as using a displacement sensor,^[129] a shadow technique^[130] or a probe beam reflection technique^[131] have been used for that purpose. The shadow technique links the dynamically changing intensity of a light source on a CCD chip with the length of the vertically aligned nanotube

forest. Dynamic reflection techniques use a laser beam which is focused on the growth side and reflection is measured to study the growth rate, size and other dynamic properties.^[131, 132] To obtain similar *in situ* information about the CNT growth process using LACVD, the same laser beam used for the local heating can be used, although to date *no research* has been published regarding *in situ* measurement of growth kinetics of a laser-assisted CVD process.

Nonetheless, the laser beam used for heating the substrate can be used for a number of other measurement techniques. Using *in situ* Raman for instance, Chiashi *et al.* were able to characterize SWNT growth as a function of time as shown in Figure 1.12.^[106] The authors were successful in growing SWNTs using a HeNe laser but for the *in situ* Raman experiments, the Raman-excitation Ar-ion laser was also used as the heating source. Hung *et al.* used a similar *in situ* Raman process to investigate and monitor the growth of the SWNT and co-induced metal oxide process as well as the temperatures involved during growth.^[113] Bock *et al.* reported on optical feedback mechanisms during growth of MWNTs.^[88] *In situ* Raman and reflection spectroscopy are related to the growth products. A strong positive feedback was observed during different stages of the growth. More laser energy is absorbed as a result of the enhanced substrate absorbance during CNT growth so the temperature increased and this eventually resulted in amorphous carbon deposition above 900°C.

1.3.5 Summary of process control

Process control in laser-assisted CVD growth of CNTs is essential. As CNT synthesis depends largely on process conditions and particularly on temperature, a well-controlled temperature is crucial. A thermocouple, optical pyrometer or Raman signal can be used to measure temperature directly where the Raman is most precise but also most difficult to implement and most expensive. With no direct temperature measurement, thermal modeling can be used to calculate temperatures involved in the process afterwards or to predict the temperature upfront. Using the fast temperature response in combination with direct temperature measurement, the growth temperature can be instantly varied. This enables direct control over the diameter of the CNT. Other attempts to increase control over the diameter of the CNTs generally consisted of more control over the catalyst size and morphology.

The localized nature of the laser-assisted growth enables fast local aligned growth as well as writing lines and patterns on substrates with temperature sensitive components making it a highly versatile process.

Finally, a direct result of the laser-assisted CVD process is the ability to *in situ* monitor the process. The dynamically changing reflected laser signal can be used to investigate growth kinetics or even be used as a Raman signal, characterizing CNT quality growth as a function of time.

In Table 1.4 a chronological overview of this literature review is presented including several process parameters such as laser type and power, substrate and catalyst that were used, time and temperature range and the most important results. Not all publications mention and discuss every parameter so a few gaps can be noticed.

Table 1.4: Chronological overview of research published on laser-assisted CVD for carbon nanotubes.

Laser (focus)	Power	Substrate	Catalyst	Feedstock gas (process gas)	Temperature range	Time range	Results	Ref.
CO ₂ unfocused	100 W	Silicon	Fe(CO) ₅	C ₂ H ₂ , C ₂ H ₄	770 - 860 °C	3 min (15-20 min)	MWNT / (aligned) SWNT	[83,84]
Ar-ion focused	180 mW	Silicon	Fe(NO ₃) ₃ ·9H ₂ O + MoO ₃ + Al ₂ O ₃	C ₂ H ₅ OH		1 min	SWNT	[101]
CO ₂ unfocused	30 W	Quartz	Au-Pd	C ₃ H ₈	1000 - 1400 °C	10 min	MWNT	[99]
CO ₂ focused	100 W	Silicon, graphite/ grafoil	Fe(CO) ₅	C ₂ H ₂ (Ar)	1130 °C	200 sec	MWNT	[89]
CO ₂ / Nd:YAG (un)focusec	20-25 W / 60 W	Silicon	Fe-Mo- Al ₂ O ₃	C ₂ H ₂ (NH ₃)	690 - 720 °C	3 - 6 min	SWNT	[107]
CO ₂ unfocused	20-45 W	Silicon	Ni-Fe	C ₂ H ₂ (NH ₃)	650 - 770 °C	5 min	SWNT MWNT	[92]
Nd:Yag focused	50 mW	Silicon	Co	C ₂ H ₅ OH	~800 °C	1 sec - 10 min	SWNT	[102]
CO ₂ unfocused	80 W	Silicon	Fe(CO) ₅ , FeC	C ₂ H ₂ , C ₂ H ₄ (NH ₃)	800 - 900 °C	5 min	MWNT	[96,97]
Diode focused	2 W	Glass, ITO	Fe-Mg	C ₂ H ₂ (Ar)	< 600 °C	5 - 30 sec	MWNT	[86]
Ar-ion unfocused	~1.5 W	Al ₂ O ₃	Ni	C ₂ H ₄	790 - 1848 °C	750 ms - 5 sec (360 sec)	Nanofibers aligned	[90,91]
Solid state focused	20 mW	Fused silica	Ni	CH ₄ , C ₂ H ₄		45 sec	MWNT	[112]
HeNe/ Ar-ion focused	30 mW / 40 mW	Silicon	Fe-Co, Mo-Co	C ₂ H ₅ OH	800 - 830 °C	15 min	SWNT	[106]
Nd:Yag (pulsed) unfocused	600 W	Silicon, SiO ₂	Fe, ferritin	CH ₄ , C ₂ H ₄	650 - 770 °C	50 ms - 30 sec	SWNT bridge/	[109]
Nd:YVO ₄ focused	57 - 125 mW	Quartz Al-Cr	Ni	C ₂ H ₂ (H ₂) / C ₂ H ₄ (H ₂)		60 sec (1 - 180 sec)	MWNT aligned / SWNT	[87] [103,104]
Diode focused	5 - 30 W	Silicon, Al ₂ O ₃	Fe	C ₂ H ₄ (Ar, H ₂)		9 - 180 sec	MWNT aligned / SWNT	[2,3,108]
Solid state focused	5 W	Si/glass	Au	CO (Ar, H ₂)	1180 °C	10 min	SWNT	[113]
CO ₂ unfocused		Silicon, SiO ₂ / Ru	Fe	C ₂ H ₂ (NH ₃)	550 °C		SWNT bridge	[116]
CO ₂ unfocused		Silicon, SiO ₂	Al-Fe-Al	C ₂ H ₂ (NH ₃)	450 - 650 °C	1 - 4 min	SWNT (aligned)	[117]
CO ₂ focused	5 W	Silicon	Fe	C ₂ H ₄ (Ar, H ₂)	~660 °C		MWNT	[128]
Nd:Yag (pulsed)		Silicon	Co-Fe	C ₂ H ₅ OH			SWNT	[110]
Solid state focused	10 - 180 mW	Fused silica, Al ₂ O ₃	Fe	C ₂ H ₂	~700 - 900 °C	2 min	MWNT	[88]

1.4 Outline and objectives

From the literature review followed that a number of opportunities, but also problems specific to the growth of CNTs with laser-assisted CVD, remained largely unexplored. The influence of the laser on the growth characteristics was found to be significant. Catalyst preparation and substrate selection introduced unique opportunities specific for laser-assisted growth. Process control however, was proven to be challenging, although essential for control over the growth product and properties, and as such ultimately over the properties of possible applications. In the literature several solutions were proposed regarding temperature-, alignment- and position control. Past and ongoing attempts enhanced the ability to tune the properties of the CNTs, as the demonstration of diameter control by fast temperature control has shown. However, an *integrated*, systematic investigation of well-controlled laser-assisted CNT growth as a function of the experimental parameters - temperature, gas and catalyst - is not yet available.

Together with temperature, the process gases influence the growth morphology and structural quality of CNTs as the bonding energy of the carbonaceous gas co-determines the decomposition rate onto the catalyst. However, the general influence of the process gases on *growth kinetics* in combination with the fast heating inherent to laser-assisted growth has not been investigated widely and systematic studies are missing.

The objective of this thesis is to investigate and optimize laser-assisted carbon nanotube growth.

On the one hand, the *technological* objectives include the feedback control of the process, the ability to control the flow and the composition of the process gases to the growth site and improving the experimental throughput and reproducibility. On the other hand, the thesis adds new *material* insights such as structural quality assessment of CNTs as a function of temperature and gas composition as well as detailed investigation of CNT growth kinetics.

This thesis follows a semi-chronological approach which helps to fully appreciate the development of the technological aspects of the project towards an understanding of the physics and chemistry behind the process. At the start of the project in 2010, open-loop growth of carbon nanotubes was successful and a paper had been published^[108] showing the time dependency of the laser-assisted CVD process on the resulting CNT growth. At the same time, other research groups were also competitively looking into the same issues.

In order to investigate and optimize the process several methods for identifying the resulting CNT growth are essential. Scanning Electron Microscopy (SEM) and Raman spectroscopy are used to *ex situ* determine geometry and structural properties of the CNTs. Two sensors are used to *in situ* monitor the growth. One sensor measures the reflected laser intensity which provides a first approximation of the growth dynamics at the laser heated zone. The other sensor monitors the emitted thermal radiation.

For a systematic investigation and identification of the key process parameters - temperature, gas and catalyst - process control in laser-assisted CVD growth of CNTs is essential. As CNT synthesis depends largely on temperature, a *well-controlled temperature* is crucial. In

chapter 2, a *closed-loop control* method based on the emitted thermal radiation is presented and discussed, to enhance the controllability and reproducibility of the CNT growth process. Together with a finite element method model it is possible to quantitatively relate growth *temperature* with structural quality of the CNTs. The influence of the temperature on the catalyst activation and formation is discussed as well.

In chapter 3, the development of a miniaturized reaction chamber is demonstrated. The necessity for this chamber followed from the fact that a large statically filled CVD reaction chamber suffers from a number of disadvantages. Firstly, the actual gas composition around the heated surface is unknown as the thermal gradients could induce local turbulence and the consumption of carbonaceous gas could result in a local minimum of that gas, resulting in an unpredictable concentration of process gases at the growth site. Furthermore, as a result of the size of the reaction chamber, experimental time is long and throughput is low. It is shown that the development of the miniaturized reaction chamber overcomes these problems by the ability to apply a *forced laminar flow* over the substrate. The precisely known gas concentration and composition enables the study of growth kinetics. At the same time the size of the chamber ensures a short experimental time and high throughput.

The dynamically changing reflected laser signal is used to investigate growth kinetics in chapter 4. Combined with the known composition of the process gases as a result of the forced laminar flow, the kinetics of the CNT growth is investigated in detail for a broad range of experimental conditions. To further optimize the growth process, the rate-limiting mechanisms are explored by determining growth regimes, correlated to the chemical rate equations governing the process.

To highlight the versatility of the process, in chapter 5, a perspective on a number of applied techniques with LACVD is demonstrated, such as writing CNT lines and transferring CNTs to a polymeric layer, as well as various potential applications. Finally, in chapter 6 the main conclusions of this thesis are listed and a perspective on future work is given.

In summary, this thesis contributes to a better understanding of the catalytic CVD growth of carbon nanotubes. It offers an integrated approach on investigating CNT growth kinetics, using a dedicated miniaturized reaction chamber in combination with both closed-loop control as well as multi-parametric thermal modeling.

Closed-loop controlled laser-assisted carbon nanotube growth

In this chapter, CNT growth results from *open-loop* experiments demonstrate the presence of different growth regimes during laser-assisted CVD growth. On basis of these observations, a closed-loop control system is designed to precisely monitor and control the process. Several sensors are used to monitor and collect *in situ* information about the growth. Emitted thermal radiation in the mid-IR range is measured from below the substrate and is used to obtain a first approximation of temperature. The variation of the reflected laser irradiance is collected and is used to investigate first order growth kinetics; also, this parameter is used for detecting the onset of catalyst formation and activation. A PID-controller is developed to accurately control on emitted thermal radiation while the reflected laser irradiance can act as a trigger or stop.

Part of this chapter has been published in

M. Haluška, Y. Bellouard, Y. van de Burgt, A. Dietzel, *In situ monitoring of single-wall carbon nanotube laser assisted growth*, Nanotechnology 21, 075602 (2010).^[2]

Y. van de Burgt, Y. Bellouard, R. Mandampambil, M. Haluška, A. Dietzel, *Closed-loop control of laser assisted chemical vapor deposition growth of carbon nanotubes*, Journal of Applied Physics 112, 034904-034904-8 (2012).^[3]

2.1 Introduction

In the previous chapter it was demonstrated that laser-assisted chemical vapor deposition (LACVD) offers an attractive method for the local growth of CNTs. Previous studies have demonstrated the possibility of growing different types of carbon nanotubes such as, single-walled^[117] or multi-walled,^[84] with different laser types^[89] and catalysts.^[103]

Apart from the temperature, an important parameter for CVD processes that co-determines the CNT properties and diameter, are the catalyst nano-particles and their preparation process.^[41,94] It is generally assumed that the catalyst layer is first oxidized^[133] in air and then has to be reduced by a heat treatment in the presence of hydrogen^[94] to finally form nanoparticles.^[41,133] In the case of a laser CVD process, the sequence of events and their dynamics leading to the formation of nanoparticles is unknown. However, the behavior is suspected to be quite different from conventional CVD as a result of the high heating rate characteristic to laser heating. This step is nevertheless crucial for controlling the growth product and its characteristics.

In this chapter, a feedback control mechanism for a laser-assisted CVD process is demonstrated, based on monitoring the mid-infrared radiation from the laser affected zone. This radiation is essentially of thermal origin and provides indirect information about the average temperature at the irradiated spot. To monitor morphological surface changes during laser exposure as well as to detect the onset for CNT growth, the reflected laser intensity is measured. In the first part of this chapter, results with the LACVD setup without feedback control are presented. In this case the process is partly controlled by modifying the laser irradiance and experimental time. By measuring the reflected laser intensity, several stages of CNTs growth are identified.

By applying feedback control to the process, an enhanced reproducibility is then demonstrated. In addition, it is shown that the reflected laser light signal can be further used for identifying the catalyst formation and their activation to catalyze the carbonaceous gas dissociation and CNT nucleation. To quantitatively relate the temperature to its influence on the quality of the CNTs, a finite element model is developed that takes into account time-dependent laser absorbed intensity.

2.2 Experimental setup

The setup is schematically shown in Figure 2.1. The substrates are 4x4 mm silicon substrates with a 20 nm aluminum-oxide (Al_2O_3) layer and a 1.5-1.8 nm iron (Fe) catalyst layer both deposited by e-beam evaporation. The stainless steel cylindrical chamber has a volume of 3.4 L with a gas inlet and outlet. A K-type thermocouple is placed at the substrate holder, a pressure sensor is placed in the gas inlet and an optical window provides visual access. A fiber-pigtailed laser diode (Unique Mode) emitting up to 30 W at $\lambda = 808 \text{ nm}$ is incident at an angle of 35° . An InGaAs photodiode is placed beneath the substrate to measure the emitted IR radiation. In this configuration, the Si substrate acts as a high-pass optical filter with a cutoff wavelength of $1 \mu\text{m}$. The reflected laser light is measured with a Si photodiode in combination with a laser line band-pass optical filter. Another Si photodetector is placed above the substrate, to monitor emitted visible light. The chamber is filled with a mixture

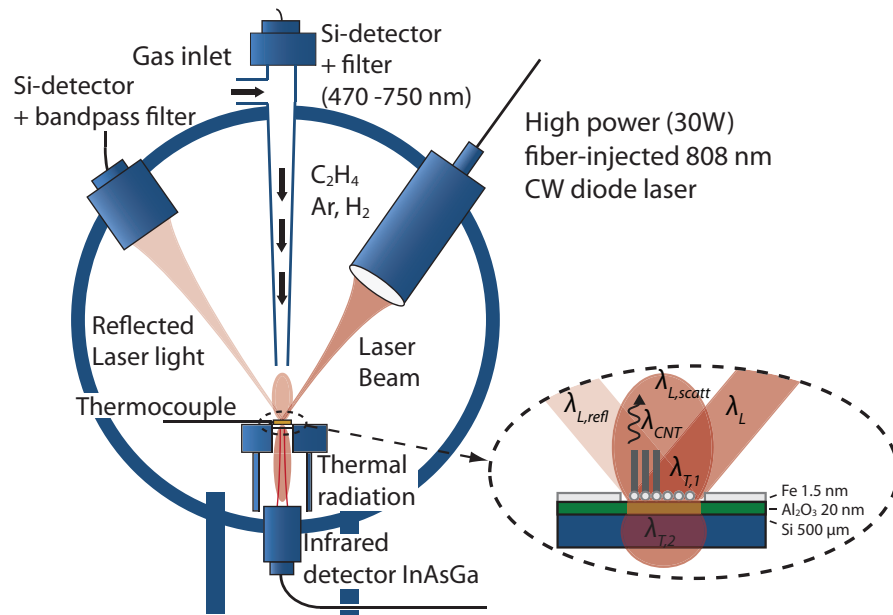


Figure 2.1: Overview of the laser-assisted chemical vapor deposition setup equipped with detectors for *in situ* measurements of the substrate temperatures as well as the intensities of reflected and emitted light. The inset illustrates the formation of the nanoparticles (right) on the catalyst followed by the CNT growth (left) on the substrate during laser irradiation. The different wavelengths of radiation present in the system are shown. The incoming laser light is λ_L (808 nm), $\lambda_{L,refl}$ is the reflected laser light, $\lambda_{L,scatt}$ is the scattered laser light, λ_{CNT} is the fluorescence of the CNTs during growth, and $\lambda_{T,1}$ and $\lambda_{T,2}$ are the emitted thermal radiation from the spot.

of argon, hydrogen and ethylene to 950 mbar in the ratio 8/2/5, respectively. The results are analyzed using a scanning electron microscope (FEI Quanta 600F ESEM) and a Raman spectrometer (632 nm, Horiba LabRAM HR).

2.3 Open-loop growth to identify characteristic regimes

To interpret the photodetector signals in the feedback control scheme and identify characteristic regimes, *in situ* and *ex situ* obtained data for each specimen was compared. For a given set of the specimens, a series of repetitive experiments were carried out with the same process parameters but with different laser exposure times.

2.3.1 Optimal irradiance level

Si/Al₂O₃/Fe substrates reflect more than 20% of incoming light as concluded from the measurement of the optical power. A vertically aligned forest of CNTs has very low reflectance as shown by Yang *et al.*^[134] The decrease of the reflected light intensity caused by the growth of vertically aligned CNTs was also shown by Puretzy *et al.*^[132] An increase of absorbed laser radiation in the CNTs raises the sample temperature and simultaneously increases the non-catalytically activated rate of thermal decomposition of ethylene. Consequently, amorphous carbon is deposited on the CNTs and catalyst particles preventing the growth of CNTs.

The LACVD process is characterized by a very fast temperature elevation at the laser spot, which helps to transform the metal film into small catalyst particles required for the SWNT nucleation and growth. These densely packed clusters form the seed structure for vertically oriented SWNTs.

Using a steeply increased laser irradiance of the substrate in a single step, the conditions for 'flash' heating were created, necessary for the formation of small clusters on which SWNTs can grow. To find the optimal irradiance level for SWNT growth, several experiments were performed at different irradiance levels. Figure 2.2(a) shows the Raman spectra of CNTs grown on Si/Al₂O₃/1.8 nm Fe substrates for different laser irradiances. The exposure time was 10 s for all the experiments except for the one performed at the lowest irradiance, where the exposure time was 15 s. In Figure 2.2(a), Si labels indicate silicon substrate Raman modes, G and D* are modes corresponding to sp² hybridized carbon and D is the mode allowed in sp² hybridized carbon only if defects are present.^[81,135] It is well known that the level of graphitization is proportional to the growth temperature.^[136] Further, the radial breathing mode (RBM) together with the position and shape of the G-mode indicate the presence of SWNTs.

Figure 2.2(b) shows the ratio of the D-mode and the G-mode intensities of the Raman spectra. The ratio is - in a first approximation - a measure of the graphitization level of nanotubes or, in other words, a sign of the CNT wall quality (i.e. the lower the ratio the higher the quality of the CNT walls). Both Figure 2.2(a) and Figure 2.2(b) indicate that for low laser irradiance more defects in the CNT wall are formed. Above $\sim 1.2 \times 10^5 \text{ W cm}^{-2}$, SWNTs are found. The dominant RBM mode at $\sim 198 \text{ cm}^{-1}$ represents SWNTs with diameter $\sim 1.2 \text{ nm}$. Above $1.33 \times 10^5 \text{ W cm}^{-2}$, the ratio I(D)/I(G) increases, indicating that this irradiance level induces the formation of defects in the nanotubes. Another possible explanation for the increase of the I(D)/I(G) ratio is that at the high irradiance level the temperature at the center of the laser spot increases above the threshold limit for thermal non-catalytic dissociation of ethylene and amorphous carbon formation.

2.3.2 Growth regimes

Figure 2.3(a)-(c) show SEM images of three samples irradiated with the power density of $1.07 \times 10^5 \text{ W cm}^{-2}$ for three different exposure times of 8, 10.5 and 16 s, respectively. From these observations, various growth regimes could be identified. Figure 2.3(a) and Figure 2.3(b) display the clusters formed from a Fe film after 8 s and CNTs obtained after 10.5 s of laser exposure, respectively. For the latter, the nanotubes probably grew partly in a short time period after the laser was turned off while the substrate was cooling down. Lower temperature may have caused the growth of lower quality nanotubes. This is clearly visible in the Raman spectrum with a high I(D)/I(G) intensity ratio shown with the black line (lower curve) in Figure 2.3(f). Figure 2.3(c) shows an aligned forest of SWNTs found after 16 s laser irradiation time. Here, the presence of SWNTs is confirmed with a red line (upper curve) Raman spectrum in Figure 2.3(f). Figure 2.3(d) and Figure 2.3(e) show the temperature and its time derivative for the three samples, respectively. Temperature starts to decrease after switching off the laser. The evolutions of the temperature are very similar and reproducible for the experiments.

Next, to further improve the LACVD process and to better interpret the *in situ* data collected with various optical sensors, a set of experiments were performed to correlate *in situ* measure-

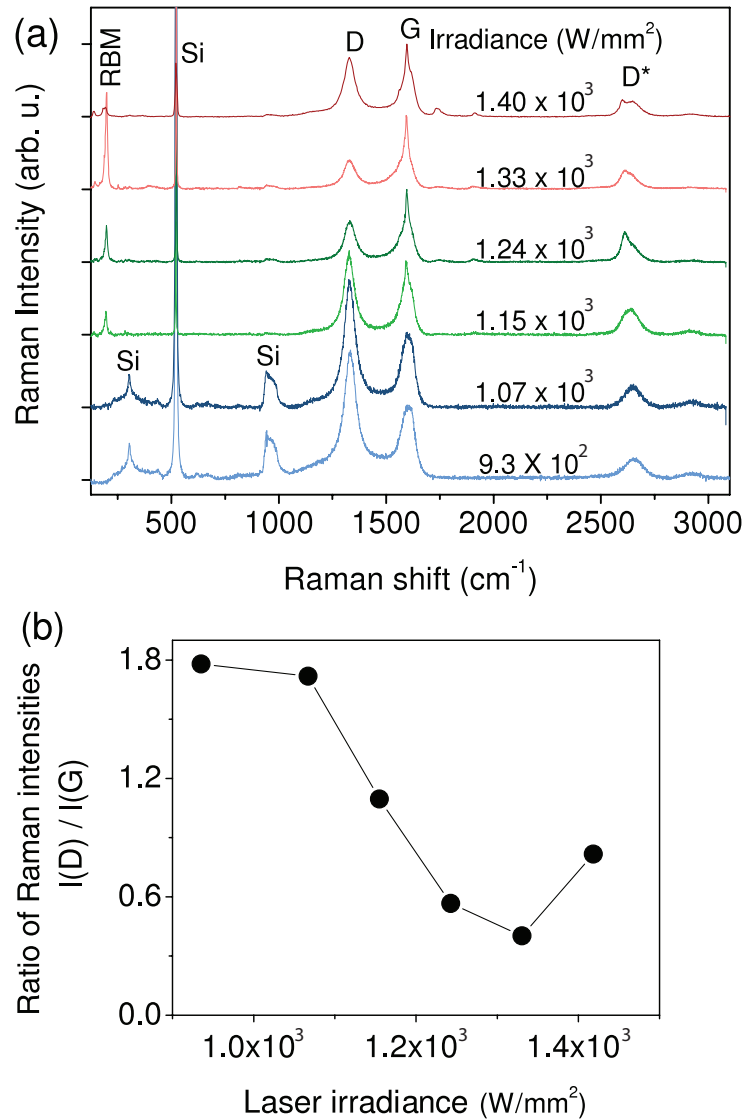


Figure 2.2: (a) Raman spectra of CNTs prepared at different laser irradiances on substrates with a 1.8 nm Fe film. The curves are shifted in the vertical direction for clarity. The level of irradiance is indicated next to each spectrum. (b) Ratio of Raman intensities of the D and the G modes from (a).

ments with *ex situ* observations. Figure 2.4 shows normalized signals of the reflected light intensity, the substrate temperature, the time derivative of the temperature as well as the IR and visible emitted light signals, obtained during a constant laser irradiance of the substrate. Three different regimes are identified.

Regime I: Fe restructuring

During this time period, the Fe film melts locally and forms clusters of catalyst nanoparticles (an example is shown in Figure 2.3(a)). Fluctuations in the photodetector signals are observed but remain difficult to interpret. This stage is attributed to the catalyst activation and may have variable duration depending on the laser irradiation power density (that controls the

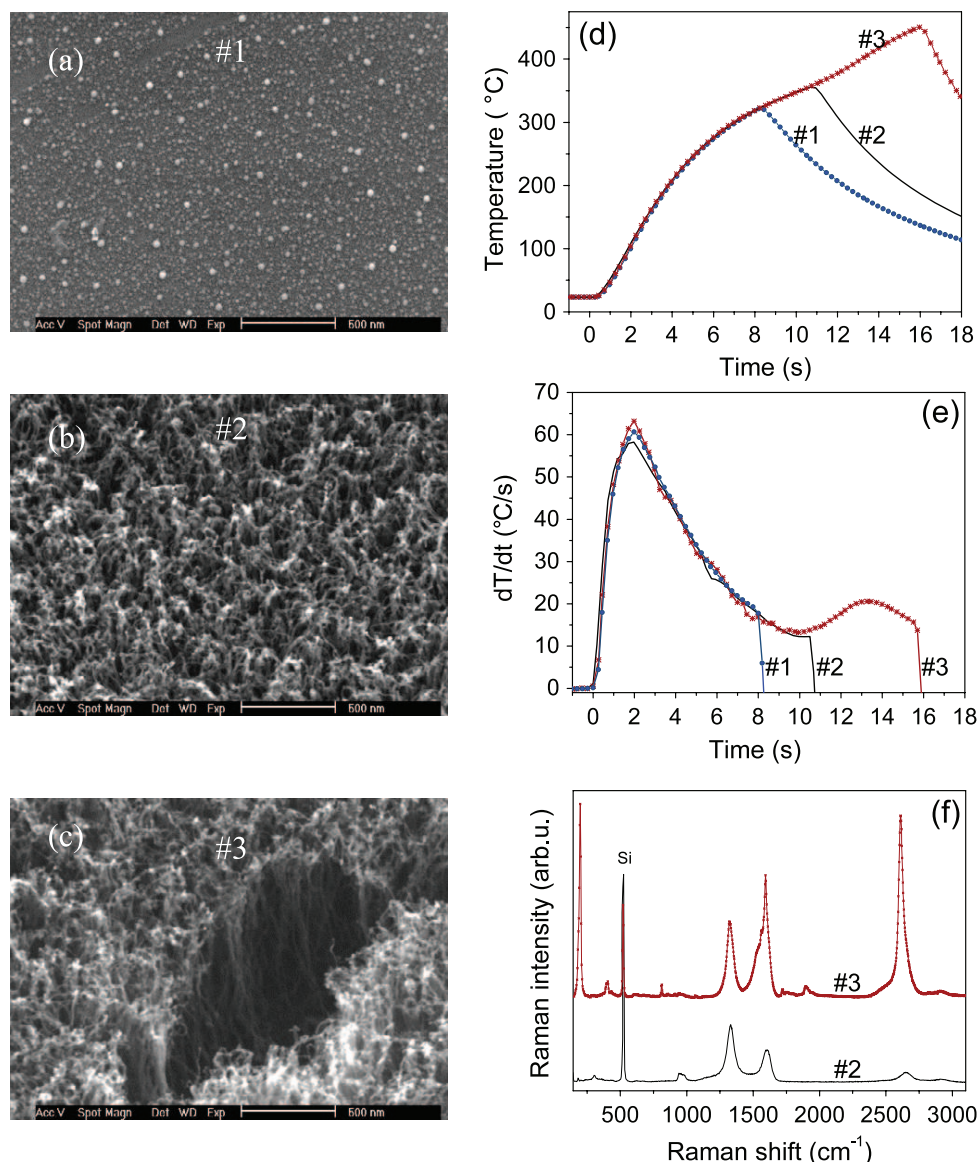


Figure 2.3: Effect of irradiation time on CNT growth. Three irradiation times are considered: 8, 10.5 and 16 s, labeled (#1), (#2) and (#3), respectively. ((a)-(c)) SEM images, (d) temperature, (e) time derivative of the temperature, and (f) Raman spectra (shifted in the vertical direction for clarity). Note that the Raman spectrum for sample #1 is not plotted because it does not show presence of carbon mods.

temperature of the laser-affected area) as well as on the metal film thickness. Rather than measuring the temperature of the irradiated area which is technically challenging, the local minimum of the time derivative of the temperature measured using the thermocouple is used to identify the onset time for the CNT growth.

Figure 2.5 shows various Raman spectra for specimens prepared at high (upper curve), intermediate (middle curve) and slow (lower curve) heating rates. Fast heating rates cause the formation and growth of SWNTs while slow heating rates yield low quality MWCNTs. The Raman spectra for specimens prepared at the intermediate heating rate indicates the presence of both SWNTs and MWCNTs since the ratio of $I(D)/I(G)$ is relatively high but an RBM-peak is present as well.

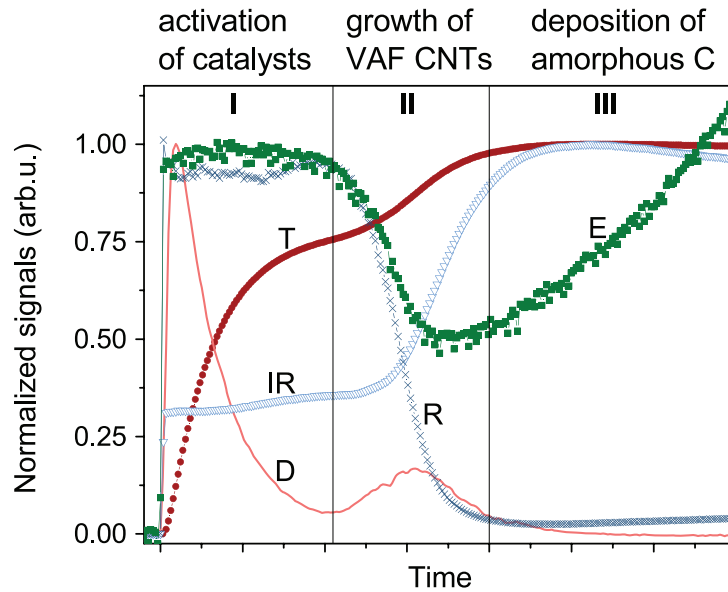


Figure 2.4: Normalized *in situ* signals that characterize the growth process. The red bullets, the blue crosses, the blue triangles and the green squares represent the temperature (T), the intensity of reflected light (R), the IR detector signal (IR), and the visible light detector signal (E), respectively. The red curve displays the time derivative of the temperature signal (D). The Roman numbers represent the process regimes.

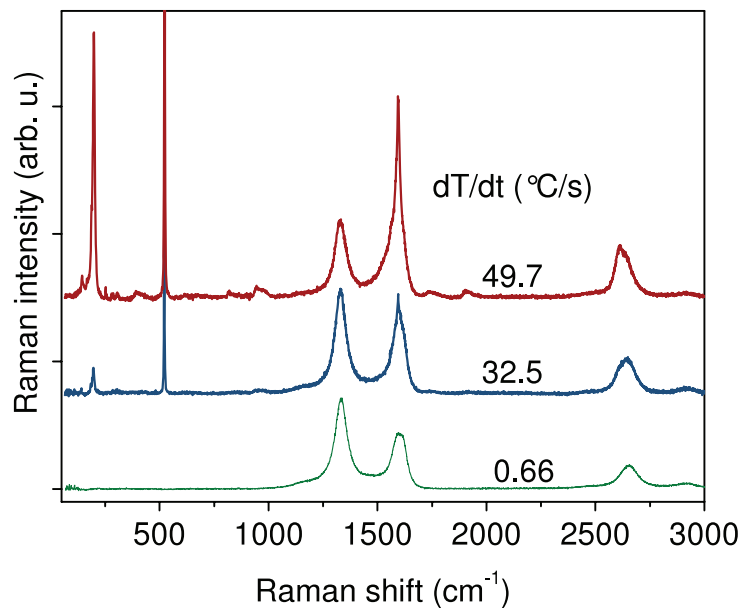


Figure 2.5: Raman spectra obtained for the samples produced at different heating rates. The heating rates are indicated.

Regime II: CNT growth

A second regime is identified triggered by a steep drop in reflected light intensity (blue crosses in Figure 2.4). The temperature measured using the thermocouple (red bullets) goes through an inflexion point after which the heating rate increases again. This temperature change is also observed with the IR photodetector (blue triangles). This second regime is attributed to

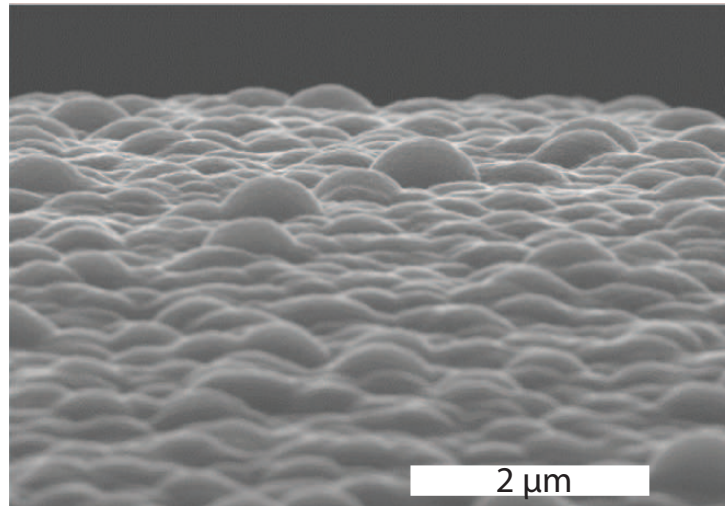


Figure 2.6: SEM image of a top layer covering the center of a vertically aligned forest of CNTs.

the growth of a CNT forest (Figure 2.3(c)).

Regime III: amorphous carbon deposition

The onset of the final regime is defined by an increase of emitted light (green squares in Figure 2.4) followed by a slight increase of the reflected light intensity. This regime seems to be directly correlated with the formation of an amorphous layer that covers the CNT forest. This amorphous deposit is shown in Figure 2.6. It terminates the growth of nanotubes and has a very interesting morphology that resembles frozen liquid droplets. Note that similar carbon spherical objects were reported for thermal non-catalyst activated dissociation of acetylene during chemical vapor deposition.^[137]

2.4 Closed-loop control

Open-loop laser-assisted CVD is intrinsically sensitive to perturbations due to the small size of the heated zone but also to rapid changes of surface properties that modify the laser absorption and in turn the temperature. A feedback control mechanism is added to the setup to overcome these problems. A schematic of the setup with feedback control is presented in Figure 2.7.

In Figure 2.8, a schematic of the open-loop system is presented in the top right blue area. In open-loop, the laser intensity determines solely the process temperature and the rate at which the temperature increases (dT/dt). During growth of CNTs the absorbance of the substrate changes, resulting in a different thermal behavior and ultimately a different temperature. Extreme situations such as overheating can occur, preventing the CNTs from growing further.

To counteract perturbations and to better control the growth process, a closed-loop model is developed as depicted in the bottom section of Figure 2.8. The reflected laser beam and the emitted thermal radiation from the irradiated spot on the substrate are given as inputs for the closed loop control. The strategy is to monitor and control the emitted radiation $E(T)$ from the laser spot which is directly related to the temperature. The reflectance of the laser

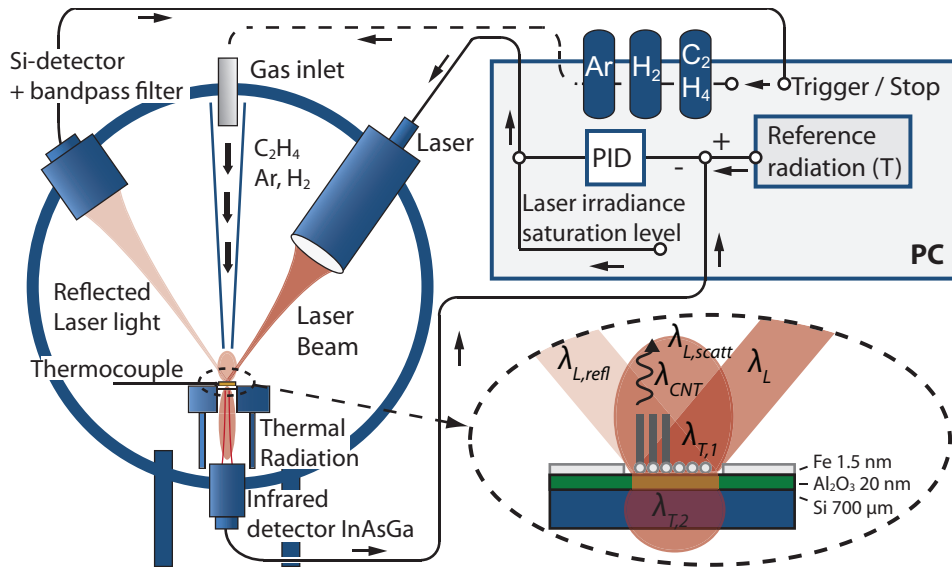


Figure 2.7: Overview of the laser-assisted chemical vapor deposition setup with feedback control. The flow of operation is depicted by arrows. The set process parameters are laser irradiance saturation level and the reference radiation. The thermal radiation from the substrate is controlled by means of a feedback signal from the infrared detector. The reflected laser light is collected by a Si-detector with a bandpass-filter to isolate the laser wavelength. The inset illustrates the formation of the nanoparticles (right) on the catalyst followed by the CNT growth (left) on the substrate during laser irradiation. The different wavelengths of radiation present in the system are shown. The incoming laser light is λ_L (808 nm), $\lambda_{L,refl}$ is the reflected laser light, $\lambda_{L,scatt}$ is the scattered laser light, λ_{CNT} is the fluorescence of the CNTs during growth, and $\lambda_{T,1}$ and $\lambda_{T,2}$ are the emitted thermal radiation from the spot.

heated surface $\rho(\lambda, T)$ is assumed to be the direct complement of the absorbance $\alpha(\lambda, T)$ of the substrate (in other words, the transmitted laser energy through the substrate can be neglected). As a consequence, a decrease in reflectance results in more absorbance of the laser irradiation and therefore an increased heating.

As shown in Figure 2.8, a PID controller is used for the feedback process. For a step response to a given reference radiation, the initial laser irradiance will be equal to the selected laser irradiance saturation level. This level determines the maximum value the controller will achieve and ensures that no integrator wind-up can occur. This phenomenon could otherwise occur when the output is limited (i.e. a maximum laser diode output) but the reference set-point is not yet reached. In this configuration it therefore also limits the maximum irradiance output for the laser diode. In contrast to the open-loop situation, at the onset of the closed-loop process, the laser saturation irradiance determines the heating rate during the start of the process. However, it does not determine the temperature at the laser spot, since the irradiance is controlled to keep the radiation constant during the continuation of the process.

In Figure 2.7, the sensors are shown in their actual configuration in the setup. The flow of operation is depicted by arrows. The inset of the figure shows a detailed schematic of the different radiated, reflected, scattered and emitted wavelengths involved in the process. The incoming laser light is λ_L (808 nm), $\lambda_{L,refl}$ is the reflected laser light after hitting the surface of the substrate, $\lambda_{L,scatt}$ is the scattered laser light, λ_{CNT} is the fluorescence emitted by the CNTs during growth and $\lambda_{T,1}$ and $\lambda_{T,2}$ are a spectrum of emitted thermal radiation from the

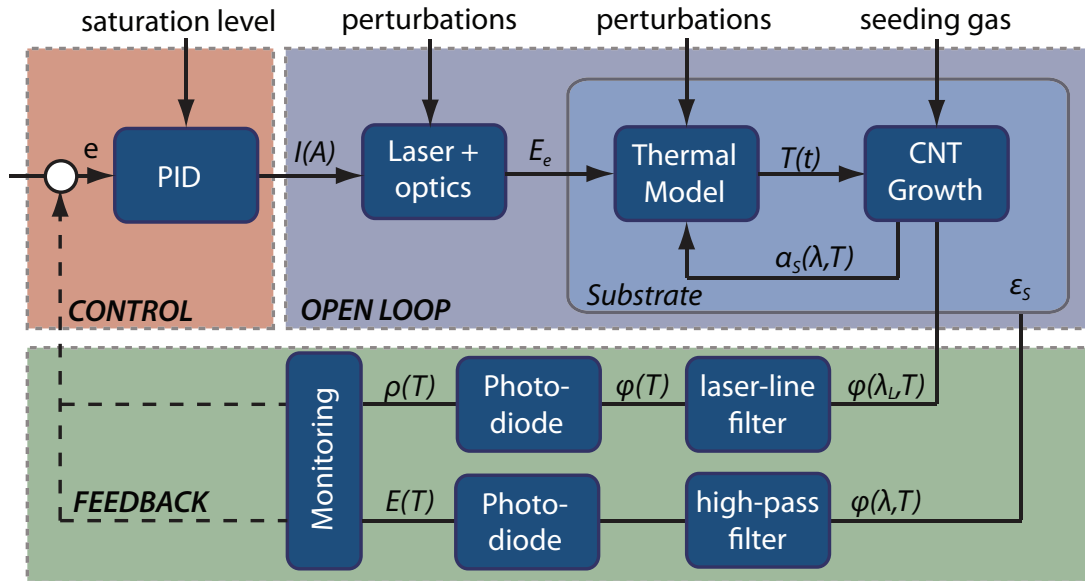


Figure 2.8: Block diagram of the laser-assisted carbon nanotube growth process and all the relevant components. In open-loop, a set current is converted into certain laser energy E_e which is irradiated on the substrate. The substrate transforms this energy into a temperature $T(t)$ at which the CNT growth starts. This growth and the temperature increase change the absorbance α_s of the substrate which in turn re-affects the thermal model. Along the open-loop process line perturbations are present. The reflected laser flux $\varphi(\lambda_L, T)$ is depending on the absorbance $\alpha(\lambda, T)$ of the substrate and is measured by a Si-photodiode. The emissivity ε_s of the system transforms the temperature of the laser spot and surroundings into a flux $\varphi(\lambda, T)$. This flux is measured by an InGaAs photodiode after passing through the silicon substrate which acts as a high-pass filter. A PID controller with a set saturation level is used to close the loop.

spot. The light emitted by the CNTs is currently not measured dynamically and therefore not taken into account in the close-loop control process.

2.5 Thermal modeling

One of the difficulties of laser-assisted growth of CNTs is to accurately predict the temperature at the laser spot. As shown in Figure 2.8, the thermal model is an essential parameter of the control process. Since the growth process is mainly dependent on temperature evolution in time it is desirable to understand and adapt the growth process in relation to that. Finite Element Analysis software (COMSOL) is used to implement the thermal model of the process to be able to calculate the temperature evolution during the growth process. A 3D sketch of the geometry used in the model is shown in Figure 2.9. The substrate holder is an aluminum cylinder with a hole in the middle covered by a fused silica slide. The silicon substrate is fixed by two iron springs on top of the fused silica. The substrate holder is itself placed on top of a steel cylindrical part of the chamber. The inside of the cylinder is hollow so that the emitted radiation can be collected beneath the substrate. In the model, the temperature is calculated for each time step using the relevant heat conduction, radiation and convection of different materials and gasses in the system.

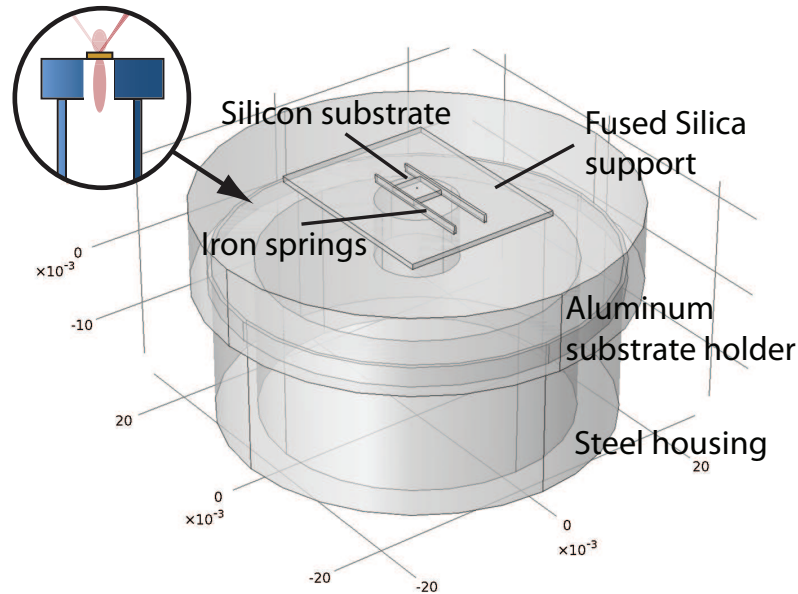


Figure 2.9: 3D Sketch of the setup used in the finite element model. In the figure, the different materials and components are labeled. The inset shows the corresponding part of the schematic setup from Figure 2.7

The temperatures at the spot and surrounding are in the order of 600 - 1100 K so the thermal conductivity and heat capacity of silicon, fused silica and iron are given temperature-dependent values, see Figure 2.10 and Figure 2.11. To model convective effects, the thermal conductivity, kinematic viscosity and thermal diffusivity of the surrounding gases (argon, ethylene and hydrogen^[138]) are also given a temperature dependency, see Figure 2.12 - Figure 2.14.

The heat transfer considered in the model is based on conduction, radiation and free convection. To calculate the heat transfer coefficient for the free convection, the Nusselt numbers for free convection from a horizontal top (Nu_{HT}) and bottom (Nu_{HB}) respectively a vertical

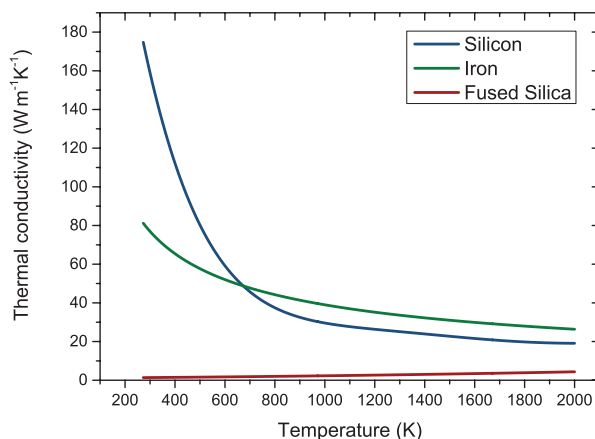


Figure 2.10: Thermal conductivity of the solids used in the model.

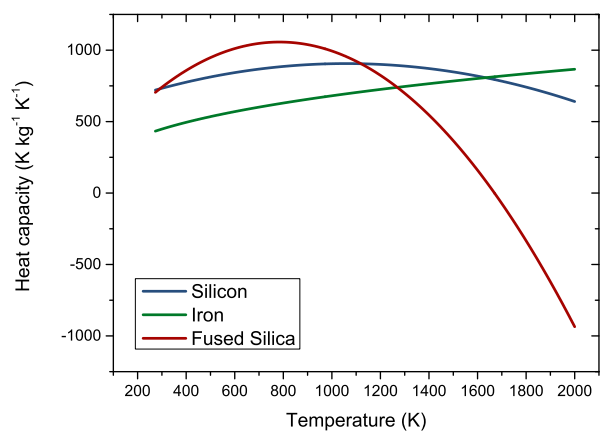


Figure 2.11: Heat capacity of the solids used in the model.

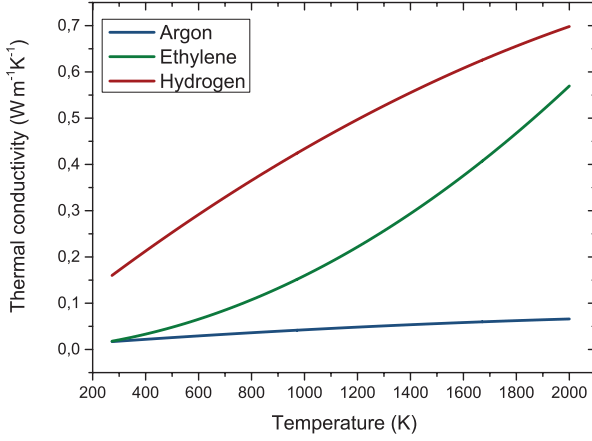


Figure 2.12: Thermal conductivity of the gases used in the model.^[138]

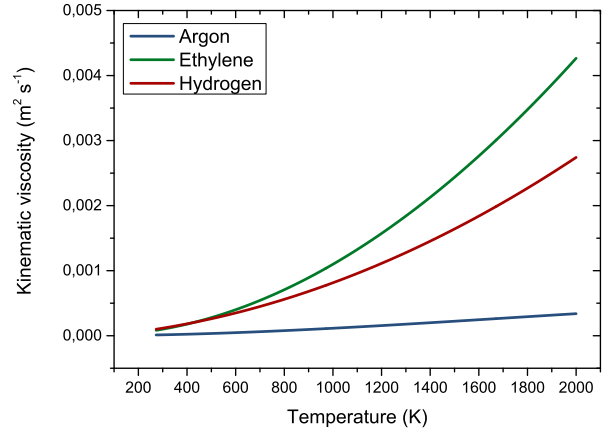


Figure 2.13: Kinematic viscosity of the gases used in the model.^[138]

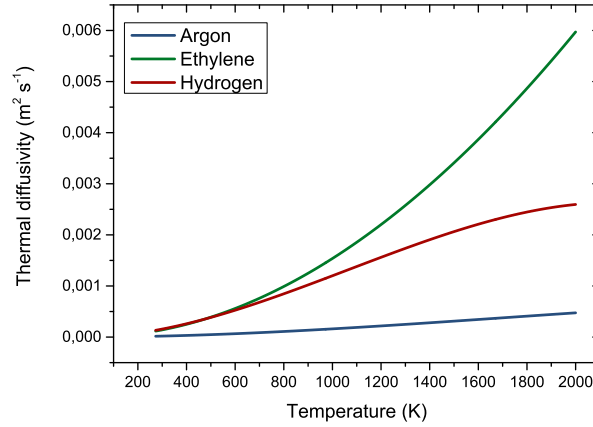


Figure 2.14: Thermal diffusivity of the gases used in the model.^[138]

plate^[139] (Nu_{VP}) are used,

$$Nu_{HT} = 0.54 Ra^{1/4} \quad (2.1)$$

$$Nu_{HB} = 0.27 Ra^{1/4} \quad (2.2)$$

$$Nu_{VP} = 0.68 + \frac{0.67 Ra^{1/4}}{1 + (0.492/Pr)^{9/16}} \quad (2.3)$$

where Ra and Pr are the Rayleigh and the Prandtl numbers. Note that these relations assume an average temperature through the substrate.

$$Ra = \frac{g\beta}{\nu\alpha}(T_s - T_{inf})L^3 \quad (2.4)$$

$$Pr = \frac{\nu}{\alpha} \quad (2.5)$$

Here, g is the gravitational constant, β the thermal expansion (ideal gas is assumed, so β equals $1/T$), ν is the kinematic viscosity (Figure 2.13), α (Figure 2.14) is the thermal diffusivity, T_s the substrate temperature, T_{inf} the (cold) wall temperature and L the characteristic length.

The Nusselt number is defined as the ratio between the convective and conductive heat transfer. The heat transfer coefficient is given by,

$$h_c = \text{Nu} \times k_f / L \quad (2.6)$$

Where k_f is the thermal conductivity of the gas mixture and L is the characteristic length. Using this method, the heat transfer coefficient was estimated for several surfaces, locations and gas composition ratios. The thermal radiation is modeled by the Stefan-Boltzmann law,

$$Q_{\text{rad}} = \varepsilon \sigma (T^4 - T_{\text{inf}}^4) \quad (2.7)$$

where Q_{rad} is the emitted thermal radiation per unit area, σ is the Boltzmann constant and T_{inf} is the surrounding temperature, in this case assumed to be room temperature.

The laser spot is modeled as an ellipsoid with dimensions $65 \times 80 \mu\text{m}$ to take into account the incidence angle of 35° . The beam is modeled with a Gaussian intensity profile and could be dynamically varied as a function of time, corresponding to experimentally obtained data.

To compare the model with reality, three different experiments are performed in an argon/hydrogen environment to ensure the absence of ethylene where no growth can take place. In Figure 2.15, the temperature evolution of these experiments using different laser irradiances is shown and compared with the experimental data from the thermocouple positioned at the edge of the substrate. The model is slightly calibrated by tweaking the heat transfer coefficient that acts on the different locations of the substrate.

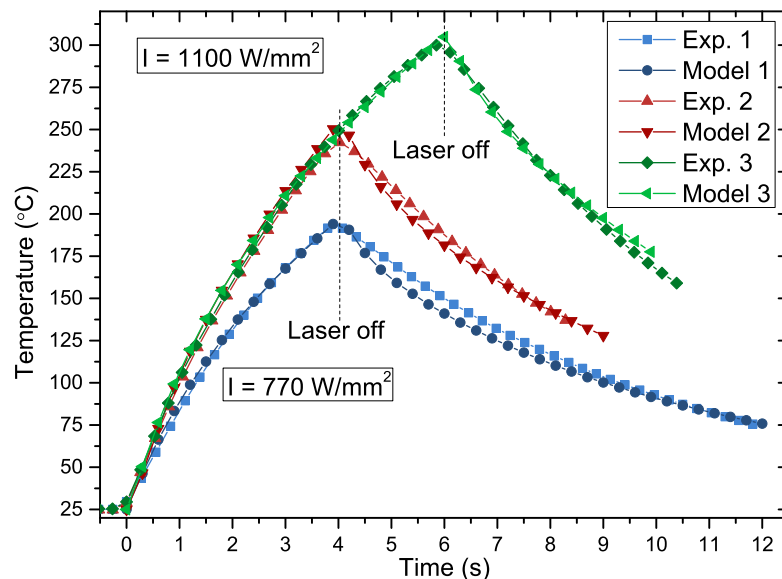


Figure 2.15: Comparison of the temperature at the edge of the silicon substrate from the thermal model with experimental data for different laser irradiances. Two different laser irradiances and two different switch off times are presented. All experiments are performed in open-loop configuration.

2.6 Catalyst

The formation of nano-particles from the catalyst layer is a crucial process since it determines the crystallographic properties and characteristics of the carbon nanotubes. To investigate the formation of the catalyst nano-particles, the substrates used in the open-loop experiments of Figure 2.15 are observed since they do not contain any carbonaceous growth. In Figure 2.16 the radiation and reflection detector responses for Exp. 1-2 are presented. The radiation is lower for Exp. 1 due to the lower laser irradiance. For both experiments, an increase of the radiation signal was observed. This increase in thermal radiation is attributed to the reduction and formation of the catalyst nano-particles. The 1.5 nm-thick iron catalyst layer is fully oxidized prior of starting the process.^[133] The absorbed energy is used to reduce with hydrogen and melt the oxidized iron layer that turns into small metallic nanoparticles on top of the Al_2O_3 layer. The higher the laser irradiance, the faster this process is completed. This is confirmed by the reflected laser signal in Figure 2.16.

In Figure 2.17, a schematic overview of the reflected laser signal over time and the proposed mechanism corresponding to the different signal intensities is given. Inset (a) illustrates the starting configuration. The reflection first drops (inset b) due the increase in absorbance of the laser irradiance as a result of the temperature increase. The reduction into metallic iron and the melting of the layer consumes energy which results in a further drop in reflection (c). However the metallic iron layer increases the reflection of that layer (d). The formation of small nano-particles reduces the actual covered area of the layer which also contributes to an increase in reflection (e). The heating of the substrate further decreases the reflectance due

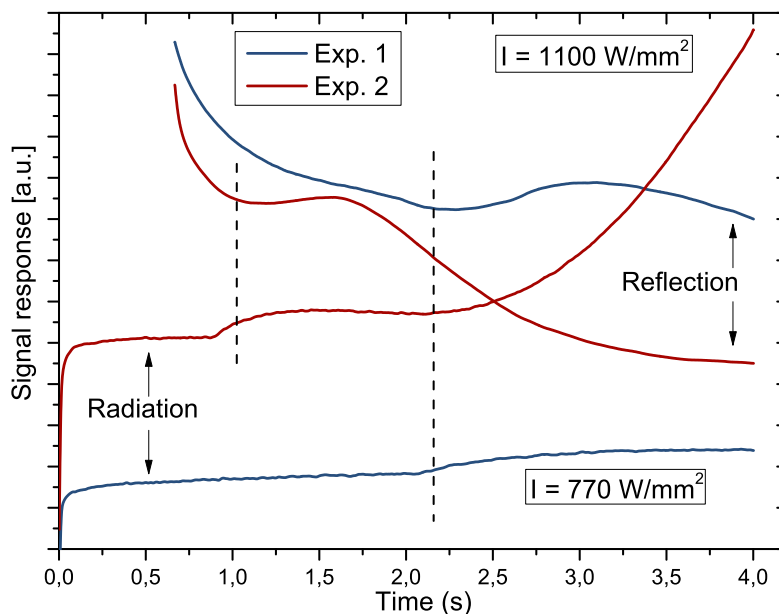


Figure 2.16: Detector response for experiment 1 (blue line) and 2 (red line). The emitted radiation of experiment 1 is lower which is due to the lower laser irradiance. For the radiation of experiments 1 and 2, an increase is visible around 1 and 2 s, respectively (see vertical dashed lines). At the same time, a small "step" in the reflection is visible. This increase is attributed to the formation and reduction of the iron catalyst nanoparticles.

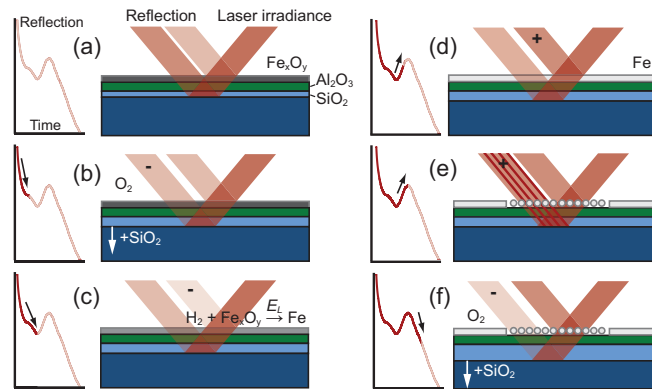


Figure 2.17: Schematic of the catalyst nano-particle formation process. (a) Starting configuration. (b) Reflection is decreased due to enhanced absorbance as a result of temperature increase. (c) Reflection is decreased due to the absorbance of energy for the reduction process. (d) Reflection is increased due to the formation of the metallic layer. (e) Reflection is increased due to the enhanced passing of the reflection from the layers beneath the catalyst as a result of the nanoparticle formation. (f) Reflection is decreased by further enhanced absorbance and interference effects as a result of the growth of SiO_2 .

to the enhanced absorbance and possible additional interference effects associated with the thermal growth of SiO_2 (f). The resulting peak in intensity takes longer to occur for the lower laser irradiance in Figure 2.16 and corresponds in time to the increase in radiation. A higher laser irradiance generally leads to smaller catalyst particles and ultimately to nanotubes with a smaller diameter.^[48, 140, 141] However, an overly long laser exposure will lead to the destruction of the catalyst layer and the formation of oxides. In Figure 2.18 the Scanning Electron Microscopy (SEM) pictures of the catalyst layer are shown for different laser irradiances and exposure time. It is observed that at higher laser irradiance and longer exposure time more discrete separation of the catalyst nano-particles occurs. This can be seen in Figure 2.18(a)-(d). However, (e) and (f) show a destruction of the catalyst layer and the formation of oxide crystals for a further increase in exposure time.

To demonstrate that the peak in the reflection signal is a result of the formation and reduction of the catalyst, the reflected laser signal from three experiments is compared; two substrates without the iron catalyst and one with the catalyst layer. These results are shown in Figure 2.19. As seen in this figure, the peak only occurs when the iron layer is present. When the substrate with the iron layer is exposed again to the same laser exposure conditions, the peak in the reflection is not observed, indicating that the formation and reduction of the iron catalyst nano-particles already took place. At this stage and due the lack of experimental data for various catalyst thicknesses, no possible correlation between the amplitude of the peak and the size of the nanoparticles can be concluded. The inset of the figure shows an extension of the reflected laser intensity for 3 minutes. Since both curves (Si and Si/ Al_2O_3 / Fe) are showing an equal oscillation pattern, these oscillations are attributed to an optical interference effect caused by the thermal growth of a SiO_2 layer, as proposed in Figure 2.17, since that is the only material present on both substrates.

To further confirm this assumption, the influence of the surrounding process gasses is investigated. Previous research has already indicated the importance of hydrogen in the formation and reduction (de-oxidation) of the iron catalyst nano-particles.^[94] It is generally believed

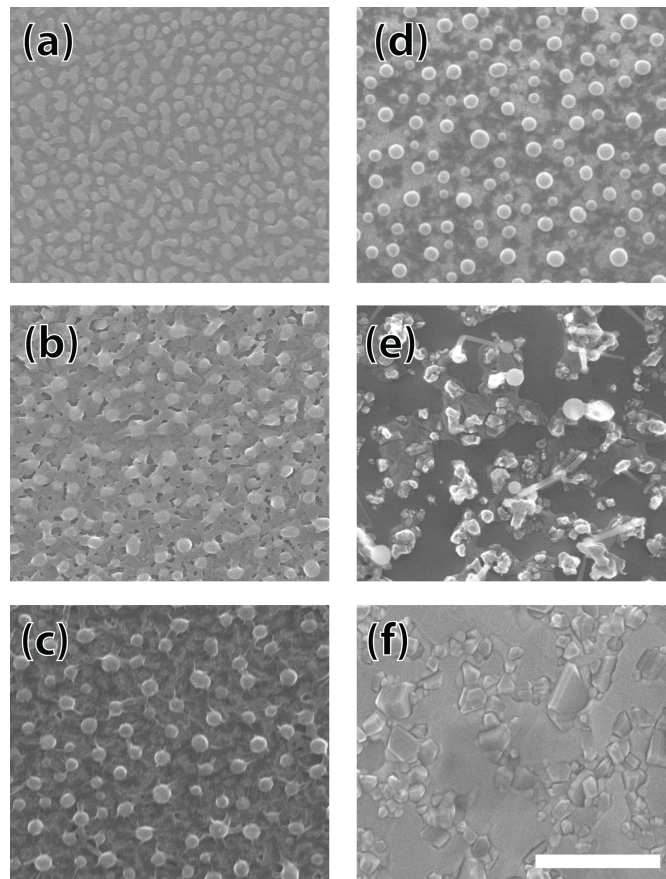


Figure 2.18: Scanning electron microscopy pictures of the laser affected zone of the catalyst layer after different exposure irradiances (I) and times (t): (a) $I = 7.7 \times 10^8 \text{ W/m}^2$ and $t = 4 \text{ sec}$. (b) $I = 9.4 \times 10^8 \text{ W/m}^2$ and $t = 4 \text{ sec}$. (c) $I = 1.1 \times 10^9 \text{ W/m}^2$ and $t = 4 \text{ sec}$. (d) $I = 1.1 \times 10^9 \text{ W/m}^2$ and $t = 6 \text{ sec}$. (e) $I = 1.1 \times 10^9 \text{ W/m}^2$ and $t = 10 \text{ sec}$. (f) $I = 1.1 \times 10^9 \text{ W/m}^2$ and $t = 40 \text{ sec}$. The scale bar represents 500 nm.

that the thin iron layer is quickly oxidized after being exposed to air into a combination of magnetite (Fe_3O_4) and maghemite ($\gamma\text{-Fe}_2\text{O}_3$), a form of hematite.^[133] The thermal energy from the laser in combination with the hydrogen reduces this iron-oxide back to iron using the following redox relations,^[142,143]



The high temperature melts the iron and surface energy minimization of the iron liquid on the alumina surface causes the formation of small nano-particles as a result of the strong catalyst-support interaction.^[144] Note that the size, mobility and distribution of the nanoparticles is also dependent on the method of deposition of both the support and the catalyst.^[145] At a temperature above 577°C , wüstite (FeO) can nucleate. This oxide is more stable and harder to reduce.^[146] To avoid the nucleation of this oxide, the time that the process exceeds

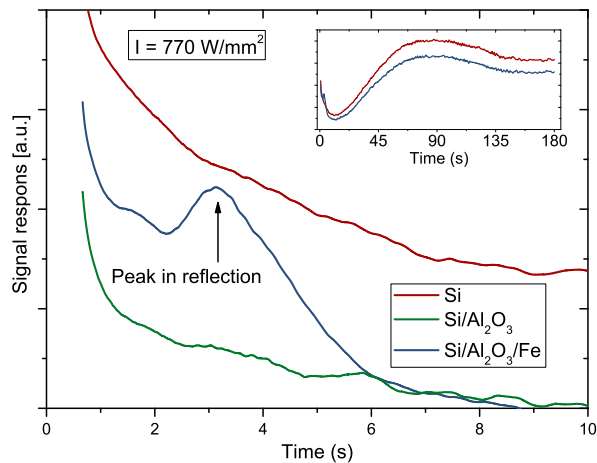


Figure 2.19: Reflected laser irradiance response for three different cases: 1: a silicon substrate with only native oxide. 2: a silicon substrate with only 20 nm Al_2O_3 and 3: the conventional substrate, a silicon substrate with 20 nm Al_2O_3 and 1.5 nm iron. It is clear to see that the peak in the reflection only occurs when the iron layer is present and is therefore attributed to the formation of the catalyst particles.

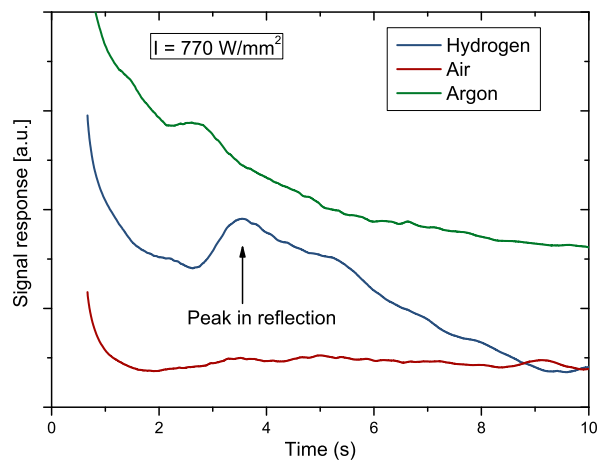


Figure 2.20: Reflected laser irradiance response for a silicon/ Al_2O_3 /Fe substrate in different environments: hydrogen, argon or air, with the same laser irradiation. Only the hydrogen case shows a peak in the signal, which indicates a reduction process which is therefore attributed to the formation and reduction of the Fe_2O_3 layer into Fe nanoparticles.

this temperature in the absence of CNT growth should be minimized. Equation 2.8 and Equation 2.9 indicate that the formation of iron nano-particles will not occur in the absence of hydrogen. In Figure 2.20 the laser reflection is shown for a substrate with the iron catalyst in the presence of different gases. When only air or argon is present, there is no observable peak in the reflection signal. When only hydrogen is present in the reaction chamber, there is a prominent peak present in the reflection. This experimentally confirms that the peak in the reflection signal is a result of the reduction and formation of the iron catalyst nano-particles. The *in-situ* catalyst observations demonstrate that the reflected signal can be used to monitor the onset of the catalyst layer activation. This important information can be used to trigger the growth process by introducing the ethylene at that time.

2.7 Results of temperature closed-loop control

Using the time dependent laser irradiance and reflected laser signal, the finite element model is used to calculate the temperature as a function of time for experiments in the closed-loop configuration as described before. In Figure 2.21, the reference radiation, measured in voltage, is compared with the modeled maximum temperature calculated from different experiments. The figure demonstrates the direct relation between the reference radiation set-point and the process temperature at the laser spot. The inset of the figure shows the relation between the selected saturation laser irradiance level and the calculated temperature for a constant reference set-point (in this case 0.4 V) for the radiation signal. It shows that there is no significant change of the temperature at the growth site for increasing laser irradiance saturation level.

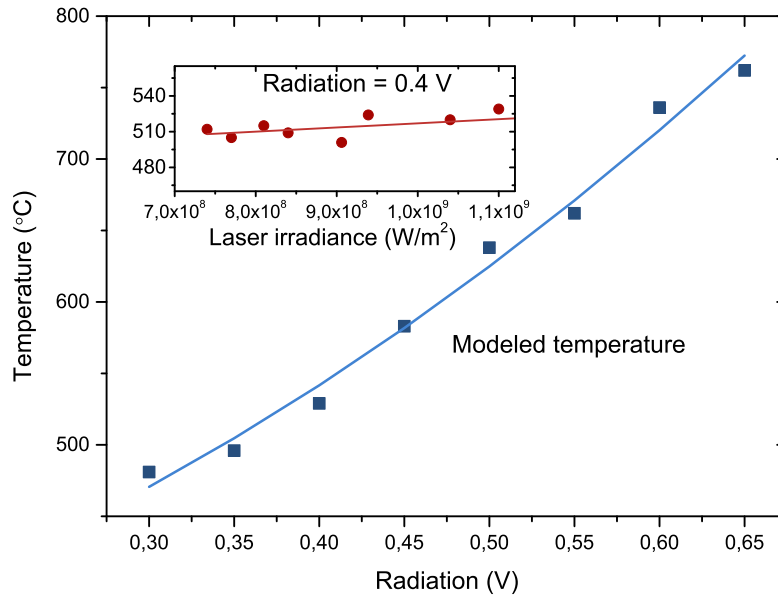


Figure 2.21: Plot of the modeled peak temperature vs the set-point reference radiation measured as voltage from the InGaAs detector. Plotted are the maximum peak values at the laser spot. The inset shows the temperature as a function of selected saturation laser irradiance with the reference radiation set at 0.4 V.

In subsection 2.3.1 it was shown that in open-loop the laser set-point, as one would expect, governs the rate of temperature increase and is related to the quality of the growth product, see Figure 2.5. A high temperature increase rate - in other words, a fast heating - yields higher quality CNTs. In the closed-loop situation, a higher laser irradiance saturation level would mean a faster response to the set-point value, which is analogue to achieving the CNT growth temperature faster. This can be seen in Figure 2.22 for two different laser irradiances. For a laser saturation irradiance of 1100 W/mm² the set point is reached faster than in the case of 770 W/mm². A too fast response (i.e. too high laser irradiance) can lead to an overshoot in the set-point (or would require adapting the PID coefficients). In Figure 2.22 the difference between the temperature at the laser spot for the controlled and uncontrolled situation is also depicted. Both experiments start with a saturation laser irradiance level of 770 W/mm². The laser irradiance of the controlled experiment, on the other hand, drops in time to keep the radiation at the constant reference value. Until around 4 seconds the temperature increase is more or less equal for both situations.

The quality of the CNTs is characterized using Raman spectroscopy^[81,82,147] as previously discussed in subsection 2.3.1. The ratio of the D-band to G-band spectral intensity is used as a measure for the quality of the nanotubes in terms of the presence of structural defects on nanotube walls and of amorphous carbon as well. High quality nanotubes with a low concentration of structural defects and amorphous carbon deposit thus have a low I(D)/I(G) ratio. At the Raman shift between 0 and ~350 cm⁻¹ the Radial Breathing Modes (RBM) of SWNTs can be found. This mode can be used to calculate the diameter of the SWNT using the following relation:^[147]

$$\omega_{RBM} = 248/d_t \tag{2.10}$$

where ω_{RBM} is the Raman shift and d_t is the diameter of the tube. The diameter of the single-

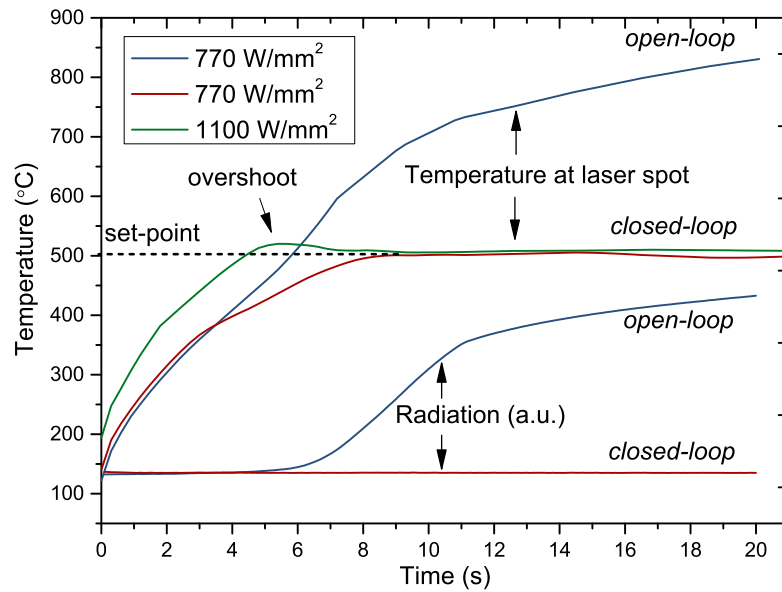


Figure 2.22: Temperature at the laser spot as a function of time for the uncontrolled, open-loop (blue lines) and radiation-controlled situation (red: 770 W/mm² and green: 1100 W/mm²). The set-point for 1100 W/mm² is shown with an overshoot. The radiation in also plotted for both situations.

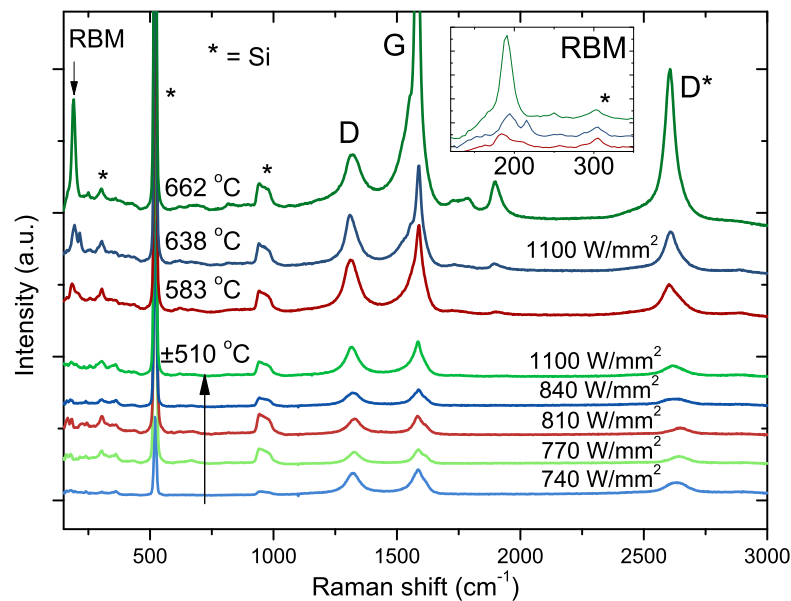


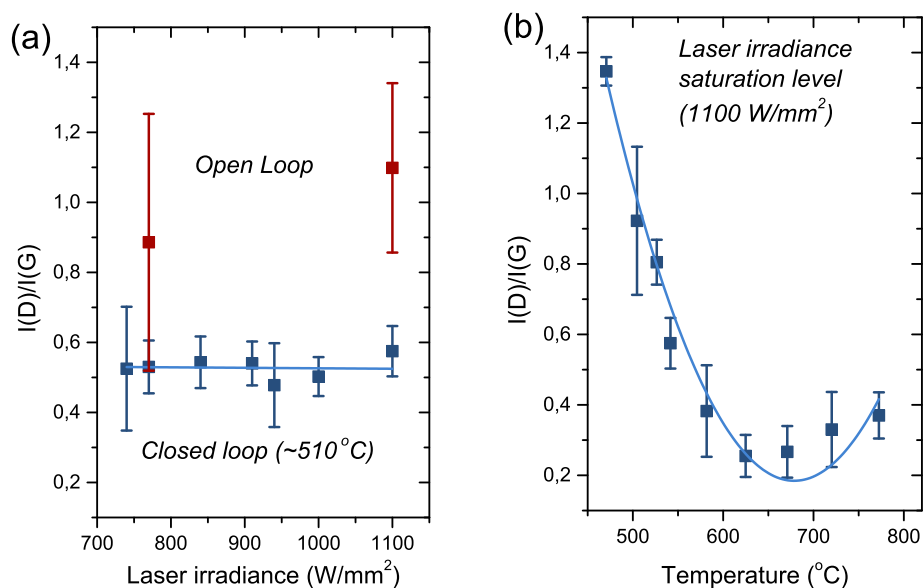
Figure 2.23: Raman spectra of CNTs prepared at different laser saturation irradiances and temperatures. All experiments are performed for the duration of 20 seconds. The curves are shifted in the vertical direction for clarity. The level of irradiance and temperature is indicated next to each spectrum or group of spectra. The inset shows a detailed zoom of the RBM area of the top three spectra.

walled CNTs grown by the LACVD method is calculated to be in the range of 1.1-1.6 nm. The most abundant diameter was 1.3 nm which is slightly smaller than the thickness of the original iron layer.

In Figure 2.23, the Raman spectra for a number of closed-loop controlled experiments are

shown. There are two types of experiments. First the laser saturation irradiance level is increased and the radiation (and thus the temperature) is kept constant. In this case, the radiation was set at 0.4 V corresponding to 510 °C. In this figure it can be seen that increasing the laser saturation level does not improve the quality of the nanotubes. This is shown in more detail in Figure 2.24(a). The black dots depict the I(D)/I(G) ratio as a function of laser intensity for the same experimental conditions which is more or less constant as confirmed by the linear fit. For comparison, two open-loop experiments are shown. It is clear that the ratio is much higher for both open-loop experiments. In the case of 1100 W/mm², the SEM analysis shows that the substrate was overheated and that a thick amorphous layer was formed (see for instance Figure 2.6). Increasing the reference radiation (i.e. the temperature) for the top three Raman spectra in Figure 2.23, the temperature at the laser spot is increased yielding higher quality nanotubes. Indeed, the I(D)/I(G) ratio decreases and the presence of the RBM peak demonstrates the presence of SWNTs. The RBM peaks are shown in more detail in the inset of Figure 2.23.

In Figure 2.24(b), the I(D)/I(G) ratio is plotted as a function of the process temperature with constant laser saturation irradiance level of 1100 W/mm². The error bars show the standard deviation over multiple experiments and positions at the center of the laser affected zone. The temperature is calculated using the finite element model as well as the time dependent laser irradiance and reflection as described before. The saturation laser irradiance level was set to the maximum value (1100 W/mm²) to achieve the highest heating rate. A quadratic



(a) I(D)/I(G) ratio as a function of laser irradiance. In open-loop the irradiance represents the set-point of the laser irradiance and in closed-loop it represents the laser irradiance saturation level.

(b) I(D)/I(G) ratio as a function of temperature for a constant laser irradiance saturation level. Squares and error bars show the mean and standard deviation respectively over multiple positions in the center of the laser spot and multiple experiments.

Figure 2.24: Structural quality of the CNTs, measured by Raman spectroscopy I(D)/I(G) ratio, versus several parameters, in closed-loop and open-loop.

fit is added and a minimum is found around 675 °C. This result demonstrates the capability of a temperature-controlled laser-assisted CNT growth process. Further, it shows that the CNT quality is a function of the growth temperature in the investigated temperature range if all other parameters are kept constant. Based on Raman spectra, SEM analysis and the non-uniform temperature distribution of the experiments, the grown CNTs are most likely to be a mix of metallic and semi-conducting CNTs as well as MWNT and SWNT.

In Figure 2.25, the SEM pictures of a number of the experiments are shown. Figure 2.25(a)-(c) correspond to the second, fourth and fifth spectra in Figure 2.23 and Figure 2.25(d)-(f) correspond to the top three spectra in Figure 2.23. In (a) to (c) the increase of the saturation laser irradiance level seems to affect the length of the CNTs forest. This might be a consequence of the temperature heating rate which influences the efficiency and the nature of the catalyst decomposition. In Figure 2.25(d)-(f) it seems that the amount of CNTs is decreased drastically by increasing temperature. The increase in temperature results in a few

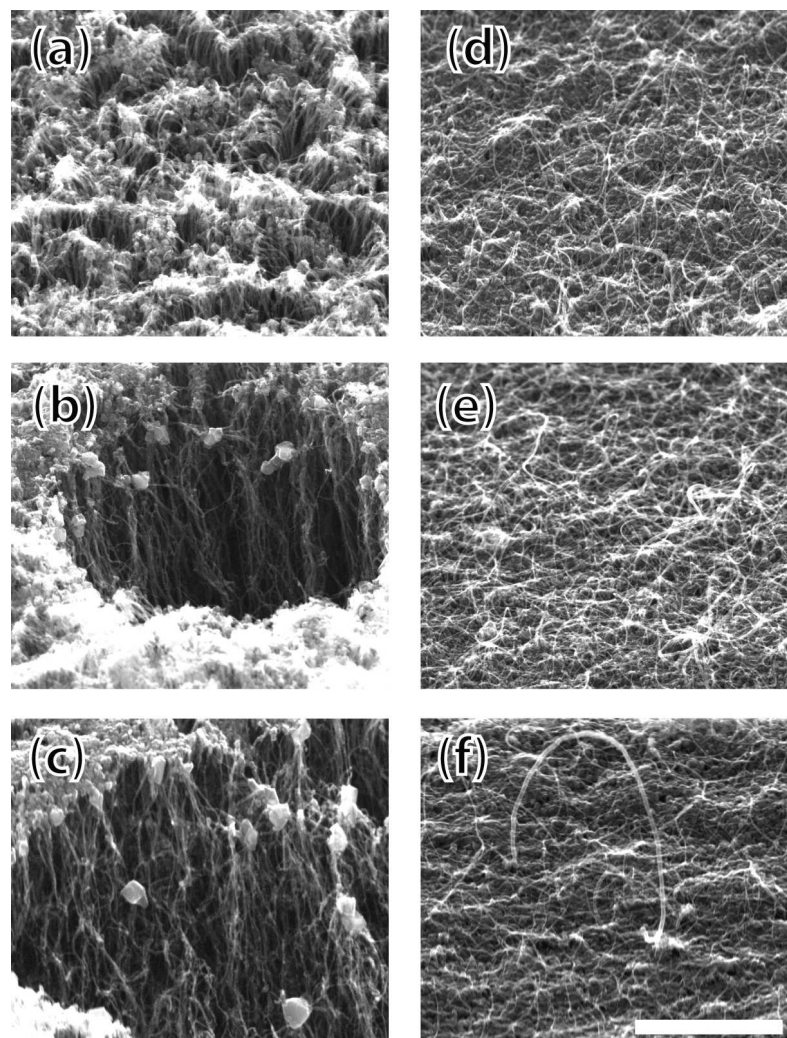


Figure 2.25: SEM pictures of the CNT growth for 6 experiments. (a) $I = 770 \text{ W/mm}^2$ and $T = 510 \text{ }^\circ\text{C}$. (b) $I = 940 \text{ W/mm}^2$ and $T = 510 \text{ }^\circ\text{C}$. (c) $I = 1100 \text{ W/mm}^2$ and $T = 510 \text{ }^\circ\text{C}$. (d) $I = 1100 \text{ W/mm}^2$ and $T = 583 \text{ }^\circ\text{C}$. (e) $I = 1100 \text{ W/mm}^2$ and $T = 638 \text{ }^\circ\text{C}$. (f) $I = 1100 \text{ W/mm}^2$ and $T = 662 \text{ }^\circ\text{C}$. The scale bar represents $1 \text{ }\mu\text{m}$.

high quality CNTs (low $I(D)/I(G)$) while at the same time the growth conditions are changed such that an overall forest growth is absent. This type of growth could be the result of the sensitive process conditions around the laser spot at those high temperatures. The temperature is high enough for SWNTs to grow but is also closer to thermal decomposition temperature of ethylene and above the wüstite formation temperature of 577°C . A formation of that oxide can slow down the reduction with hydrogen bringing the growth to a pre-mature stand-still. Although there is no clear evidence to support it, the crystal structure of the oxide nevertheless resembles that of other iron-oxides.

2.8 Catalyst activation control

Using the information from the reflected laser irradiation as described earlier, the onset of the catalyst layer decomposition can be detected, which could be used to optimize the gas feeding schedule. For non-laser CVD, a catalyst preparation step is common prior to the CNT growth. Here, it is shown that the same preparation step can be done with laser-assisted CVD. As a consequence of the fast heating rate due to the low thermal inertia of the system, the catalyst preparation step is considerably shortened.

The catalyst activation and carbon nanotube growth processes are strongly coupled. In order to investigate and identify the complete process and growth kinetics (chapter 4), de-coupling of the two processes is desirable. It follows from the results of this chapter that the closed-loop controlled LACVD method developed here has the ability to do so.

2.9 Summary

In this chapter, a *closed-loop control* process based on the infrared emission from the laser spot is presented and developed, for reproducibly growing local CNT forests using a laser-assisted CVD method. Open-loop CNT growth revealed different growth regimes which are related to the sensors used to monitor the process. The results from these experiments demonstrated the necessity of closed-loop control.

In combination with closed-loop control, finite element modeling, calibrated with experimental data, is used to determine and compare *process temperatures*. From experiments in a non-growth environment, the iron catalyst properties were investigated and it was found that the optimal catalyst reduction and formation occurs when the maximum laser irradiance of 1100 W/mm^2 is used to expose the catalyst layer for 6 seconds to ensure formation of small particles but to avoid the formation of oxide crystals. A unique method to detect the *onset* of the catalyst layer was found, by monitoring the reflected laser irradiance. Increasing the growth temperature yields the same trend as for conventional CVD growth with respect to the quality of the CNTs. A minimum of the $I(D)/I(G)$ ratio in the Raman spectra is observed around 675°C for a fixed laser irradiance of 1100 W/mm^2 in this setup. However, the amount and alignment of the CNTs changes rapidly for high temperatures suggesting iron-oxide formation and thermal decomposition of ethylene at high temperatures. This novel laser-assisted CVD method successfully demonstrated that growing local CNT structures is possible in a controlled manner.

This chapter demonstrates the necessity of closed-loop control, with respect to open-loop CNT growth in enhancing reproducibility and preventing overheating. Closed-loop controlled growth is also essential to simulate the temperature of the process, in itself crucial for qualitatively evaluating the CNT growth as well as studying growth kinetics. However, to further investigate and optimize the process, a precise knowledge of gas composition at the growth site is necessary and local induced turbulence should be avoided.

Chapter 3 |

Miniaturized reaction-chamber for optimized carbon nanotube growth

To overcome the challenges of the large statically filled reaction chamber, such as low throughput time, local induced turbulence and process gas depletion, and to be able to study growth kinetics, a miniaturized reaction chamber is presented in this chapter. The chamber provides a laminar gas flow over the substrate with precise control of the gas composition at the laser growth-site. The particular design of this miniaturized reactor results in a high reproducibility as well as fast growth cycle time. A multi-parameter finite element method (FEM) model is implemented to link substrate temperature at the laser spot with emitted radiation, taking into account the gas flow, the process time and other temperature-dependent physical parameters such as forced convection, thermal conductivity and heat capacity. The resulting growth of carbon nanotubes is assessed using Scanning Electron Microscopy (SEM) and Raman spectroscopy. Combined with results from the thermal model, process information is used to calculate activation energy for the nanotube nucleation.

Part of this chapter has been accepted for publication in

Y. van de Burgt, Y. Bellouard, W. van Loon, R. Mandamparambil, *Miniaturized Reaction Chamber for Optimized Laser-Assisted Carbon Nanotube Growth*, Journal of Laser Micro / Nanoengineering (2014).^[4]

3.1 Introduction

In the previous chapter, a feedback control in the laser-assisted CVD process for CNT growth was introduced. The process itself is monitored and controlled by different optical sensors, controlling temperature and monitoring the CNT growth. To further optimize the process, laser-assisted CVD also requires a localized gas flow control, eliminating possible effects of turbulence.

In this chapter, a miniaturized LACVD reactor is presented (shown in Figure 3.1), where a precise control of the gas flow at the laser-growth site is provided. The particular design of this miniaturized reactor results in a high reproducibility as well as a high production yield. A multi-parameter finite element model (FEM) is implemented to link substrate temperature at the laser spot with emitted radiation, taking into account gas flow, process time and other temperature-dependent physical parameters such as forced convection, thermal conductivity and heat capacity.

To validate and calibrate the model, a series of test-experiments is performed. The thermal model then is applied to find a relation between reference radiation and temperature at the laser spot. The resulting CNT growth for certain process parameters is assessed using Raman spectroscopy and Scanning Electron Microscopy. To illustrate the versatility of the process, the ability to calculate the characteristic activation energy for nanotube nucleation is demonstrated.

3.2 Design and setup

The necessity for a small reaction chamber originated from limitations of the large, statically filled gas reaction chamber described in the previous chapter. Growth kinetics requires a precisely known gas composition at the growth site. For accurate predictions of gas concentration around the laser hot-spot a laminar flow is required with the ability to control the gas flow. A miniaturized CVD reaction chamber was designed for this purpose, at the same time significantly reducing the experimental cycle time.

The laser-assisted chemical vapor deposition process for the growth of local carbon nanotube structures comprises of three main components. All three are essential to the growth of carbon nanotubes. Thermal energy, gas supply and catalyst are the building blocks for any CVD process. Here, a CW short-IR laser (808 nm) is used to heat up the substrate. In this case the laser hits the substrate from the top surface. Although this method allows a higher spatial resolution for localized growth, it suffers from the fact that the substrate absorptivity dynamically evolves as CNTs start to grow. The enhanced absorbance during CNT growth results in overheating of the CNTs and amorphous carbon deposition as was described in subsection 2.3.2. To overcome this problem, in the previous chapter a closed-loop control synthesis method was developed, which uses the emitted radiation in the mid-IR spectrum from the laser hot-spot as the controller input. This radiation is directly related to the temperature at the laser spot and enables a better control over the process and prevent overheating. The growth itself is monitored by means of the intensity variation of the reflected laser beam, providing a first approximation of the growth kinetics.^[131]

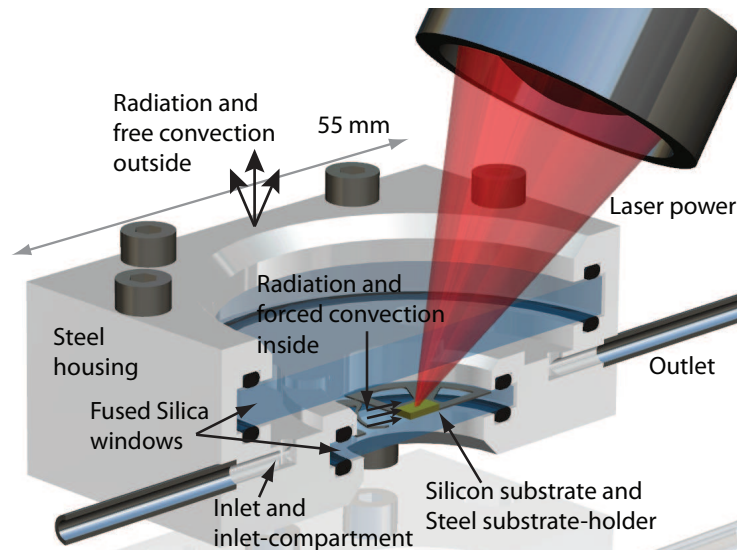


Figure 3.1: CAD overview of half of the reaction chamber including the focused laser beam. Also indicated are the thermal properties and materials that are used in the FEM model.

3.2.1 Design

The miniaturized reaction chamber design requirements comprised a laminar gas flow over the substrate and the ability to easily replace substrates and specimens while remaining optically accessible for the laser path and sensors. Further, by decreasing the size of the reaction-chamber, the system can be placed onto an x-y-z stage, enabling the creation of lines, patterns and arrays of CNT structures. The laser source is placed completely outside of the chamber. Taking advantage of its optical and thermal properties, fused silica was chosen as a covering top window. For similar reasons fused silica was also used as the bottom window. Especially, the low thermal conductivity and shock resistance of fused silica were proven to be essential for the growth process where the former enhances the thermal confinement.

The chamber is schematically shown in Figure 3.1. To ensure a laminar flow, the reaction chamber was designed with an "inlet-compartment" to reduce any turbulence possibly present in the gas before entering the main reaction compartment of the chamber. The dimensions of the chamber ensure the Reynolds number (defined as the ratio between inertial forces and viscous forces) does not exceed 35 for the maximum flow rates of the flow controller, significantly lower than 2000, where the transition to turbulent flow starts.

The chamber is sealed with flexible O-rings and clamped with bolts to avoid leaking. The substrate is held to its place by a substrate-holder fabricated by Electrical Discharge Machining (EDM) from stainless steel and comprises a small spring pushing the substrate on its place.

3.2.2 Experimental setup

The optical setup for the chamber is more or less similar to the optical setup presented in the previous chapter, section 2.2. In the current setup however, the laser beam is focused through the window onto the substrate under an angle of 45° and the reflection signal is captured by the Si-detector under the same angle. A schematic of the setup is shown in Figure 3.2. The

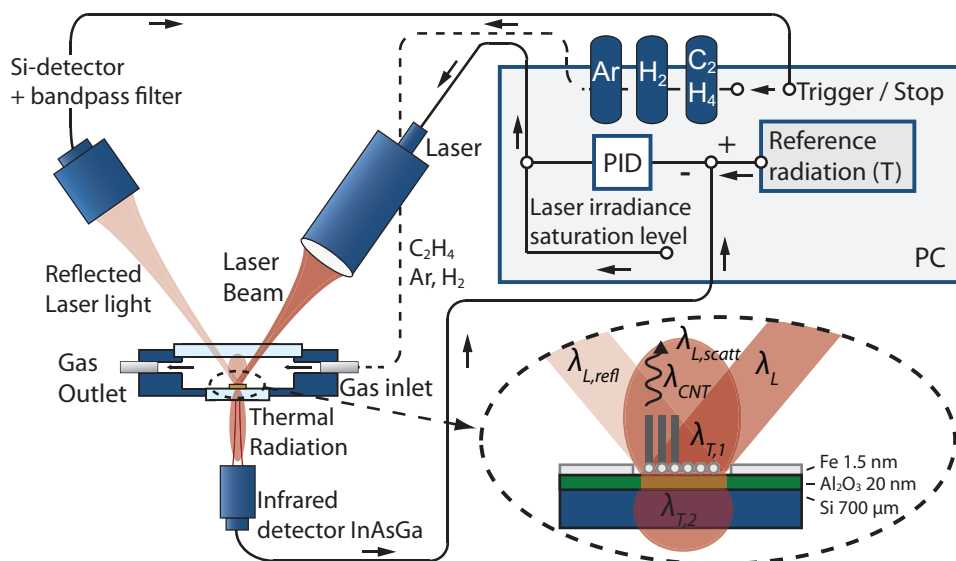


Figure 3.2: Overview of the laser-assisted chemical vapor deposition setup with feedback control similar to Figure 2.7 in chapter 2. In this miniaturized setup the laser is placed outside the chamber and is focused through the fused silica window. The gas flow is controlled and flows in laminar fashion over the substrate.

chamber is placed on an x-y-z stage by an extended clamping plate to ensure the bottom window is visible by the radiation detector from beneath the chamber. The laser diode is connected to the computer by a data acquisition board enabling real-time control over the laser irradiance. Simulink is used to create a PID-controller that controls the radiation. The process gases, argon, hydrogen and ethylene can be individually controlled with a maximum flow rate of 500 sccm (standard cubic centimeter per minute).

3.3 Thermal modeling

A finite element method (FEM) model is developed in COMSOL Multiphysics 4.3a. Like for the model described the previous chapter, in section 2.5, this thermal model is necessary in order to investigate temperature evolution in time and space. A schematic of the model including the heat transfer properties was shown in Figure 3.1. In this particular design, heat and flow are strongly coupled. Here the model evaluates forced and natural convection as a function of input parameters such as gas flow and laser irradiance.

3.3.1 Modeling of heat transfer

The miniaturized reaction chamber designed in this chapter allows for the heat and flow problems to be coupled so that heat transfer through forced and natural convection is calculated by the model itself. This means that the input gas flow and the concentration will be directly related to the calculated temperature and vary for different input conditions.

All the materials and gases described in the model have temperature dependent properties. That is, heat capacity, thermal conductivity, and thermal diffusivity for the gases; heat capacity,

thermal conductivity and thermal expansion for the solids. See section 2.5 and Figure 2.10- Figure 2.14. Gases are modeled using the ideal gas law, which is assumed to be valid within the pressure and temperature range considered here. The inlet and outlet boundary conditions are prescribed *mass flow* and *constant pressure*, respectively. Further, on all exterior and interior free boundaries *surface radiation* is applied and *natural convection in air* is applied on the exterior free boundaries. From estimations of the Grashoff and Rayleigh numbers it followed that forced nor natural convection can be neglected. Since the thermal model couples gas flow with heat transfer this is incorporated for the internal domains. The laser is modeled with a Gaussian intensity profile and can be stationary, in the case of open-loop experiments, or time-dependent, in the case of closed-loop experiments. The laser irradiance is applied as a *boundary heat source* and for the latter the recorded laser irradiance in time is used as the input instead of a constant laser irradiance.

3.3.2 Experimental validation of the model

To validate the model, two different flow conditions (flow of Argon of 50 sccm and 500 sccm) are selected and the corresponding temperature is calculated for a range of laser irradiances. Since measuring the temperature directly in the laser spot is not possible, a thermocouple has been placed at the edge of the substrate. Stationary temperature is measured when the substrate is exposed to various preselected laser irradiance levels. The results are shown in Table 3.1. It appears that the model slightly over-estimates the temperature at high laser power and under-estimates the temperature at lower laser power. This effect seems to be larger for the lower flow rate of 50 sccm. The discrepancy can be explained by a number of factors. Most importantly, the calculation is done on a highly complex multi-parameter model and therefore the coupling between the forced gas flow and the thermal heat transfer in solids is very sensitive. It could be that the gas inlet flow differs somewhat from reality, changing the kinetics and ultimately the temperature. Furthermore, an ideal gas is assumed, which is reasonable under the current conditions but not perfect. Considering the complexity of the model and the multiple approximations made, the results show a rather good agreement between the measured temperature and the predicted one with a relative error between -13 and 4 %.

Table 3.1: Stationary temperature at edge substrate for different laser irradiances and flow conditions.

Irradiance (W/mm ²)	Ar flow (sccm)	Experimental	Model	Rel. error (%)
9.7	500 sccm	278 °C	241 °C	-13.4
	50 sccm	303 °C	275 °C	-9.2
17.9	500 sccm	429 °C	406 °C	-5.4
	50 sccm	472 °C	454 °C	-3.8
26	500 sccm	546 °C	548 °C	0.4
	50 sccm	583 °C	605 °C	3.8

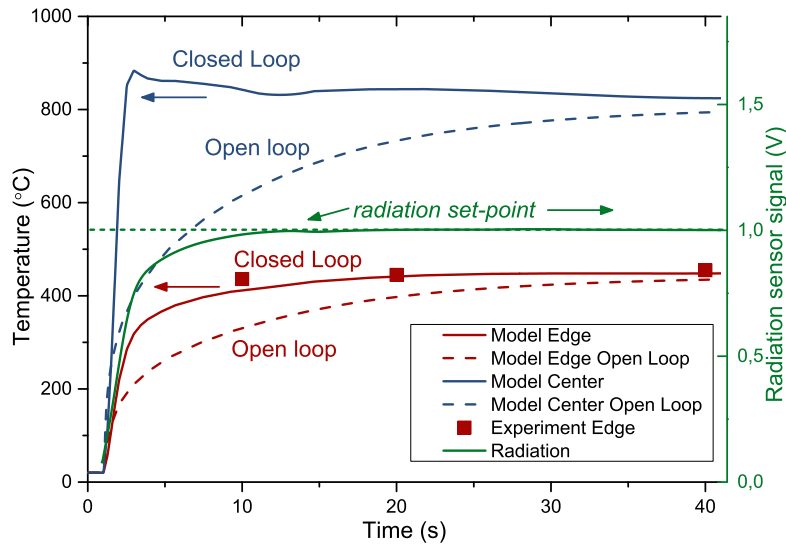


Figure 3.3: Modeled temperature as a function of time in closed-loop setup compared with modeled temperature in open-loop. Also plotted is the radiation in volts as a function of time. This radiation is the controlled parameter.

3.4 Results

Our miniaturized reaction chamber, in combination with the closed-loop control system results in fast, temperature-controlled growth of carbon nanotubes with a precise known gas composition. These benefits can be demonstrated by comparing the closed-loop process with the open-loop case.

3.4.1 Experimental results

To evaluate and quantify the temperature response of the system, the thermal model is used to compare the closed-loop control system operation with an open-loop system. The results are plotted in Figure 3.3. As the emitted radiation is used as the controlled variable this signal (solid line) is plotted together with the reference set-point (dashed line). The particular choice of the PID-controller values results in this case in an over-damped response, without any overshoot. The result is that the radiation set-point is reached after about 15 seconds. A similar response is found in the model, when looking at the temperature at the edge of the substrate (solid line). The real values measured by thermocouple at certain times (squares) are compared with the model and correspond well. The temperature in the center of the laser-spot (solid line) shows a small overshoot but settles around 12 seconds as well. The nature of the overshoot in temperature is not fully understood as the controlled radiation shows no sign of overshooting. It is assumed that the high sensitivity to the input power over time as well as the still simplified model and assumptions could account for the difference between temperature and emitted radiation. The time-step used in the FEM solution might be too large and the real, non-linear response to an instant laser pulse is difficult to model. This assumption is to some extent confirmed by the temperature response at the edge of the substrate. This position is further from the spot and is thus less affected by near non-linear effects. The smooth temperature response, very similar to the radiation signal confirms this.

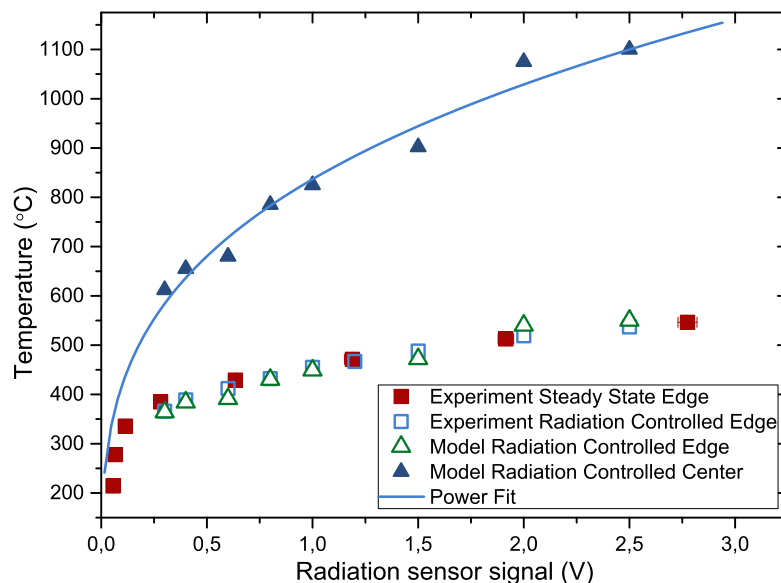


Figure 3.4: Modeled temperature as a function of set-point radiation. The temperatures at the center of the spot (triangles) are fitted with a power law. The temperature at the edge of the substrate is given both by experimentally measuring for open-loop (filled squares) and closed-loop (open squares) as well as the modeled temperature (open triangle).

To find a direct relation between the radiation set-point and temperature, closed-loop experiments were carried out for a range of different radiation set-points. Similar responses as shown in Figure 3.3 were found and the steady-state temperatures of both the center at the laser spot as well as at the edge of the substrate are plotted against the set-point radiation. This is shown in Figure 3.4. The triangles (filled and open) represent the modeled temperature at the center of the laser spot and the edge of the substrate, respectively. To further validate the thermal model, the measured temperature at the edge of the substrate is plotted in this figure. The filled black squares are temperatures obtained with an open-loop experiment reaching a steady-state value and the corresponding emitted radiation. The open squares represent the temperature of the radiation-controlled experiments, measured by thermocouple. Note that the thermocouple could have a systematic error of about 4 °C at 500 °C.

Using the miniaturized reaction chamber, with a radiation-controlled temperature of 850 °C and flow rates of 200, 250 and 50 sccm, for argon, ethylene and hydrogen, respectively a localized hill of aligned carbon nanotubes has been grown, as depicted in Figure 3.5.

3.4.2 Flow simulation results

The forced flow coupled with heat transfer that is solved in the FEM-model allows for a closer investigation of the interaction between applied heat transfer and the corresponding gas flow alteration. In Figure 3.6(a), a typical result is depicted of half of the chamber where the arrows show the direction of the flow and the different colors show the temperature. The gas flow is laminar over the substrate. Looking more closely to the flow, by zooming in to the hotspot, it can be seen that just before (Figure 3.6(b)) the laser is switched on, the flow is laminar but right after the laser is switched on (Figure 3.6(c)) a sudden change in streamlines is apparent.

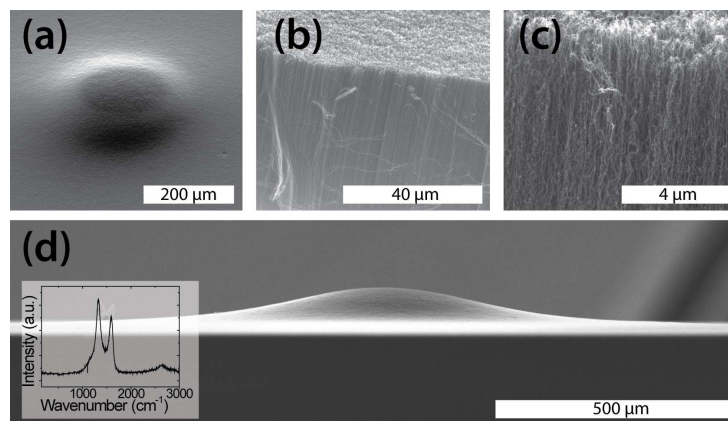


Figure 3.5: SEM Micrographs of a localized hill of vertically aligned carbon nanotube forest created with the miniaturized reaction chamber. (a) Overview. (b) Zoom of the aligned nanotubes after scratching the surface. (c) Enhanced zoom of the top of the nanotubes. (d) Side view. Inset shows Raman intensity signal and indicates multi-walled nanotubes.

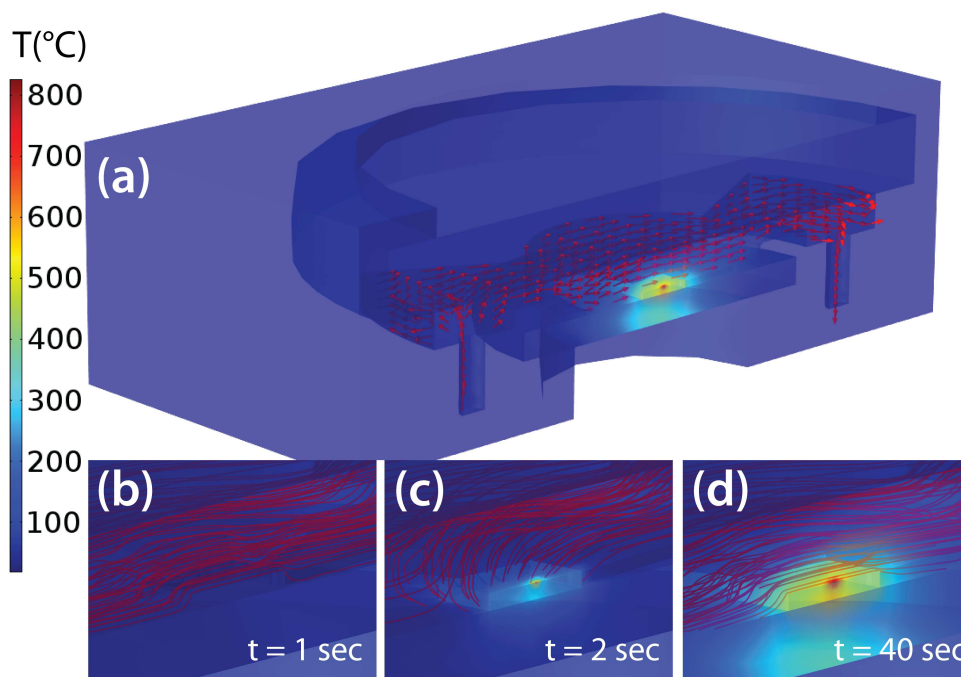


Figure 3.6: Finite Element Modeling results depicted for different times. The red lines are streamlines while the colors depict temperature. (a) Overview of half of the chamber. (b) Zoom of the substrate with flow streamlines at 1 sec. (c) Zoom of the substrate just after laser has been switched on. The flow streamlines show a sudden increase in pressure which affects the flow direction. (d) Zoom of the substrate after 40 sec. The flow has been normalized again.

This effect is due to the instant temperature increase which results in a localized high pressure affecting the flow. After some time (Figure 3.6(d)), the flow is stabilized again, indicating that using this chamber, the forced flow ensures a stable well-known flow of process gases at the growth site.

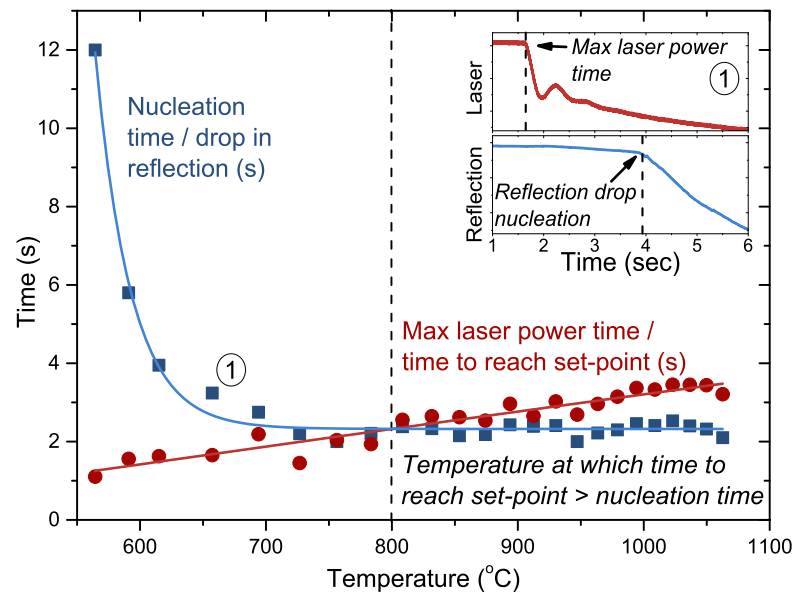


Figure 3.7: Graph comparing nucleation time to reference temperature. Also depicted is the time to reach the reference temperature, which is equal to the time the laser irradiates at maximum irradiance. When that time exceeds the nucleation time, the nucleation time does not decrease anymore. The inset shows the laser and signal response for experiment 1. Indicated are the max laser power time and the nucleation time.

3.4.3 Nucleation

The miniaturized reaction chamber has the advantage of being optically accessible. To investigate growth kinetics, the Si-detector is used to collect the reflected laser light (see subsection 2.3.2). Any growth of carbon nanotubes absorbs laser irradiance, decreasing the reflected laser light. This sensor can thus be used for investigating certain basic growth characteristics. As a proof-of-concept of the capabilities of this method, the nucleation characteristics are investigated. The nucleation and onset of the growth is characterized by a sudden drop in the reflection signal, as was shown in Figure 2.4. The time it takes for the drop in reflection to occur depends on the temperature and the catalyst characteristics. The temperature dependency of the nucleation is shown in Figure 3.7.

At a certain temperature, the nucleation time does not decrease anymore. This is a consequence of the closed-loop system. The laser has a maximum laser irradiance level and for temperatures above 800 °C the time it takes to reach the radiation set-point at the maximum laser irradiance exceeds the nucleation time. Therefore, the nucleation starts while the laser is still ramping up to the reference temperature. The time to reach the set-point is plotted in circles in the figure. Notice that this time does not exceed four seconds, a consequence of the specific PID-controller characteristics which result in a faster reaching of the set-point, allowing some overshoot to occur. The inset of the figure shows the laser and reflection characteristics for the experiment labeled "1" in the figure. The top part of the inset shows a typical laser irradiance response to a certain input reference radiation set-point. The drop of the laser irradiance shows the set-point is (almost) reached ensuring the radiation to remain constant. The resulting reflection is also characterized by a drop, indicating the start of the growth process.

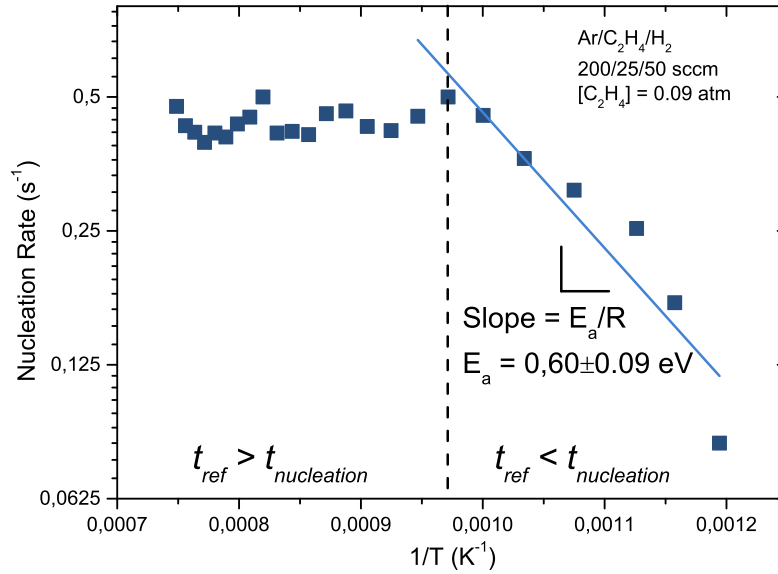


Figure 3.8: Arrhenius plot of the nucleation of the process where the inverse of the temperature is plotted against the nucleation rate, the inverse of the nucleation time. Above a certain temperature the time to reach the reference temperature exceeds the nucleation time, so the rate doesn't increase anymore.

For temperatures below the threshold of 800 °C, it is possible to make an Arrhenius plot where the inverse of the temperature is plotted versus the natural logarithm of the nucleation rate. Arrhenius law states that a process can be characterized by a rate constant k which is given by,

$$k(T) = \nu e^{-E_A/RT} \tag{3.1}$$

Here, ν is the prefactor which is reaction dependent, E_A , the activation energy, R the universal gas constant and T the temperature. In this case, the nucleation rate is defined as the inverse of the nucleation time. The slope can be calculated by taking the natural logarithm of the rate and plotting it against the inverse of calculated temperature. The results are presented in Figure 3.8. The linear fit of the part below 800 °C is shown as a straight line. From the slope of this line, the apparent activation energy for this nucleation process can be extracted. The apparent activation energy is calculated to be 0.60 eV. The activation energy is usually calculated from measuring the growth rate of the nanotubes instead of measuring the onset of growth, as is done in this study. Nevertheless, the catalyst reduction and re-structuring process are important processes with respect to the resulting CNT growth and morphology. However, as seen in section 2.6, the catalyst preparation process is difficult to comprehend. To fully model the multi-parameter problem, molecular dynamical simulations are required which goes beyond the scope of this thesis.

To validate the experimentally obtained activation energy, the results from the thermal model are used to evaluate the internal energy of the process around the laser hot spot. For the different experiments the specific internal energy is evaluated at the time the nucleation starts (see Figure 3.7). The internal energy is calculated by multiplying it by the molar mass of the iron catalyst. The values obtained from the thermal model range from 0.52 eV to 0.62 eV, in good agreement to the experimentally obtained value. In the next chapter, the activation

energy of carbon nanotube growth will be discussed in more detail and the characterization of the process will be continued.

3.5 Summary

This chapter shows the versatility of the specifically designed miniaturized reaction chamber. As a direct result from the laser-assisted growth process, a fast heating rate is achieved while the radiation feedback control prevents overheating. A precise knowledge of gas composition during synthesis is now available due the forced laminar flow over the substrate. This resulted in the ability to grow a well defined forest of vertically aligned CNTs.

Thanks to an enhanced FEM thermal model combining heat and flow, the temperature is known with an accuracy of within 13% in open-loop. With this information, nucleation kinetics and corresponding apparent activation energy can be investigated as demonstrated by the proof-of-principle in subsection 3.4.3. An additional result of the small reaction chamber is the much shorter experimentation time and the ability to move the chamber during laser irradiance as will be discussed in chapter 5, *Application perspectives*.

Chapter 4 |

Growth kinetics

In this chapter, a detailed investigation of carbon nanotube growth kinetics related to physical and chemical process characteristics is presented. Specifically, the growth kinetics is investigated by monitoring the dynamical changes of reflected laser beam intensity during growth. Benefiting from the fast growth and high experimental throughput, a wide range of experimental conditions is investigated and several growth regimes are proposed. Rate-limiting steps are determined using rate equations linked to the proposed growth regimes, which are further characterized by Raman spectroscopy and Scanning Electron Microscopy (SEM). Activation energies for the proposed regimes are found in the range of 0.3 - 0.8 eV.

Part of this chapter has been published in

Y. van de Burgt, Y. Bellouard, R. Mandamparambil, *Kinetics of Laser-Assisted Carbon Nanotube Growth*, Physical Chemistry Chemical Physics 16, 5162-5173 (2014).^[5]

4.1 Introduction

Vertically aligned carbon nanotube (CNT) structures are desirable for many applications. Their unique structural, electronic and thermal properties make them ideal candidates for applications such as field emitters,^[18,19] field effect transistors,^{[15][16]} filters,^[25–27] interconnects^[28] and sensors.^[22] So far, producing aligned nanotube structures has been achieved almost exclusively by chemical vapor deposition (CVD). This process allows a high degree of control over the resulting growth and morphology by tailoring the catalyst that adsorbs and dissociates the carbonaceous gas. Despite enhanced control, the quality of CVD-produced nanotubes is generally poor as a result of a relatively high defect presence. Further improvements can be achieved through a better understanding of the growth kinetics and the various catalytic mechanisms.

Carbon nanotube growth kinetics and its dependence on process gases are currently not fully understood. The precise reaction process is still under debate.^[114] Growth-limiting reaction steps depend on precise growth conditions and resulting activation energies vary widely between experimental conditions such as temperature, pressure, catalyst and gas composition but also between subsequent experiments with seemingly identical conditions.

The small reaction chamber with precise control of the composition of the laminar flow of process gases is used, as described in the previous chapter. This allows for *in situ* determination of the growth kinetics while maintaining a higher experimental throughput than conventional CVD growth. Specifically, the influence of feedstock gas flow and composition as well as the corresponding kinetics involved in laser-assisted CVD growth of carbon nanotubes is investigated. From kinetic relations, several different growth regimes and corresponding rate constants are derived and proposed. The regimes are linked to elementary steps of the CNT growth process, as schematically proposed in Figure 4.1. The influence of the three different process gases, ethylene, argon and hydrogen, is related to the proposed regimes and confirmed by micro-Raman spectroscopy quality measurements. Using time-resolved reflectivity measurements, first order dynamics of the growth of carbon nanotubes are obtained which are used to calculate activation energies for the different regimes. Finally, by exploring the growth rate of the carbon nanotubes as a function of several partial pressures, the various reaction orders are derived.

The laser-assisted growth method investigated in this thesis is of specific interest for determining carbon nanotube growth kinetics in general, as the nature of the localized laser-heated process allows for a fast and high throughput *in situ* investigation of the growth characteristics with respect to the experimental conditions.

4.2 Experimental setup for measuring growth kinetics

The experimental setup consists of a feedback-controlled laser-assisted carbon nanotube growth process, as described in chapter 2, combined with the miniaturized reaction chamber from chapter 3 that allows the process gases (argon, hydrogen and ethylene) to flow in a controlled manner over the substrate. To investigate growth kinetics, the reflected laser signal is dynamically measured. A sudden drop in reflection is attributed to the initiation and growth of the

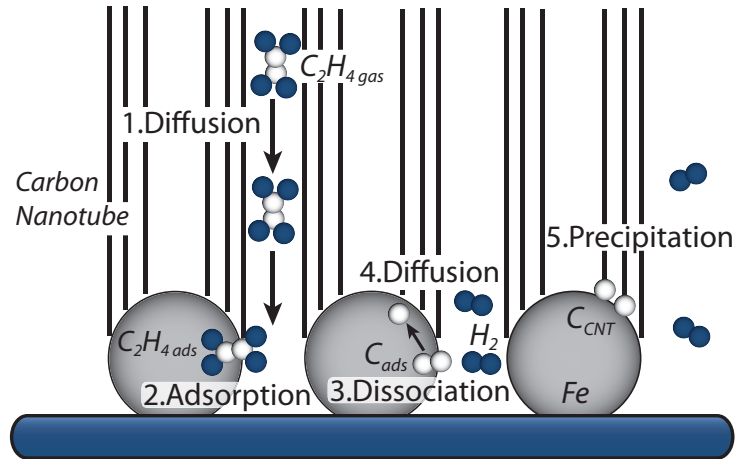


Figure 4.1: Schematic of the carbon nanotube growth process investigated in this study. 1. Diffusion of the ethylene through the CNT forest. 2. Adsorption of ethylene onto the catalyst. 3. Dissociation of ethylene into adsorbed carbon and hydrogen gas. 4. Diffusion through the catalyst. 5. Growth of the carbon nanotube.

carbon nanoforest (see subsection 2.3.2), indicated with t_n in Figure 4.2. The average growth rate is calculated by dividing the estimated length of the nanotube forest by the growth time ($t_{20\%} - t_n$) as indicated for two cases in the figure. This is done for several process conditions to confirm the CNT length for a specific intensity. The time $t_{20\%}$ is chosen to be shorter than the lifetime of the catalyst since the growth continues, demonstrated by the exponential decay of the reflected laser intensity. Combined with FEM modeling, the temperatures involved in an experiment can be calculated which allows for the investigation of activation energies. The decay of the intensity seems to follow the Beer-Lambert law,

$$I(z, t) = I_0 e^{-2\alpha z(t)} \quad (4.1)$$

where I is the intensity, z is the average thickness of the layer and α its absorbance. In that case the absorbance α can be estimated with,

$$\alpha = \frac{\ln(I_0/I)}{2z} \quad (4.2)$$

Several lengths of CNTs and corresponding intensities were used to estimate α . Surprisingly, this resulted in a variation of the absorbance over time in contrast to results from Poretzky *et al.*^[132] This dynamically changing absorbance might imply a CNT density variation during growth. For that reason, the CNT forest lengths at their highest point under different experimental conditions is manually measured. This method bypasses the uncertainties in the growth rate calculations as a result of the varying absorbance α and an estimation of the average growth rate can be made.

4.2.1 Growth rate

The growth rate changes dynamically over time as well, where a much higher growth rate is measured at the beginning than at the end of the process. This can also be seen in Figure 4.2,

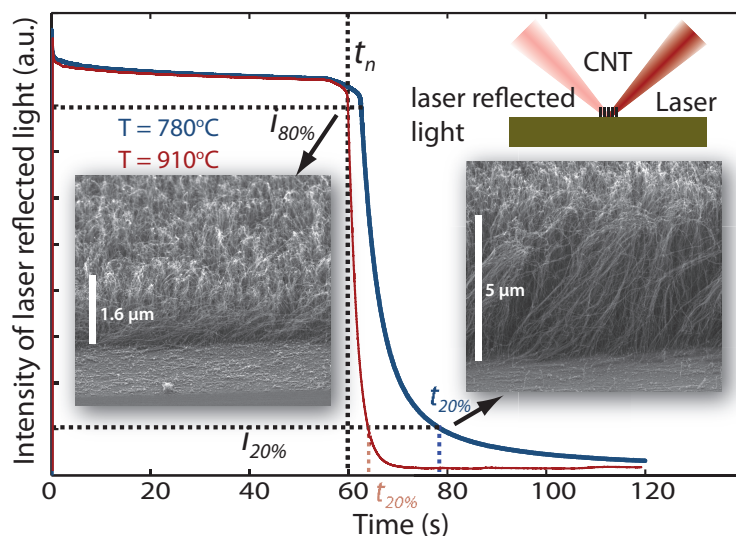


Figure 4.2: Plot of the intensity of reflected laser signal versus time for two different experiments. Indicated in the figure are the nucleation time t_n and the intensity level of the signal of 80% and 20% of the maximum value, $I_{80\%}$ and $I_{20\%}$ respectively. For the 20% intensity the time at which this is reached is depicted for both experiments as well. Also shown are the corresponding SEM pictures of the nanotube forest at the intensity levels 80% and 20%. The inset shows a schematic representation of the growth of CNTs by laser irradiance and the laser reflected signal.

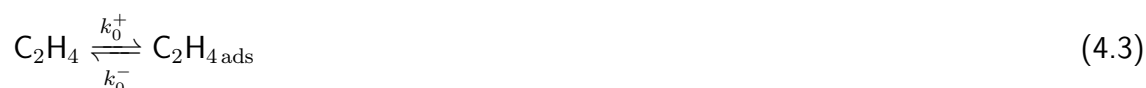
where the CNTs have a length of already $1.6 \mu\text{m}$ at $I_{80\%}$ and grow only to about $5 \mu\text{m}$ at $I_{20\%}$, significantly later. At $I_{40\%}$ the length was estimated to be $2 \mu\text{m}$. The corresponding growth rates for 780°C were found to be $3.3 \mu\text{m/s}$, $0.75 \mu\text{m/s}$ and $0.74 \mu\text{m/s}$ respectively. These results indicate that the initial growth rate is much higher but eventually becomes constant.

4.3 Growth kinetics

The catalytic chemical vapor deposition growth of carbon nanotubes can be schematically represented by a number of elementary steps.^[132,148] Those steps are graphically presented in Figure 4.1. The ethylene gas has to reach the catalyst, by a forced flow or natural diffusion. Diffusing through the nanotube forest might play a role, although that process is assumed to be very fast; giving notable effects only at nanotube lengths much greater (in the order of mm) than what is expected here.^[149] When the ethylene reaches the catalyst, it is adsorbed onto the iron catalyst surface. This step is followed by a dissociation step, resulting in adsorbed carbon and hydrogen. The adsorbed carbon diffuses through or over the catalyst to the growth side where it precipitates as part of the carbon nanotube.

4.3.1 Rate equations

The following relations can be given regarding the growth kinetics of the different elementary steps,





Here k^+ and k^- are the rate constants for the forward and backward reaction, for respectively the reaction from ethylene gas into adsorbed ethylene k_0 , from adsorbed ethylene into adsorbed carbon and hydrogen k_1 , and from adsorbed carbon into carbon nanotube k_2 .

Equilibrium of gas phase ethylene with adsorbed ethylene under normal process conditions is assumed. With the further assumption that the gas phase concentration of ethylene does not change, i.e. a sufficient supply of ethylene gas is present, Equation 4.3 becomes,

$$\frac{d[\text{C}_2\text{H}_4]}{dt} = 0, \rightarrow K_0 = \frac{k_0^+}{k_0^-} = \frac{[\text{C}_2\text{H}_{4\text{ads}}]}{[\text{C}_2\text{H}_4]} \quad (4.5)$$

where K_0 is an equilibrium constant for the reaction between ethylene and adsorbed ethylene. From the theory of kinetics and Equation 4.4, the rate equation for the adsorbed carbon as a function of the concentration (or partial pressure) of the different components can be written,

$$\frac{d[\text{C}_{\text{ads}}]}{dt} = 2k_1^+ [\text{C}_2\text{H}_{4\text{ads}}] - (k_2^+ + k_1^-) [\text{C}_{\text{ads}}] [\text{H}_2] \quad (4.6)$$

Note that for a total pressure of 1 bar, the concentration and partial pressure of the different gases are interchangeable in these relations. The hydrogen concentration is assumed to be constant, i.e. the produced hydrogen from dissociation is much less than the feedstock hydrogen. In other words,

$$\frac{d[\text{H}_2]}{dt} = 0, \quad [\text{H}_{2\text{diss}}] \ll [\text{H}_{2\text{feed}}] \quad (4.7)$$

Solving the linear differential Equation 4.6 results in

$$[\text{C}_{\text{ads}}] = \frac{C}{e^{(k_2^+ + k_1^-)[\text{H}_2]t}} + \frac{2k_1^+}{k_2^+ + k_1^-} \frac{[\text{C}_2\text{H}_{4\text{ads}}]}{[\text{H}_2]} \quad (4.8)$$

where C is an integration constant. With the assumption that no carbon is adsorbed at $t = 0$ this can be further reduced to

$$[\text{C}_{\text{ads}}] = \frac{2k_1^+}{k_2^+ + k_1^-} \frac{[\text{C}_2\text{H}_{4\text{ads}}]}{[\text{H}_2]} (1 - e^{-k_2^+[\text{H}_2]t}) \quad (4.9)$$

In this expression the exponential term defines the "start-up" phase, which depends on the hydrogen partial pressure. In steady-state, i.e. for sufficiently large t , the exponential term disappears. The growth rate, R_G , of the carbon nanotubes can be expressed as,

$$R_G = \frac{d[\text{C}_{\text{CNT}}]}{dt} = k_2^+ [\text{C}_{\text{ads}}] \quad (4.10)$$

Taking into account all elementary steps depicted in Figure 4.1, different growth regimes are identified, having specific rate-limiting steps that arise for different process conditions.

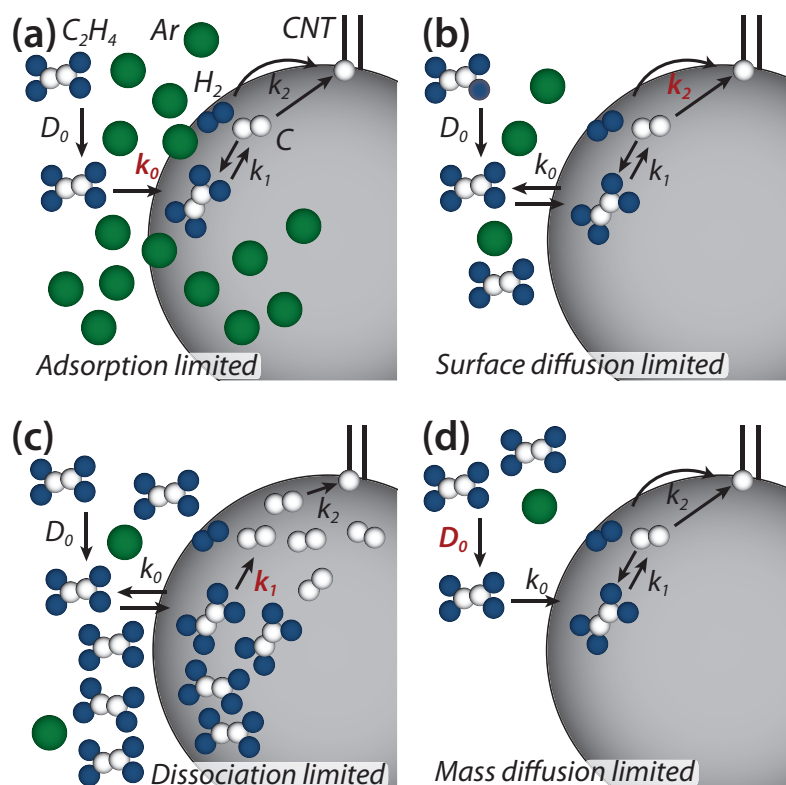


Figure 4.3: Schematic overview of different catalytic carbon nanotube growth regimes. (a) Adsorption-limited: For low ethylene partial pressure, the adsorption on the catalyst is the rate-limiting step. (b) Surface diffusion-limited regime: diffusion through the catalyst and precipitation of the nanotube are expected to be the rate-limiting step. (c) Dissociation limited regime: the dissociation of ethylene into carbon is considered the rate-limiting step. (d) Mass diffusion-limited: for low velocities, the renewal rate is low which results in local under-supply of ethylene.

It is generally assumed that the rate-determining step is equal to the process step with the highest energy barrier. However, different experimental conditions can lead to different energy barriers and corresponding growth regimes. This can be explained by the fact that energy barriers are usually a combination of different elementary steps, which can act differently under different conditions such as temperature and partial pressure but also the coverage degree of the catalyst. The resulting activation energies have been found to vary widely in literature depending on the rate-limiting mechanism. The rate-limiting growth regimes for the catalytic CVD growth of carbon nanotubes that are considered here are *adsorption-limited*,^[150] *surface diffusion-limited*,^[150, 151] *dissociation-limited*,^[152, 153] and *mass diffusion-limited*^[154, 155] and are schematically depicted in Figure 4.3. By varying the experimental conditions, the characteristics of these regimes are investigated.

4.3.2 Growth regimes

Adsorption-limited regime

It was shown by Lebeveda *et al.*^[150] that for low ethylene partial pressure, the adsorption of ethylene on the catalyst surface is the rate determining step. Although in the system described

in this thesis also a carrier gas is present, this inert gas does not participate in the chemical reaction and as such this regime is assumed to be equivalent to the one described by Lebeveda *et al.* The effective coverage of ethylene on the catalyst is very low and the dissociation step, k_0^+ , becomes the pre-dominant step. This is schematically shown in Figure 4.3(a) where the red colored rate constant k indicates the rate determining step. For this, the dissociation step from adsorbed ethylene to adsorbed carbon, k_1^+ is assumed to be much faster. Furthermore, k_0^+ is lower than the surface diffusion and precipitation step, k_2^+ . This will result in low growth rates and, without sufficient carbon supply, the introduction of defects.

For a constant pressure of 1 bar, this regime only occurs with a high partial pressure of argon gas and corresponding high flow rate. These high flow rates ensure a steady-state ethylene concentration around the catalyst and as a result the local gas phase ethylene concentration and partial pressure do not change.

Surface diffusion-limited regime

With increasing ethylene partial pressure, sufficient ethylene can reach the surface of the catalyst and can reach equilibrium with the adsorbed ethylene and carbon. The surface diffusion and nanotube precipitation become the rate-determining step, where the reaction rate of the growth k_2^+ is much lower than the rate of reaction back to ethylene, k_1^- , see Figure 4.3(b). This means the first step is virtually at equilibrium and a steady-state of the adsorbed carbon can be assumed; in which the carbon nanotube growth does not affect the concentration of the adsorbed carbon

$$\frac{d[C_{\text{ads}}]}{dt} = 0, \quad k_2^+ \ll k_1^- \quad (4.11)$$

This further simplifies Equation 4.6,

$$K_1 = \frac{2k_1^+}{k_1^-} = \frac{[C_{\text{ads}}][\text{H}_2]}{[C_2\text{H}_4]_{\text{ads}}} \quad (4.12)$$

where K_1 is an equilibrium constant. Using Equation 4.10 and K_0 from Equation 4.5, it then follows that

$$[C_{\text{ads}}] = K_1 K_0 \frac{[C_2\text{H}_4]}{[\text{H}_2]} \quad (4.13)$$

$$R_G = k_2^+ [C_{\text{ads}}] = k_2^+ K_1 K_0 \frac{[C_2\text{H}_4]}{[\text{H}_2]} \quad (4.14)$$

This relation suggests that the growth rate in this regime is depending on both the ethylene and hydrogen concentration. The growth rate is also proportional to the equilibrium constants K_0 and K_1 of the reaction between gas phase ethylene and adsorbed ethylene and the reaction between adsorbed ethylene and carbon and hydrogen, respectively.

Dissociation-limited regime

A further increase of the ethylene partial pressure causes the equilibrium of adsorbed ethylene and carbon to shift towards a nearly complete covering of adsorbed ethylene on the catalyst. In this case any dissociated ethylene will almost immediately be incorporated into a nanotube. Typical for the dissociation-limited regime is that the dissociation rate becomes the rate-limiting step. In this case, the rate-determining chemical equation is,



Because the dissociation transition from adsorbed ethylene into adsorbed carbon is the rate-determining step, the process of diffusion and incorporation of the carbon into a nanotube is assumed to be faster and thus k_1^- is assumed to be negligible. In fact, a very high partial pressure of ethylene could cover the whole catalytic active surface. The saturated catalyst could prevent the reaction back into adsorbed ethylene. This is schematically represented in Figure 4.3(c).

Overall, this reaction is limited by the reaction rate constant k_1^+ and as such the concentration of adsorbed ethylene is assumed to be in equilibrium with the gas phase ethylene via the equilibrium constant K_0 . Using Equation 4.9, for the steady-state situation can be written,

$$[\text{C}_{\text{ ads}}] = \frac{2k_1^+ [\text{C}_2\text{H}_4_{\text{ ads}}]}{k_2^+ [\text{H}_2]} \quad (4.16)$$

where the k_1^- term is neglected. Using Equation 4.10 and Equation 4.5 the growth rate can then be written as,

$$R_G = k_2^+ [\text{C}_{\text{ ads}}] = 2k_1^+ K_0 \frac{[\text{C}_2\text{H}_4]}{[\text{H}_2]} \quad (4.17)$$

This result suggests that the growth rate is similar to the surface diffusion-limited regime except it is now only depending on k_1^+ and K_0 , where k_1^+ is the dissociation term.

Mass diffusion-limited regime

Finally, the mass diffusion regime is considered, which also occurs at a high ethylene partial pressure. However, this regime is characterized by very low flow velocity around the catalyst so that the mass diffusion of ethylene to the catalyst becomes the rate-limiting step. In this case, the consumption of ethylene exceeds its supply by diffusion. On increasing ethylene partial pressure, as a result of a decreasing argon flow, the diffusion constant decreases which can finally result in an undersupply of carbon at the catalyst.^[150] This regime is characterized by a low activation energy.^[148]

4.4 Results

With the different proposed regimes, combined with the rate equations for CNT growth, the rate-limiting steps as proposed in Figure 4.1 can be investigated. A wide range of experimental conditions is considered in order to study and optimize the carbon nanotube growth. The quality and morphology of the resulting growth is compared as a function of temperature and partial pressure of the different process gases, linking the results to the growth regimes described in the previous section. The fast *in situ* growth of the laser-assisted CVD method results in the ability to rapidly explore a wide range of different experimental conditions and to determine the activation energies for the different rate-limiting mechanisms.

4.4.1 Influence of temperature

Thermal modeling of the process, as described in chapter 3 is used to investigate the influence of temperature. For ideal gases, the rates of reaction are dependent on the temperature T , the universal gas constant R and the activation energy E_A following Arrhenius law,^[156]

$$k(T) = \nu e^{-E_A/RT} \quad (4.18)$$

where ν is the frequency factor. Similarly, the equilibrium constant K is dependent on the temperature and gas constant through the following relation,

$$K(T) = e^{-\Delta H/RT} \quad (4.19)$$

where H is the reaction enthalpy. As a direct consequence, the growth rate of CNTs generally is higher for higher temperatures. To investigate the quality of the grown nanotubes, micro-Raman spectroscopy is used.^[81] The Raman signal includes several peaks that are characteristic for certain vibrational modes of molecules. The quality of the carbon nanotubes is usually assessed by the ratio of the intensity of the defect-peak (D) with the graphite peak (G). The lower this ratio, the higher the quality.

In general, the quality of the nanotubes grown with a CVD process with ethylene and iron increases until about 900 °C.^[109,157] A similar trend is found in Figure 4.4, where the ratio of D and G intensity is plotted against estimated process temperature. The data is fitted with a polynomial fit and shows a minimum around 950 °C. The figure inset shows two typical Raman spectroscopy graphs, with graph 1 showing low quality mostly multi-wall CNTs while graph 2 clearly shows single-walled high quality CNTs. These results indicate the highest quality CNTs at a higher temperature than proposed in section 2.7. The reason for that could lie in the different experimental conditions. The local gas composition in the statically filled reaction chamber in chapter 2 is unknown as a result of possible higher carbon consumption than supply. Together with a high thermal gradient that could induce local turbulence, this could result in a different temperature for the highest quality. The enhanced accuracy of the thermal model could play role as well. The thermal model of the miniaturized chamber does not include an estimated natural convection term but relies on the numerically calculated value of this term instead.

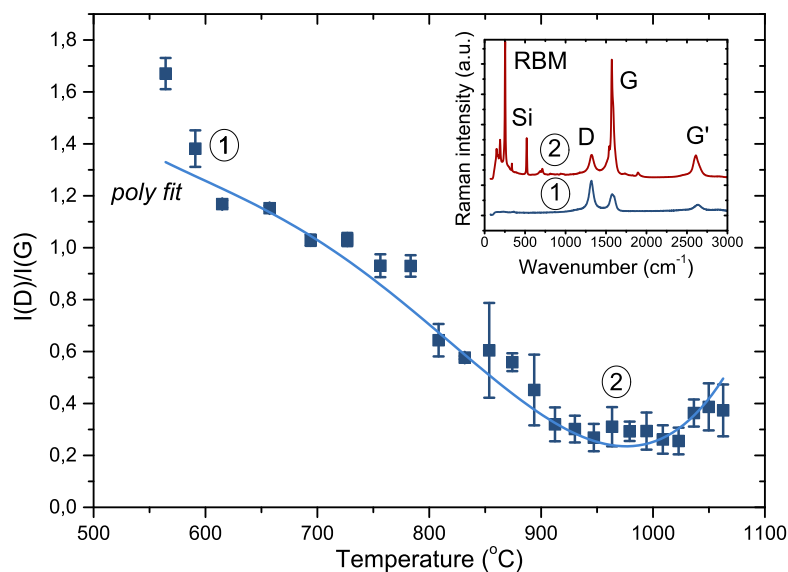


Figure 4.4: Estimated process temperature versus $I(D)/I(G)$. The figure inset shows typical Raman intensity spectra for two different experiments specified in the figure. Indicated in the figure are characteristic peaks for the radial breathing modes (RBM), Silicon (Si), the defect-peak (D), the graphite-peak (G) and the second order graphite peak (G').

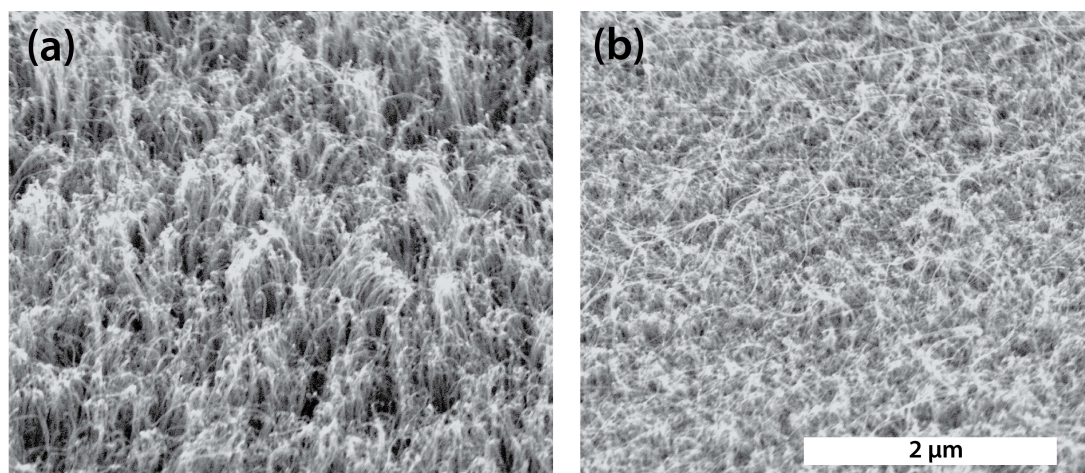


Figure 4.5: SEM pictures showing the influence of the temperature. (a) 718°C (b) 1044°C.

The decrease in the quality after a certain temperature can be attributed to an increase in the pyrolysis of ethylene. At high temperature the non-catalytic decomposition of ethylene increases, usually in the form of amorphous carbon deposition. This trend can also be a consequence of the increased reaction rate in the surface diffusion-limited regime. Higher temperatures can also lead to a more efficient dissociation and thickening of the nanotube walls, introducing defects and decreasing overall quality of the CNTs.^[97] Although the growth rate and quality generally are higher for higher temperatures, at very high temperatures the resulting growth morphology consists of predominantly un-aligned CNTs forming a thin spaghetti-like nano-carpet (see Figure 4.5). Most probably a few high quality single-wall nanotubes contribute to the low $I(D)/I(G)$ ratio and the growth terminates quickly, hampering the formation of forests. In the growth rate study, the structure of the CNTs are assumed to be more or less identical, i.e. aligned multi-wall CNTs.

4.4.2 Growth rate and activation energy

The CNT growth rate is proportional to the reaction rate k and the concentration or partial pressure of adsorbed carbon, according to Equation 4.10. Using Equation 4.18 the activation energy, E_A , of a reaction rate process can be found. Assuming the CNT growth rate R_G is proportional to k , the natural logarithm of the growth rate can be plotted against the inverse of the temperature and the same Arrhenius law can be used to find the activation energy for R_G using

$$R_G \sim e^{-E_A/RT} \quad (4.20)$$

In this case E_A , is the apparent activation energy, since it includes all elementary steps included in the carbon nanotube growth. Although the precise underlying mechanism is still under debate, different groups have determined the rate-limiting step and activation energy for carbon nanotube growth.^[70, 130, 148, 150–153, 158–175]

Baker *et al.* argued that the rate-limiting step must be carbon diffusion in bulk iron resulting from the resemblance of the activation energy of bulk diffusion with their calculated activation energy.^[159] Other groups found similar results relating the activation energy to bulk carbon diffusion^[161, 164, 169] as the activation energy was between 1.3 and 2 eV corresponding to the bulk diffusion energy of fcc-iron of 1.53 - 1.57 eV.^[85, 176] On the other hand, diffusion of carbon in bulk bcc-iron has an activation energy of about 0.8 eV.^[85, 176] In contrast, other research has shown that the surface diffusion of carbon has a much lower activation energy of about 0.2 - 0.3 eV and is thus energetically favorable.^[151, 160]

The activation energies that were found must be a combination of both dissociation as well as diffusion, as was also proposed by Bronikowski *et al.*^[167] The low values of 0.2 - 0.3 eV were also found in fluidized bed reactors.^[171, 173] Nessim *et al.*^[172] found a very low activation energy of 0.1 eV if the process was carried out without pre-heating of the process gases while with pre-heating an activation energy of 0.9 eV was reported.

Liu *et al.*^[152] and Pirard *et al.*^[153] argued that the mechanism must be surface reaction- or dissociation- limited and reported activation energies of 1.65 eV and 1.25 - 1.4 eV respectively. In comparison, acetylene and ethylene dissociate on the iron surface via CH_x radicals with an activation energy of about 0.6 - 1.4 eV.^[177]

Without experimental estimation of the activation energy, mass diffusion was proposed as the limited process by Zhu *et al.*^[154] and Louchev *et al.*^[165]

These results illustrate the diversity between the attributed underlying mechanisms that determine the apparent activation energy. It is fair to say that the growth process is not fully understood and the variation of the activation energy between 0.1 and 2 eV reflect the strong influence that different process parameters have on the growth mechanism. The direct *in situ* laser-assisted growth process proposed in this thesis offers a quick and versatile method to investigate activation energy for multiple growth regimes.

4.4.3 Influence of ethylene

Using a constant flow of argon and hydrogen, the influence of the flow of ethylene on the growth has been investigated. The partial pressure of ethylene was increased from 0.04 bar

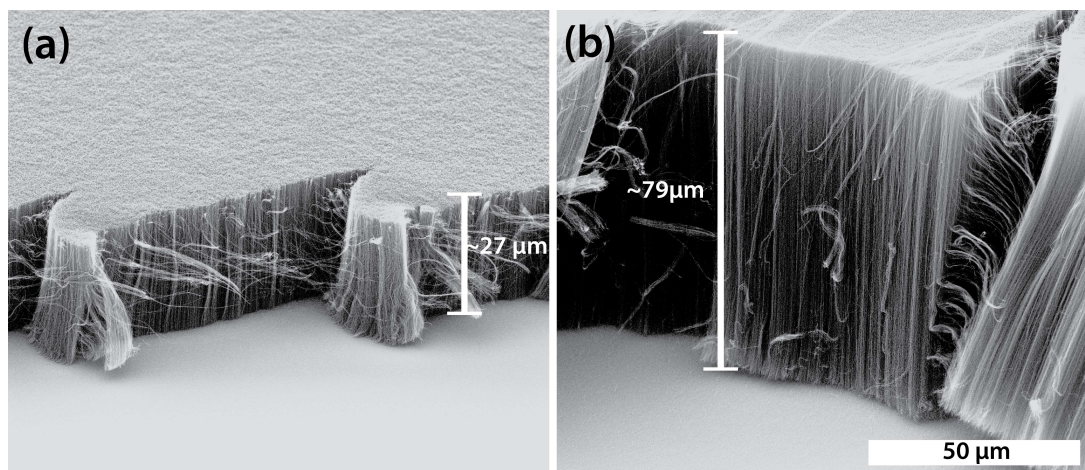


Figure 4.6: SEM pictures showing vertically aligned nanotube forests grown under similar conditions with only partial pressure of ethylene changed. (a) Flow of ethylene 20 sccm (partial pressure = 0.07 bar). (b) Flow of ethylene 250 sccm (partial pressure = 0.5 bar).

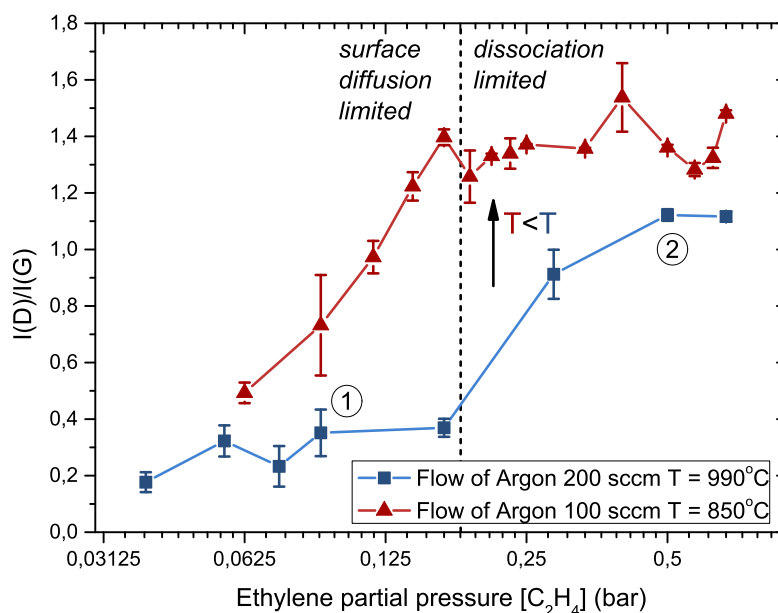


Figure 4.7: Quality of grown CNTs plotted versus ethylene partial pressure for two growth temperatures. Different growth regimes are indicated in the figure.

to 0.7 bar. This was achieved by flowing argon and hydrogen at a constant flow of 200 and 50 sccm respectively and changing the flow rate of ethylene from 10 to 500 sccm. From Equation 4.9 and Equation 4.10, it is expected that a higher ethylene partial pressure leads to higher growth rates. To confirm this, the length of the CNTs is estimated using SEM. This is shown in Figure 4.6. It is clear that the CNT length is lower for a partial pressure of 0.07 bar (ethylene flow of 20 sccm) than for 0.5 bar (ethylene flow of 250 sccm).

By comparing Raman spectroscopy intensity signals a clear trend for increasing ethylene partial pressure is found. Higher pressures, thus higher growth rates, result in lower CNT quality. This could be attributed to defect formation at high growth rates.^[97] An additional reason could

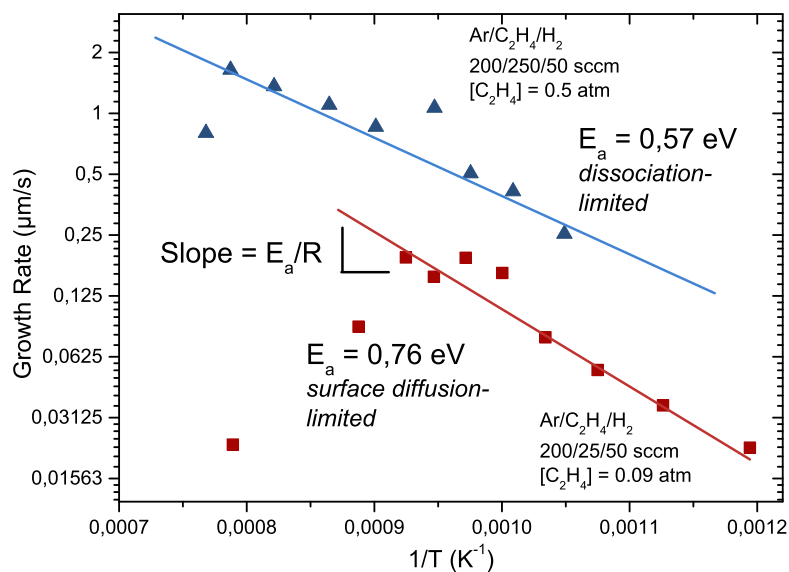


Figure 4.8: Arrhenius plot of the surface diffusion-limited and the dissociation-limited regimes. The CNT growth rate is shown versus the inverse of the growth temperature. Indicated is the partial pressure of ethylene for both graphs as well as the experimental flow conditions.

be the transition to a different regime with a higher density of defects due to the oversupply of carbon and poisoning of the catalyst. In Figure 4.7, the quality of nanotubes is shown as a function of the ethylene partial pressure for two different temperatures and argon flow rates. In this figure, a distinction is made between surface diffusion-limited growth and dissociation-limited growth. The transition between both regimes is positioned around a partial pressure of ethylene of 0.2 bar. For the lower temperature graph (triangles), the decrease in quality starts at a slightly lower ethylene partial pressure, resulting from the lower total flow rate. The overall quality is also lower, in accordance with Figure 4.4.

Activation energies for both regimes are calculated using Arrhenius law, see Figure 4.8. The activation energies for the surface diffusion-limited regime (ethylene partial pressure of 0.09 bar) and for the dissociation-limited regime (ethylene partial pressure of 0.5 bar) are found to be 0.8 and 0.6 eV, respectively. The dissociation-limited regime has the lowest activation energy of about 0.6 eV with a growth rate that is generally higher, in accordance with Equation 4.17. This seems realistic, as the dissociation step is always present and the surface diffusion can vary as a result of the total coverage of carbon on the catalyst surface. High temperatures are excluded from the analysis as they show a sudden decrease in growth rate, a result of the non-aligned growth as discussed before.

Our calculated activation energies are lower than other reported activation energies for surface diffusion- and dissociation-limited processes. However, using plasma-enhanced CVD, Hofmann *et al.*^[151] also reported a very low activation energy of 0.2 eV, which was attributed to surface diffusion only; the plasma involved accounted for the decomposition of the ethylene. Such effects cannot be excluded from these experiments. Another possibility is that in the process the catalyst is quickly transferred into iron-carbide, Fe₃C, where the diffusion of carbon is calculated to be 0.38 eV by Liu *et al.*^[152] Sharma *et al.*^[178] have proposed that the growth of CNTs takes place on cementite that is formed during the reduction process of iron-oxide. A more detailed study of the catalyst chemical composition is necessary to confirm or disprove

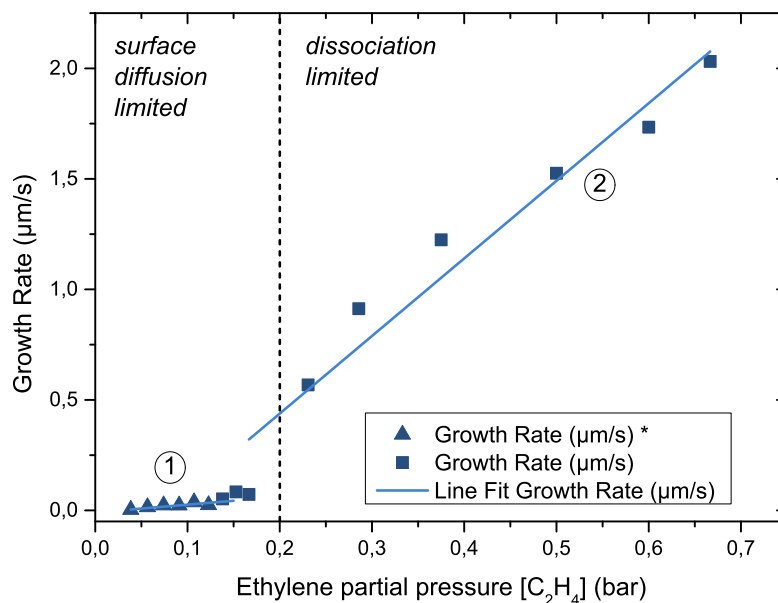


Figure 4.9: Growth rate versus ethylene partial pressure. In both regimes a linear relation was found and the reaction order is therefore assumed to be 1. *Growth rate is calculated using a less significant drop in reflection. Experiments 1 and 2 correspond to experiments 1 and 2 in Figure 4.7.

these assumptions. Finally, the results exhibit uncertainties due to errors introduced by fitting with this amount of data points^[70] and the average growth rate used in the calculations could also account for some deviations.

The reaction rate order of ethylene is investigated by measuring growth rate as a function of ethylene partial pressure. The results are illustrated in Figure 4.9. For both regimes a linear relation is found and as such the reaction order is assumed to be 1, in correspondence with other reported results^[130,150,169] and Equation 4.17. The surface diffusion-limited growth has a much lower linear relation to the ethylene partial pressure than the dissociation-limited growth, which corresponds to both a lower reaction rate constant k and the weaker dependence on ethylene partial pressure for diffusion-limited growth.^[152]

4.4.4 Influence of argon

The rate equations do not include a term for the partial pressure of argon. In fact, the flow of argon and the partial pressure do not influence the ratio of the partial pressures of ethylene and hydrogen, as they will both be changed equally by any change of partial pressure of argon and as such Equation 4.14 will not change. However, the carrier gas argon still influences the growth of the carbon nanotubes. The dilution of the process gases by argon can indeed change the rate-limiting process steps. In effect, the argon flow rate determines the flow speed through the chamber. At the same time, a high argon flow results in a low concentration of both ethylene and hydrogen which may result in an undersupply of those gases at the catalyst site. In that case, the argon molecules will shield the surface sites, decreasing the mean free path of ethylene molecules, effectively preventing them to reach the catalytic surface. On the other hand, with no argon flow, the flow velocity is low which could result in a local

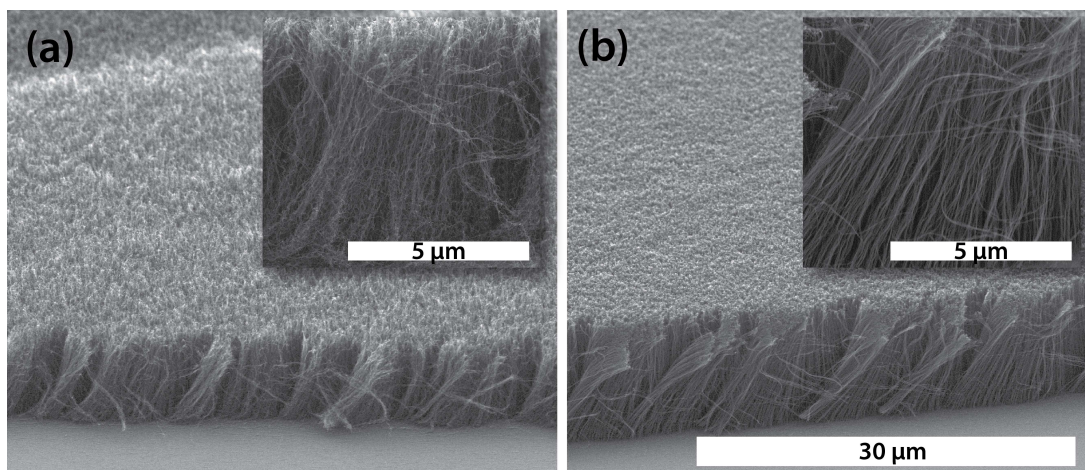


Figure 4.10: SEM pictures showing influence of argon flow and partial pressure on growth rate. (a) Argon flow 10 sccm (partial pressure = 0.14 bar). (b) Argon flow 500 sccm (partial pressure = 0.9 bar). Both insets show a detailed zoom of the morphology of the aligned nanotube forest.

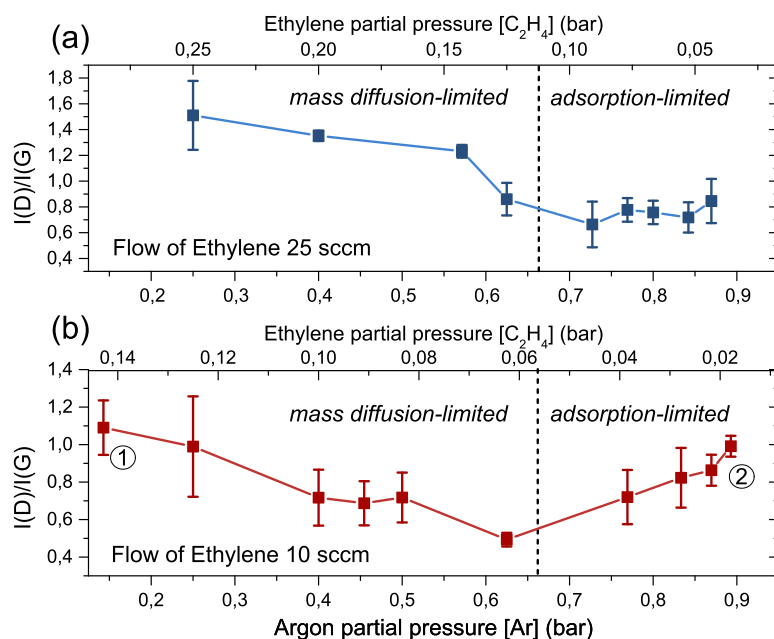


Figure 4.11: Quality of nanotube growth versus argon partial pressure. Indicated are also the ethylene partial pressure and the separation between both regimes. Experiments 1 and 2 correspond to the SEM pictures of Figure 4.10(a) and (b), respectively.

undersupply of carbon, when consumption is higher than supply. For both a low and a high argon partial pressure, the resulting growth is analyzed. This can be seen in Figure 4.10. The SEM pictures show the growth for similar experimental conditions where only the argon flow is changed and demonstrate the similarity of the growth rate of both cases. The insets in the figure show the morphology of the aligned CNT forest which indicates that although the growth rate might be comparable; the morphology of the CNTs is not.

In Figure 4.11 the quality of the CNTs is assessed as a function of argon partial pressure. The other two gases, ethylene and hydrogen, are kept constant. The quality of CNTs is assessed for

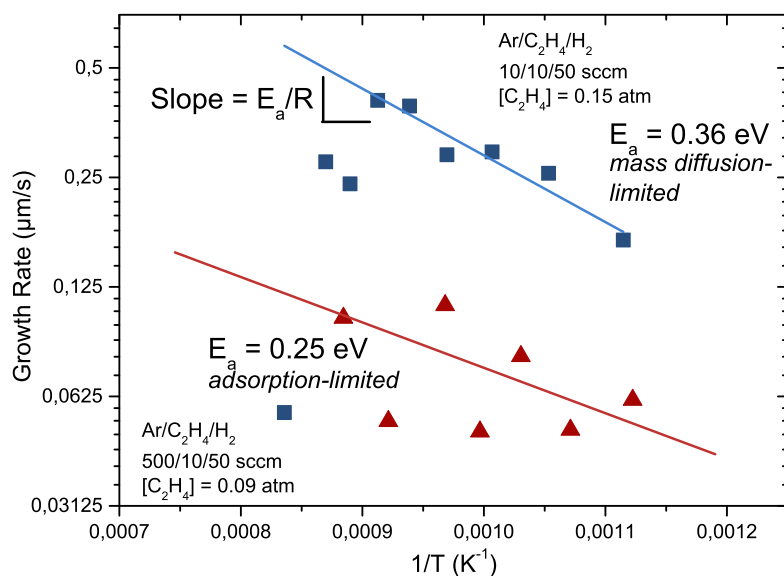


Figure 4.12: Arrhenius plot of the mass diffusion-limited and the adsorption-limited regime. The growth rate is plotted against the inverse of the calculated growth temperature. The partial pressure of ethylene is indicated for both graphs as well as the experimental flow conditions.

two different ethylene flows, 10 sccm, Figure 4.11(a) and 25 sccm, Figure 4.11(b), respectively while the hydrogen flow was 50 sccm throughout.

A clear trend is visible in both graphs. For low argon partial pressures, the quality of the nanotubes is low. This is attributed to the mass diffusion-limited regime where the local consumption of ethylene by the catalyst is higher than the supply of ethylene by diffusion as a result of the very slow flow rate of gases around the hot-spot. In this case that means $k_0^+ < k_1^+$. With insufficient carbon in the catalyst, the growth is not stable which results in low quality CNTs. An optimum value of the quality is found around 0.65 - 0.75 bar argon partial pressure where the change between growth regimes is assumed to be located.

In contrast, an increase in argon flow to high partial pressure also leads to a reduction in the quality. It is hypothesized that this regime is dominated by the adsorption-limited regime. With a high argon flow, the surface coverage of the ethylene is low and not enough carbon atoms are absorbed to ensure a stable growth. This results in both low quality nanotubes as well as lower growth rates. This effect seems to be larger for the ethylene flow of 10 sccm which is plausible considering the amount of ethylene molecules around the catalyst is much lower in that case.

To qualitatively assess both regimes, the activation energy for experimental conditions 1 and 2 from Figure 4.11(b) is calculated. The result is shown in Figure 4.12 where both regimes are fitted with an Arrhenius plot. The resulting calculated activation energies are very low. However, note that the fits are rather inaccurate due to the large scatter of the experimental data; the adsorption-limited regime in particular shows large deviation from the fit. A high sensitivity to changes in process conditions is assumed to be the cause for the large errors. In the adsorption-limited regime, the argon partial pressure is very high, preventing ethylene molecules from reaching the catalyst surface; small deviations in process conditions might therefore have a large impact on the growth rate.

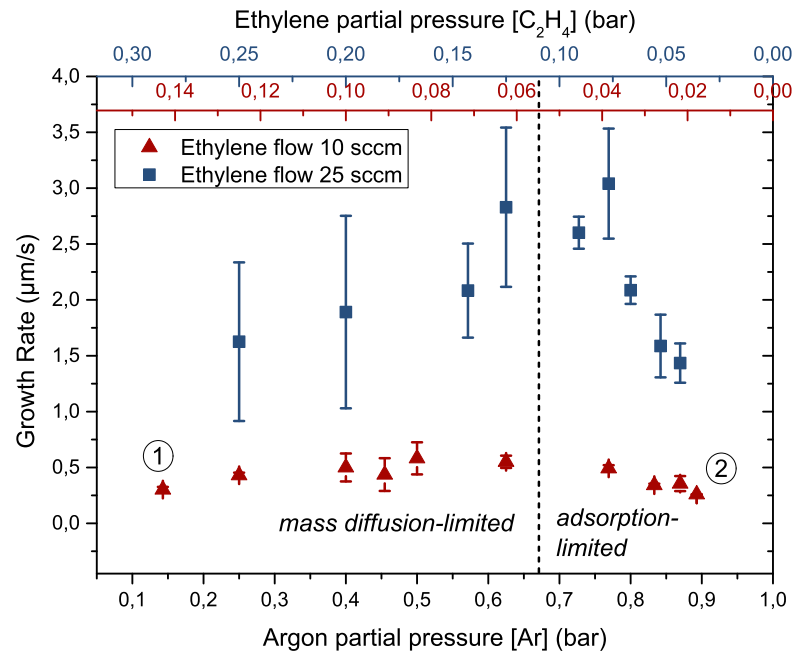


Figure 4.13: Growth rate as a function of argon and ethylene partial pressure for two different ethylene gas flows, 10 and 25 sccm, respectively. From the graph it is clear that argon has negligible influence on the growth rate. The growth rate for the ethylene flow of 25 sccm is larger than that of 10 sccm and larger errors are present in the mass diffusion-limited regime. Indicated in the figure is the transition between the mass diffusion-limited and adsorption-limited regime. Experiments 1 and 2 correspond to experiments 1 and 2 in Figure 4.11 as well as Figure 4.10(a) and (b), respectively.

The mass diffusion-limited regime is expected to have a low dependence on temperature^[150] and thus a low activation energy. Because the driving force is diffusion by concentration difference, it is an unstable regime and also sensitive to small deviations in experimental conditions.

The reaction rate order of argon is investigated by plotting the growth rate as a function of argon partial pressure Figure 4.13. In the figure the proposed growth regimes from Figure 4.11 are indicated. From the figure it is clear that the reaction rate order is not zero but the influence on the growth rate is minimal in the case of an ethylene flow of 10 sccm. For the higher ethylene flow, an increase in argon partial pressure leads to a slight increase in growth rate up to a maximum around an argon partial pressure of 0.67 bar. This can be explained by the increased total flow rate, ultimately overcoming the diffusion-limited growth by forced flow of new ethylene supply. At high argon partial pressure and high flow rates, a visible reduction of the growth rate predicts a reaction order of -1, which can be explained by the increased coverage of the argon molecules on the catalyst, preventing the ethylene from adsorbing and dissociating on the catalyst.

Nucleation rate

In subsection 3.4.3 the nucleation of the process for a certain combination of experimental conditions was discussed, as a proof-of-concept of the abilities of the miniaturized reaction chamber. The nucleation rate N_R was defined as the inverse of the nucleation time t_N . The

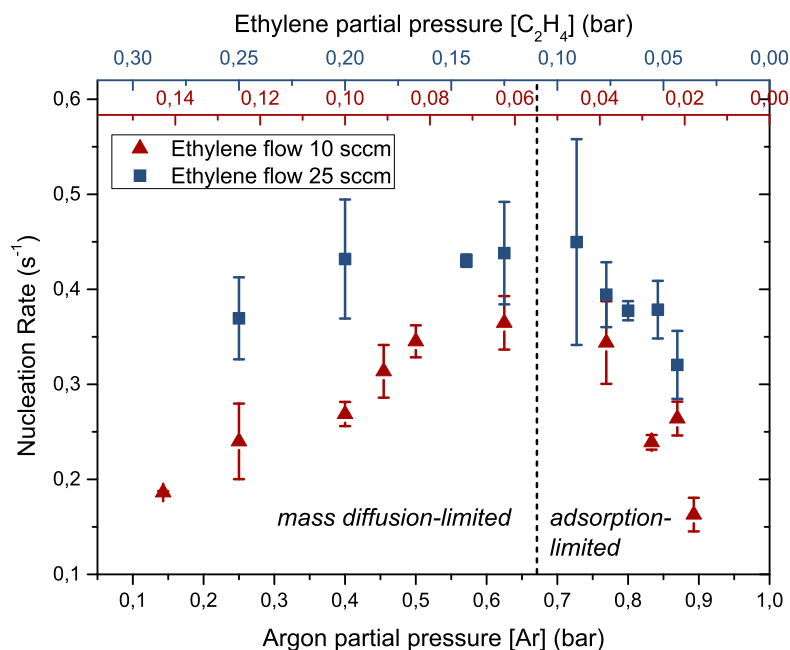


Figure 4.14: Nucleation rate as a function of partial pressure of argon and ethylene for two different flows. The nucleation rate has an optimum around 0.67 bar, i.e. around the transition between the mass diffusion-limited and adsorption-limited growth regimes.

nucleation rate may be seen as a measure of the efficiency of the process. For the nucleation rate experiments, all three gases are flowing through the chamber before the experiment starts, so that the exact time of the nucleation can be extracted as a function of input gas ratio. Similarly as described in subsection 3.4.3. For both ethylene flows, the nucleation rate is plotted in Figure 4.14 as a function of argon partial pressure and ethylene partial pressure. In this figure the maximum nucleation rate is reached around 0.65 bar of argon partial pressure. This value corresponds to the assumed separation of regimes indicated in Figure 4.11. The change in nucleation rate between both regimes is more profound in the case of an ethylene flow of 10 sccm, which follows naturally from the fact that ethylene gas is necessary for the nucleation to start. The trend in the figure can be explained the same way as the trend in Figure 4.11. In the adsorption-limited regime, the amount of argon covering the catalyst is very high; this results in a non-ideal adsorption and decomposition of ethylene on the catalyst and thus a low nucleation rate. In the mass diffusion-limited regime the partial pressure of the ethylene is high enough, but the amount of ethylene around the catalyst is expected to be depleted fast, resulting in a slower nucleation.

4.4.5 Influence of hydrogen

Hydrogen has previously been found to be a key player in the CNT growth process. For instance, it plays a significant role in the reduction process of the iron-oxide catalyst layer and is an excellent thermal conductor and as such has been used as a carrier gas, optimizing growth kinetics. Hydrogen has also been suggested to decompose inactive metal carbides^[179, 180] and plays a significant role in the removal of amorphous carbon from the catalyst surface, preventing catalyst poisoning and increasing the process lifetime.^[181, 182] In contrast, hydrogen has also

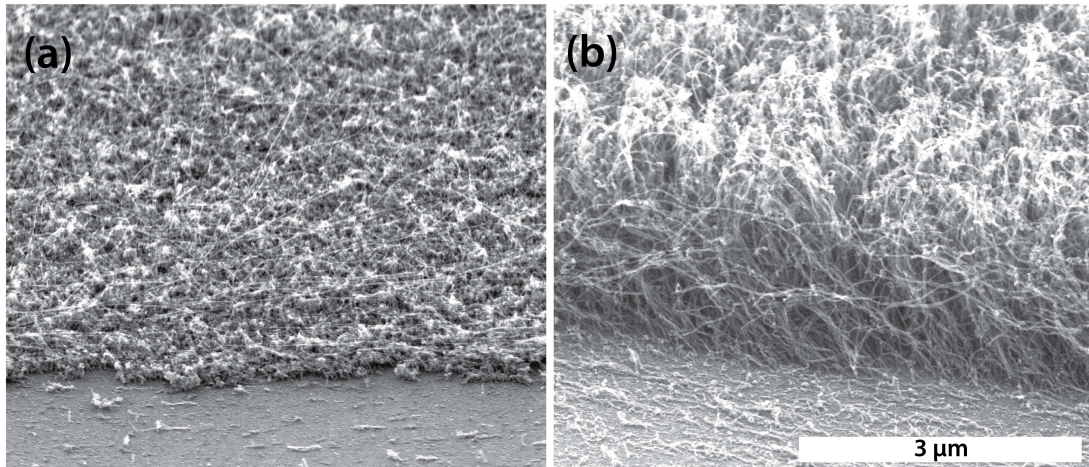


Figure 4.15: SEM pictures of the influence of hydrogen on resulting CNT growth. (a) Hydrogen flow 400 sccm (0.64 bar). (b) Hydrogen flow 25 sccm (0.1 bar).

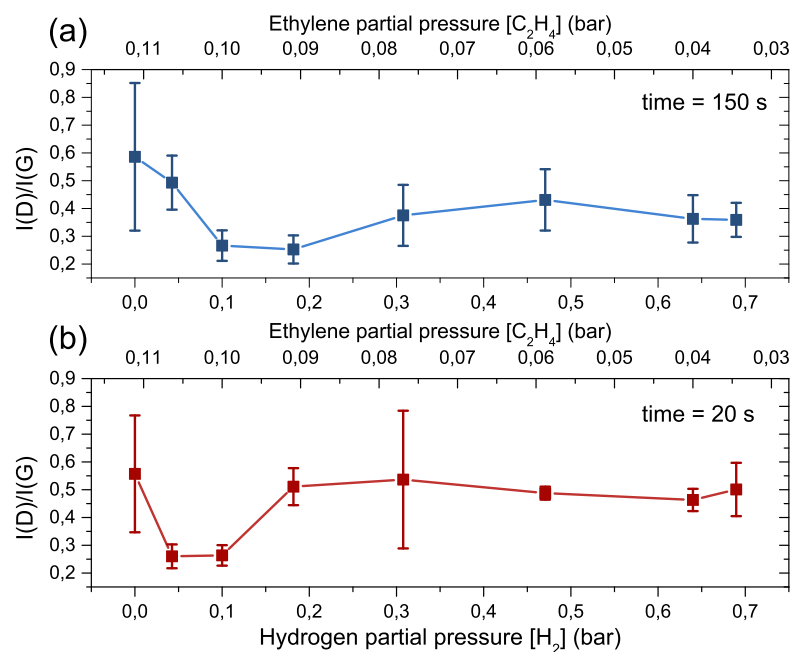


Figure 4.16: Quality of CNTs as a function of hydrogen and ethylene partial pressure for two experimental growth times: (a) 150 seconds and (b) 20 seconds.

been reported to suppress the CNT growth by the formation of methane from carbon.^[179, 180]

The hydrogen incorporated in the ethylene gas can also be used in the reduction process at high temperatures, therefore the influence of hydrogen on CNT morphology and quality is investigated by varying the flow between 0 and 200 sccm (partial pressure 0 - 0.47 bar) while keeping the argon and ethylene flow at 200 and 25 sccm, respectively. The growth rate equations, Equation 4.9 and Equation 4.10 suggest that the hydrogen partial pressure influences the growth rate negatively. In Figure 4.15, two SEM pictures are presented with similar growth conditions except for the hydrogen partial pressure. A high hydrogen partial pressure, Figure 4.15(a), results in a very thin layer of nanotubes while a low hydrogen partial pressure, Figure 4.15(b), results in a forest of longer CNTs.

Since hydrogen is involved in multiple stages of the growth process, the quality of the CNTs is also expected to be influenced by the hydrogen partial pressure. In Figure 4.16, the quality of CNTs is plotted as a function of hydrogen partial pressure and ethylene partial pressure for two durations of laser exposure, 150 and 20 seconds respectively.

A small shift in the minimum $I(D)/I(G)$ ratio can be noticed between the two graphs towards the lower hydrogen partial pressure for shorter laser exposure. Although the overall quality of the 150 second experiments is generally better, the best quality is reached at a higher hydrogen partial pressure than in the 20 second case. As an explanation, Equation 4.9 and Equation 4.10 are considered. The exponential term goes to zero for sufficiently large t . However, the hydrogen partial pressure also plays a role in this term. The difference between both experimental times is that the extra time in the longer experiment, will ensure that the growth rate is stabilized, i.e. an equilibrium is reached, even for low hydrogen partial pressures, and will result in high growth rates due to the inverse relation with hydrogen. High growth rates can introduce more defects. On one hand, a low hydrogen partial pressure for the 20 second case might still be outside equilibrium, resulting in a lower growth rate and more defect free growth. On the other hand, a high hydrogen partial pressure will result in lower growth rates and generally higher quality CNTs. However, the resulting ethylene partial pressure also drops, i.e. the coverage of the catalyst surface by ethylene molecules becomes very low which could result in a transfer to the adsorption-limited regime, similar to the case of high argon partial pressure.

Nucleation rate

Since hydrogen pre-dominantly determines the start and nucleation of the growth process, due to its influence in reduction of the oxidized catalyst and the exponential term in Equation 4.9, the nucleation rate of the process is investigated as a function of hydrogen partial pressure. The temperature set-point was set to 950 °C. The experiment already starts (and all three gases are present) during the ramping to this set-point to investigate nucleation characteristics. The nucleation rate N_R was defined as the inverse of the nucleation time t_n and can be extracted from Equation 4.9 by introducing a nucleation constant C_N ,

$$N_R = C_N \frac{[C_2H_4]}{[H_2]} (1 - e^{-k_2^+ [H_2]}) \quad (4.21)$$

The nucleation rate is plotted against the hydrogen partial pressure in Figure 4.17. Two parts can be distinguished in this figure. The first (left) part shows an increase in nucleation rate while the second (right) part shows an exponential decay. The decline can be explained by fitting Equation 4.21. However, in this equation no hydrogen would result in an infinitely high nucleation rate. Since hydrogen also plays a role with the reduction of the catalyst, the first part of the figure can be explained by an increase in catalyst activity. Without hydrogen, the ethylene has to provide the hydrogen, which can only decompose thermally at high temperatures. So the catalyst is reduced faster with more hydrogen, until the point at which more hydrogen would start suppressing the nucleation rate. A similar trend for the influence of hydrogen concentration was found by Pérez-Cabero *et al.* for acetylene on iron catalyst.^[183]

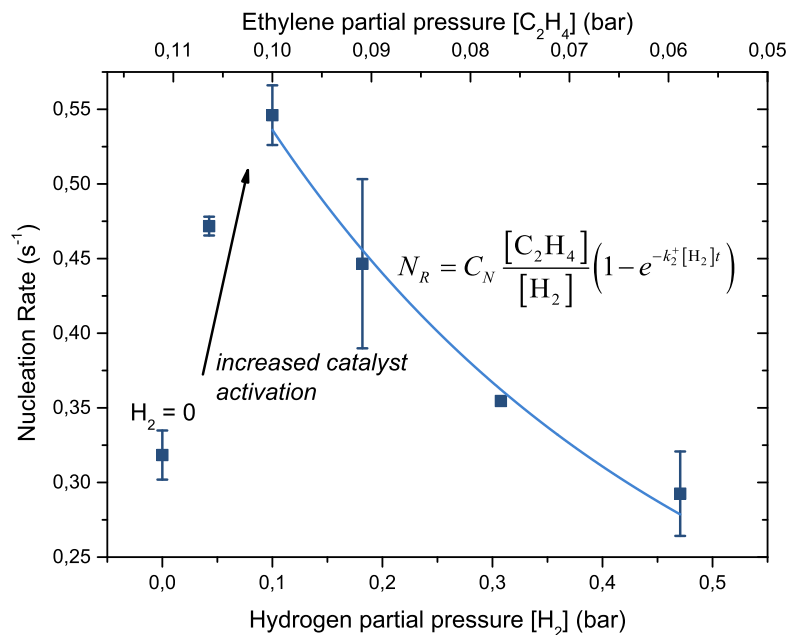


Figure 4.17: Nucleation rate as a function of hydrogen partial pressure. Also indicated is the resulting ethylene partial pressure. The nucleation rate first shown an increase due to increased catalyst activity. The resulting part of the graph is fitted with with an exponential decay.

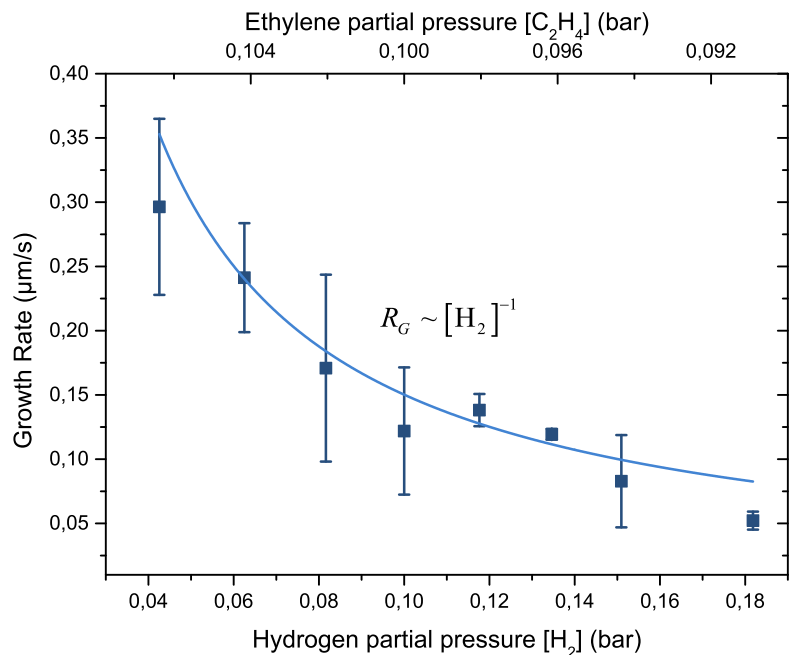


Figure 4.18: Carbon nanotube growth rate as a function of hydrogen partial pressure. Also indicated is the resulting ethylene partial pressure. The growth rate shows an inverse relation to the hydrogen which is fitted by the blue line.

The reaction rate order of hydrogen is estimated in Figure 4.18 where the hydrogen flow is varied between 10 and 50 sccm (partial pressure 0.04 - 0.18 bar). The ethylene gas is added after the temperature set-point is reached to exclude the influence of start-up and nucleation.

From Equation 4.9 an inverse relation between growth rate and hydrogen partial pressure is expected, i.e. growth rate $\propto [\text{H}_2]^{-1}$. In the figure the growth rate is fitted with this relation, which shows that the reaction rate order of -1 proposed in the rate equations seems probable. Note that for these experiments the growth temperature was too low ($\sim 850^\circ\text{C}$) to result in CNT growth without any hydrogen.

4.5 Summary

In this chapter the growth kinetics of laser-assisted carbon nanotube growth is investigated. The localized nature of the laser-assisted process allows for a fast *in situ* determination of growth kinetics with high throughput in comparison to conventional CVD. As a result, the investigation of the influence of the process gases over a wide range of partial pressures is possible and several growth regimes are proposed. Each of the growth regimes has a unique rate-limiting step which is determined by the governing rate equations. The quality and morphology of the CNTs is assessed as a function of temperature and partial pressure for ethylene, argon and hydrogen. A maximum CNT quality occurs around 950°C . The growth rate is calculated using the dynamically changing reflected intensity from the laser beam. From the growth rate it is possible to determine reaction rates and activation energies. The activation energies found are in the range between 0.3 - 0.8 eV. The results are linked to growth regimes, depending on the partial pressure and flow rates of the different process gases.

An increase in the partial pressure of ethylene shifts the growth regime from *surface diffusion-limited* to *dissociation-limited* growth. The quality decreases with increasing ethylene partial pressure while the growth rate increases. This is confirmed by SEM and Raman analysis, which indicate the largest forest to consist of low quality multi-walled CNTs grown in the dissociation-limited regime. The reaction rate order of ethylene is found to be 1, in accordance with derived rate equations.

The partial pressure of argon in itself does not change the growth rate but in effect changes the flow speed of the process gases over the substrate. With a very low argon partial pressure the mass diffusion of ethylene to the growth site is the rate-limiting step. The quality of the growth decreases for lower partial pressure in the *mass diffusion-limited* regime. In contrast, a high argon partial pressure can affect the surface coverage of the catalyst. That is, the argon molecules shield the surface sites, preventing the ethylene molecules to reach the catalytic surface, resulting in the *adsorption-limited* regime. In this regime the quality reduces with increasing argon partial pressure. As expected, this effect is larger with a lower ethylene flow and partial pressure.

The influence of hydrogen on the growth is largely attributed to its ability to reduce the catalyst and its presence in the exponential "start-up" term. However, the quality of the CNTs shows a dependence on the partial pressure of hydrogen as well. The existence of start-up effects are confirmed by comparing the results of experiments with two different runtimes. The influence of hydrogen on the start-up phase of the process is further confirmed by investigating the nucleation rate of the process. Finally, the reaction rate order of hydrogen is confirmed to be -1.

In Table 4.1 a summary of the different proposed growth regimes and the resulting growth is presented. To obtain the longest CNTs, a high ethylene partial pressure within the dissociation-

limited regime is necessary. The quality of the resulting vertically aligned multi-walled CNTs is generally low. The highest quality un-aligned CNTs are obtained with a low ethylene partial pressure, within the surface diffusion-limited regime. Also indicated in the table is the ethylene partial pressure range corresponding to the proposed growth regimes and the gas variable that was varied.

Table 4.1: Growth regimes and resulting CNT growth.

Growth regime	C₂H₄ pressure	Gas variable	Results
Surface diffusion limited	0.04 - 0.2 bar	C ₂ H ₄	High quality, un-aligned CNTs
Dissociation limited	0.2 - 0.7 bar	C ₂ H ₄	Low quality, vertically aligned CNTs
Mass diffusion limited	0.2 - 0.6 bar	Ar	Low quality, thin layer of vertically aligned CNTs
Adsorption limited	0.6 - 0.9 bar	Ar	Low quality, thin layer of vertically aligned CNTs

Chapter 5 |

Application perspectives

Carbon nanotube assemblies can be used for specific applications such as sensors and filters, as well as electronic interconnects in for instance flexible electronics. In this chapter a number potential applications and perspectives are given along with proof-of-concepts. A simple method to transfer a hill of vertically aligned nanotubes into a polymeric substrate is introduced. Secondly, the miniaturized reaction chamber is used to directly grow lines and patterns of CNTs as well as demonstrate the ability to grow in a narrow enclosure. Finally, a method and proof-of-concept to directly grow vertically-aligned carbon nanotube structures within sealed enclosures is presented by means of the feedback-controlled laser-assisted chemical vapor deposition technique. The process is compatible with a variety of micro-fabrication processes and bypasses the need for post-process packaging. These experiments include interesting observations related to the gas diffusion dynamics in micro-scale and sub-micron enclosures.

Part of this chapter has been published in

Y. van de Burgt, A. Champion, Y. Bellouard, *In-situ localized carbon nanotube growth inside partially sealed enclosures*, AIP Advances 3, 092119 (2013).^[6]

Y. van de Burgt, Y. Bellouard, W. van Loon, R. Mandamparambil, *Miniaturized Reaction Chamber for Optimized Laser-Assisted Carbon Nanotube Growth*, accepted for publication in Journal of Laser Micro / Nanoengineering (2013).^[4]

5.1 Introduction

Owing to their special geometrical, structural and electrical properties, carbon nanotubes have been found useful in a variety of applications^[12,13] such as field effect transistors and logic operators,^[14–17] field emitters,^[18–20] displays,^[21] sensors,^[22,23] flexible electronics,^[24] filters,^[25–27] interconnects,^[28] scanning probe microscopy tips,^[29] solar cell technology,^[30] and computers.^[31] More specifically, vertically aligned carbon nanotube embedded structures have been proposed for enhanced particle interception in cell separation^[184,185] and as blood pressure sensors.^[186]

The localized growth inherent to laser-assisted CVD growth allows for a number of specific potential applications. Especially, applications where local CNT structures are desirable, for instance interconnects or filters, could be advantageous to be created with a laser-assisted CVD process.

In this chapter, a number of potential applications using the controlled laser-assisted CVD growth method are explored. Four examples are discussed, a post-processing method, the advantage of the local growth process itself and growth inside enclosures. The chapter ends with an outlook for the future, summarizing the capabilities of this technique and what are possible future applications.

5.2 Transfer of carbon nanotubes into polymers

Because of the structural and electronic properties of CNTs, local aligned forests could be used as interconnects in flexible electronics. To demonstrate this, a proof-of-concept of a method in which a forest of vertically aligned carbon nanotubes is transferred into a flexible polymeric layer is presented. After the laser-assisted CVD growth of a CNT hill, a thin Polydimethylsiloxane (PDMS) layer is spincoated onto the substrate containing the forest. By varying the speed and time of the spincoating process the thickness of the PDMS layer can be adjusted to match the thickness of the forest.

After spincoating, the PDMS is cured in an oven at 100 °C. Finally, the layer with the embedded CNT forest is removed from the substrate. The result is shown in Figure 5.1.

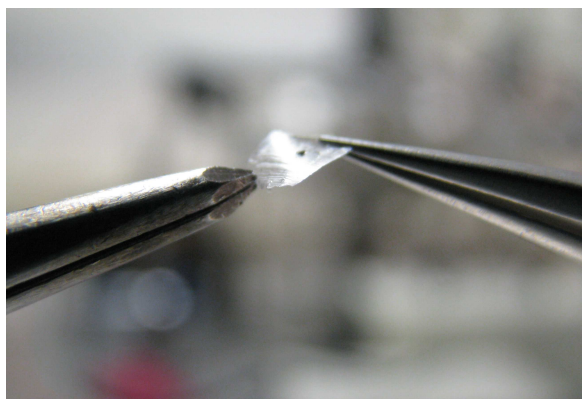


Figure 5.1: Photo of transferred aligned CNT forest into flexible polymer (PDMS).

To verify the conducting nature of the nanotubes, necessary for interconnecting purposes, a simple two-point probe resistance measurement is carried out through the nanotube forest inside a scanning electron microscope. The results look promising as the resistance measured is in the range of 15 - 60 Ω . Note that the planar resistance in CNT forest is much higher than along the nanotube length and that these measurements also include contact resistance.

5.3 Growth in a narrow enclosure

The laser is used to grow carbon nanotubes on the substrate in a narrow enclosure. Taking into account the heat resistance of this enclosure, it is possible to use any material as enclosure. One can think of electronic components that already surround the position where carbon nanotube growth is desirable. Also polymers such as PDMS can be used as long as the growth is sufficiently distant enough to not damage the polymer. In this case, a U-shaped patterned piece of fused silica is created by femto-second laser machining in combination with an etch process.^[187] A schematic of this fused silica part on top of the substrate is shown in Figure 5.2(a). The fused silica part is attached to the silicon substrate by a heat resistant epoxy. The gas flow is from the right side, into the U-shape. In Figure 5.2(b) an SEM picture shows the resulting hill of aligned nanotubes that was grown. The inset of the figure shows a zoom to the side of the hill where the aligned nanotubes are clearly visible. Despite the major thermodynamic changes introduced by the addition of such part, the closed-loop system combined with a well-defined gas flow results in a controlled growth of aligned nanotubes.

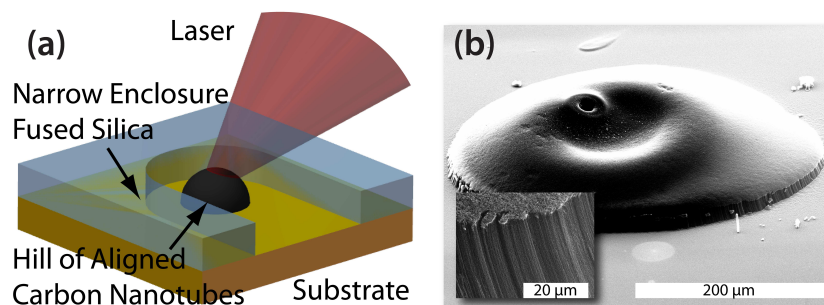


Figure 5.2: Demonstration of growth in a narrow enclosure. (a) Schematic of the process. The width of the enclosure is 2 mm (b) SEM picture showing the resulting hill of aligned carbon nanotubes. Inset shows a zoom of the side of the hill clearly indicating the vertically aligned nanotubes.

5.4 Writing lines of carbon nanotubes

The miniaturized reaction chamber is attached to an x-y-z table which allows for movement of the chamber during the synthesis of nanotubes. As a demonstration of this, a line of aligned nanotubes is grown by moving the complete chamber under the laser for about 1.5 mm. The resulting growth is shown in Figure 5.3. In Figure 5.3(a) an overview of the line is shown including an indication of the laser spot size and write direction. In Figure 5.3(b) and (c) the line is visualized from the side while the latter is after scratching the surface, clearly showing the aligned nanotubes. In Figure 5.3(d) a part of this is zoomed to show the alignment better.

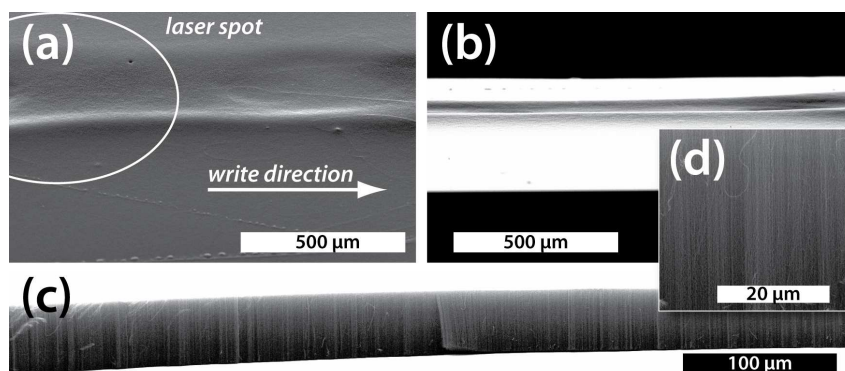


Figure 5.3: SEM pictures of a line of aligned nanotubes grown by moving the complete reaction chamber under the laser. (a) Overview including an indication of the laser spot size and the write direction. (b) Side view. (c) Side view after scratching the surface. (d) Zoom of a part of the aligned nanotubes.

5.5 *In situ* carbon nanotube growth inside partially sealed enclosures

The organic nature of carbon nanotube structures also allows them to be used in micro-fluidic (biological) applications and makes them compatible with many materials commonly used in micro-fluidics, such as PDMS or glass. For instance, vertically aligned carbon nanotube embedded structures have been proposed for enhanced particle interception in cell separation^[184, 185] and as blood pressure sensors.^[186]

These applications use lithography in combination with thermal chemical vapor deposition to control the geometry of the nanotube structure and embed the nanotubes inside the device by creating the micro-channel on top of the nanotubes. More convenient would be to directly grow the nanotubes inside the micro-channel without the need of an extra structuring or transfer step. Various techniques for local growth of carbon nanotube structures such as micro-resistive heating^[68] or micro-induction^[73] have been proposed. Although these techniques provide the possibility of localized heating and CNTs growth, they have intrinsically limited flexibility.

In this section, a laser-assisted fabrication method is presented for local *in-situ* growth of carbon nanotube structures inside enclosures. This technique eliminates the lithography structuring step and increases the versatility of the process since a laser-beam can be used virtually anywhere in the channel. Specifically, as a proof-of-principle, the growth of a hill of vertically aligned carbon nanotubes inside a micro-channel is presented, created by femtosecond laser processing. Furthermore, the growth of CNTs on a silicon substrate covered with a transparent window is also demonstrated. This result raises interesting questions related to gas diffusion kinetics.

5.5.1 Experimental details

Carbon nanotube chemical vapor deposition (CVD) growth consists of a thermal energy supply, a catalyst and a carbon-containing precursor gas. This growth method provides a high degree of control making it the most promising method for carbon nanotube growth.

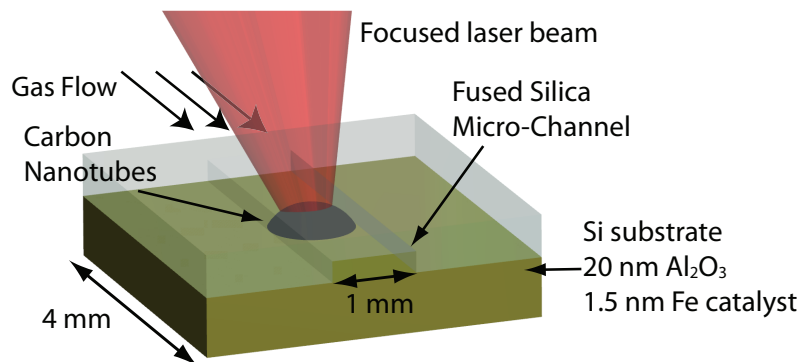


Figure 5.4: Schematic of the direct local growth of carbon nanotubes inside a sealed micro-channel. For the second experiment, the same setup is used but without channel and with a window covering the substrate.

Among CVD processes, laser-assisted ones differ from conventional CVD by using a laser to provide the thermal energy. This opens up new possibilities for direct-write growth as well as fast and local heating, enabling the growth site to be surrounded by temperature-sensitive elements and/or materials, as was shown in the previous sections. Indeed, the laser-assisted CVD growth method is compatible with most polymers and other materials or adhesives used in micro-fluidics.

In this experiment, the closed-loop control growth process, described in detail in chapter 2 and chapter 3, is used. The micro-channel is fabricated in a 500 μm -thick fused-silica glass slide with lateral dimensions similar to the substrate, 4 \times 4 mm to which it will be attached. A femtosecond laser process was combined with etching for 24 hours in 2.5% hydrogen-fluoride (HF) solution to create the channel.^[187] The open channel is 1 mm wide, 120 μm in height and has a length of 4 mm. For the aligned carbon nanotube growth, the standard silicon substrate, covered with a 20 nm Al₂O₃ and a 1.5 nm iron catalyst layer, is used. The laser used is a continuous-wave (CW) diode laser operating at a wavelength of 808 nm, focused to a spot of about 500 μm . To visualize and analyze the resulting CNT structures grown inside the channel by scanning electron microscopy (SEM), the channel was not permanently attached to the substrate. However, to show the proof-of-concept, Epotek 355nd epoxy is used to glue the two parts together at the side-edges of the substrate, so that the material combination can withstand the elevated temperatures around the laser hot spot. Other bonding processes such as anodic bonding could also be considered and are assumed to be more stable for the high temperatures involved here.

In Figure 5.4 a schematic of the channel growth is presented. The laser beam is focused onto the substrate through the fused silica channel, which is transparent to the wavelength of the laser, 808 nm. The channel itself only has two openings where the gas flows through.

5.5.2 Results

The proof-of-concept is presented in Figure 5.5(a) with a photo of the locally grown CNT structure inside the attached micro-channel. In Figure 5.5(b) a photo of the transparent micro-channel attached to the substrate is shown with the inset showing the (infrared) light emission from inside the channel during growth.

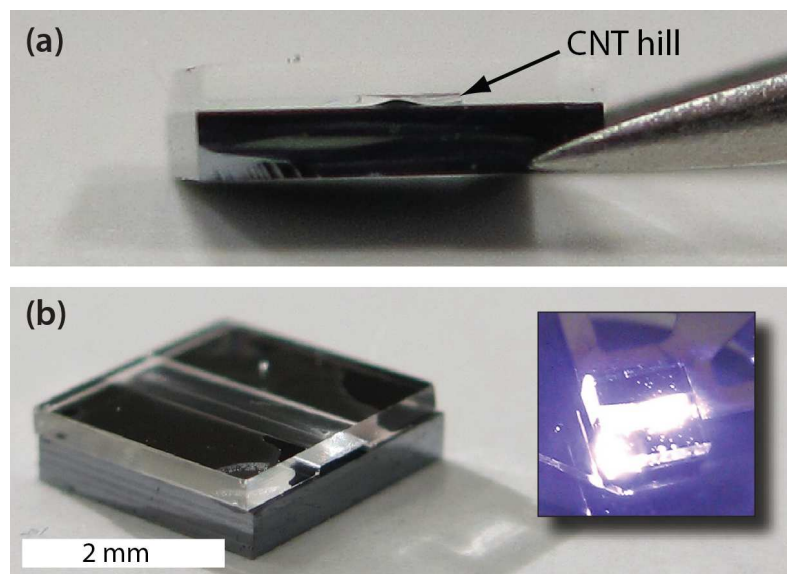


Figure 5.5: Photo of the hill of aligned CNTs grown inside a sealed fused silica micro-channel attached to a silicon substrate. B. View of the channel. Inset shows a photo of the channel during laser-assisted growth.

The nucleation of nanotube growth is typically indicated by a drop in the reflected laser signal, as was shown in subsection 2.3.2. This can be seen in Figure 5.6 which shows a characteristic graph relating laser irradiance and sensor signals. The laser irradiance starts at the maximum level while ramping to the temperature set-point. Just before reaching this set-point, the reflected laser signal shows a clear drop, indicating the nucleation of the nanotube growth. The temperature reached at the laser spot is estimated using the finite element simulation from chapter 3 and is about 900°C . The lateral distribution is of Gaussian nature and reaches about 420°C at the edges (i.e. at a distance of 2 mm). The heat can be significantly confined using a less conductive substrate than silicon, such as fused silica with a thermal conductivity of about 100 times lower.

From the reflected laser irradiance signal in Figure 5.6, forest height is also extracted by measuring an interference effect of the reflected laser signal with the nanotube forest. This is shown in the inset of the figure. The calculated growth rate is $0.97\ \mu\text{m/s}$ which corresponds to estimates made from scanning electron micrographs.

In Figure 5.7 corresponding scanning electron micrographs of the resulting growth are presented. This particular nanotube structure was grown in 150 sec and has an estimated height of about $100\ \mu\text{m}$. The lateral dimensions of the structure are about $800 \times 600\ \mu\text{m}$. An overview of the substrate with corresponding CNT growth is shown in Figure 5.7(a). In Figure 5.7(b) a view of the side of the hill is given, from which the height was estimated. The insets show the Raman intensity signals for two positions on the sample. The ratio of D- and G-band intensities of the Raman signal can be used to evaluate the quality of the CNTs. Here, both signals indicate multi-walled CNTs, predicting the presence of a vertically aligned forest of multi-wall carbon nanotubes. In Figure 5.7(c) and Figure 5.7(d) detailed zooms of the aligned nanotubes are given. These pictures were obtained after scratching the nanotubes grown layer from the side in the direction of the gas flow. Figure 5.7(c) shows a zoom of the left side of the hill while the Figure 5.7(d) shows an enhanced zoom of the right side of the hill, visible

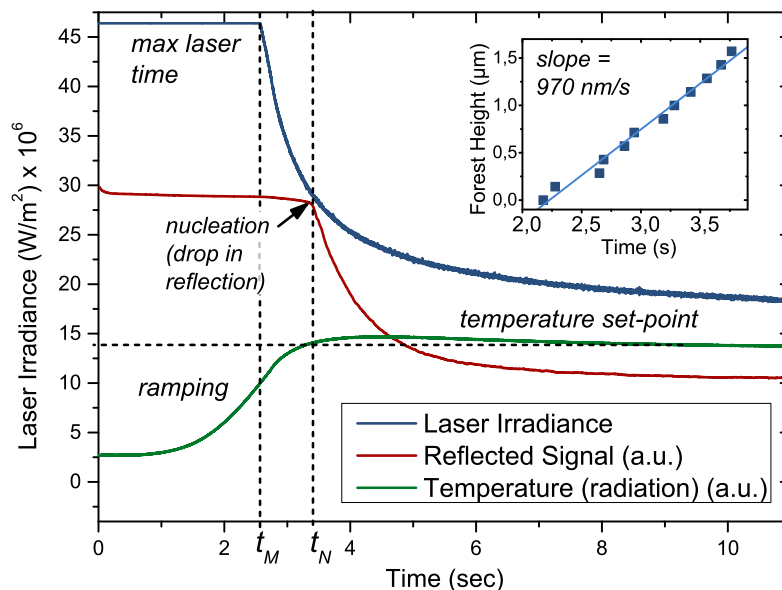


Figure 5.6: Typical graphs plotting laser power and sensor signals as a function of time for *in situ* localized closed-loop controlled growth inside a micro-channel. The laser power is at a maximum level while ramping to the radiation set-point and drops (t_M) when this level is reached to keep the radiation constant. The reflection shows a clear drop indicating the nucleation of nanotube growth (t_N). Inset shows calculated forest height and corresponding growth rate.

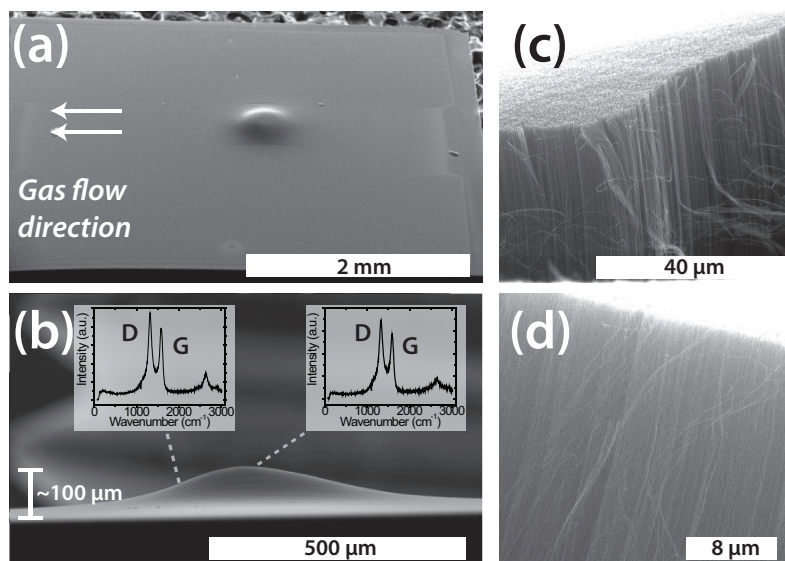


Figure 5.7: SEM pictures of nanotube growth inside the micro-channel. (a) Overview of the substrate with the hill of aligned nanotubes visible. Also depicted is the gas flow direction. (b) Side view of the hill. Indicated is the estimated height. Inset shows a Raman intensity plot for this experiment. The ratio of D and G-band intensities indicate multiwall carbon nanotubes. (c) Detailed zoom of the alignment of the nanotubes after scratching the hill. (d) Detailed zoom of the other side after scratching.

by the slopes of the top of the nanotubes in both pictures.

Using a heat/flow coupled finite element simulation of the laser heated micro-channel, the

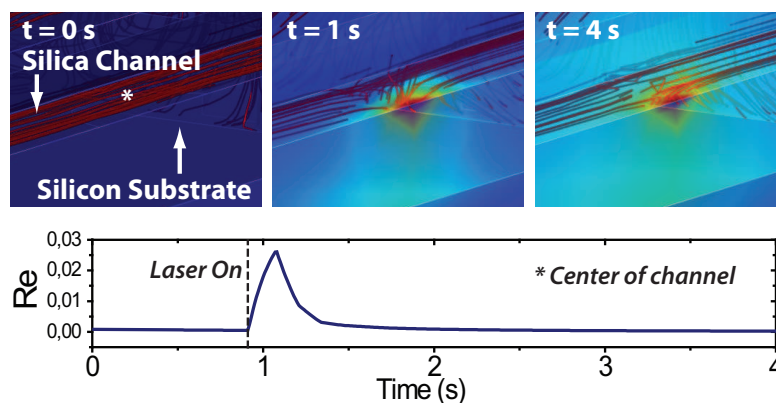


Figure 5.8: Simulation of flow alteration by switching on the laser and corresponding Reynolds number measured in the center of the channel, just above the laser heated zone. At $t = 0$ s, the laminar flow is clearly visible and at $t = 1$ s, the streamlines are disrupted by the sudden increase in temperature as a result of the laser heating. At $t = 4$ s, the flow is stabilized again. The corresponding Reynolds number confirms this trend.

effects of laser heating on the laminar flow could be investigated (see Figure 5.8). The laminar flow is essential for carbon nanotube growth as it ensures a stable and known gas feed to the laser heated spot. The simulation suggests that the sudden increase in temperature by laser heating increases the Reynolds number significantly but still within laminar flow conditions. The flow quickly stabilizes again.

During these experiments "side-growth" of CNTs was also observed. It appears that when the fused-silica channel is not permanently attached to the substrate, nanotubes can grow in between the silicon substrate and the fused silica cover. Assuming both the silicon and the fused silica have a surface roughness in the nanometers range, it seems unlikely that the nanotubes can grow to lengths of 10 - 20 μm with only the carbon already present in between the two surfaces.

To investigate the phenomena, a series of test-experiments were performed on a substrate simply covered by a unattached fused silica window and using different process times, ranging from 25 seconds to 150 seconds with different gas flow ratios. From these experiments it appeared that the further from the side, thus the closer to the laser irradiated center, the longer the nanotubes were. Two other direct relations between nanotube lengths were found with time and carbonaceous gas concentration. These results suggest that the process showed conventional growth behavior, where it appeared that it did not matter there was a fused silica cover covering the substrate and catalyst. In other words, the carbonaceous gas found its way to the laser-induced hot spot rather easy. Much easier as one would expect by estimating diffusion lengths for the nano-channels in between the two surfaces.

A possible explanation is the very fast heating of both surfaces by the laser irradiance. In Figure 5.6 it can be seen that for certain conditions the laser can operate at its maximum irradiance level for about 3 seconds. During this time the substrate and covering fused silica locally heat up quickly resulting in a temperature gradient which can result in thermally-induced bending. The bending of both surfaces could result in a large enough opening to allow the carbonaceous gas to flow to the nucleation site.

In Figure 5.9 the results of a Finite Element Method simulation of material expansion with

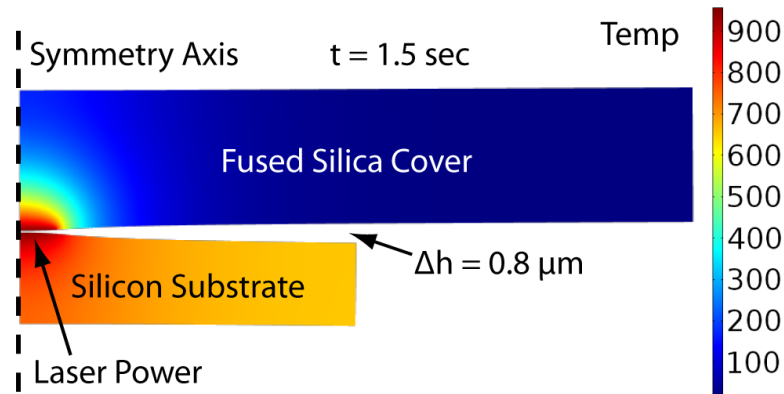


Figure 5.9: Finite Element Method simulation in COMSOL linking the expansion to temperature for a given input laser irradiance. The figure shows the scaled result after 1.5 seconds. A gap of $0.8 \mu\text{m}$ has been created with the substrate reaching 900°C

COMSOL Multiphysics are presented. A radial symmetric model of the substrate is simulated with heating by a constant laser irradiance corresponding to the maximum laser power in Figure 5.6. The resulting temperature variation over time is used as the input on a similar model of the fused silica glass. The two pictures are assembled for clarification. The time after which the resulting gap is calculated is chosen to be 1.5 seconds for two reasons. First of all, the gap does not increase much more after this time, due to heat conduction through the material. Secondly, after 1.5 seconds the temperature in the model starts to deviate from reality due to the simplified thermal conditions in the model. The resulting gap of $0.8 \mu\text{m}$ might be enough for the carbonaceous gas to enter and flow to the laser hot spot nucleation site. Due to the consumption of the ethylene gas and precipitation into carbon nanotubes in the center, a pressure difference is created between the center of the laser-heated zone and the outside. An estimation of the diffusion length of ethylene yields about 9 mm for these particular conditions. However, the walls of the sub-micro enclosure are expected to reduce this length significantly. Despite the temperature gradient in the channel, the diffusion in combination with the pressure driven flow, seem like a plausible explanation for the growth. However, further analysis is desirable.

5.6 Summary and outlook

Laser-assisted CVD growth of carbon nanotubes has developed into a very attractive process for local, rapid, and well defined growth of CNT structures. The ability to grow virtually anywhere on a substrate, write patterns and lines, inside micro-channels and close to temperature sensitive elements and components opens up new application areas for CNTs.

In this chapter, several possible applications of the laser-assisted CVD process are demonstrated. The transfer of an aligned forest of CNTs into a polymeric layer was demonstrated. By moving the complete miniaturized reaction chamber lines of aligned CNTs were grown and finally by using the localized nature of the growth process, the possibility of growing CNT structures in narrow enclosures and directly inside a micro-channel is demonstrated. The latter is a unique technique only possible because the micro-channel is transparent to the wavelength of the laser.

To add even more flexibility to the process by removing the requirement of a deposited nanolayer, the catalyst could also be part of the gas feed, for instance using iron-pentacarbonyl gas, $\text{Fe}(\text{CO})_5$. In addition, to get absorption within a fluidic channel made of a transparent material, a non-linear absorption process such as multi-photons could be used. For instance, using femtosecond laser exposure of silica in the cumulative regime produces localized heat affected zones.^[188]

As recent successes on carbon nanotube computing have proven,^[31] the ability to grow controlled local suspended CNTs on specific positions might be a next step. Laser-assisted CVD has a major advantage in selectively heating the growth site and the ability to grow single suspended CNTs, capable of displaying transistor behavior. In that perspective, LACVD could be expected to be a basis for cheap printed full carbon electronics, especially for flexible electronics and/or prototyping, allowing the user to quickly produce specifically designed devices. Competing with classical techniques by easiness and cheapness, not by fabrication volume.

A further enhancement of the local gas flow growth of Kwok *et al.*^[99] could be the development of a miniaturized reaction chamber with incorporated laser to be able to selectively grow CNTs on large wafers or devices. This way, local, aligned structures of carbon nanotubes can be created without the need for a static CVD chamber, anywhere desired. Of course, scientific focus has been shifting towards other molecular carbon structures such as graphene, where the laser-assisted CVD method could also be expected to provide major advantages for local, controlled growth as some first results already suggests.^[189,190]

To utilize the capabilities of the CNTs to the full extend in applications, it is necessary to further enhance control of the process. Unlike conventional CVD process where the difficulty is placing the CNTs on the desired position, LACVD can grow CNTs on the spot. The main problem to overcome is direct control on the process. In particular, CNT type, length, size, morphology and direction are crucial parameters to control if CNTs integrated with applications are to be successful.

Chapter 6 |

Conclusions and Outlook

*"Nobody ever figures out what life is all about, and it doesn't matter. Explore the world.
Nearly everything is really interesting if you go into it deeply enough."*

Richard P. Feynman

6.1 Conclusions

Laser-assisted chemical vapor deposition has been demonstrated as a versatile technique for fast local growth of carbon nanotube (CNT) structures. The growth of carbon nanotubes depends on three main parameters - thermal energy, catalyst and process gases. The nature of the laser-assisted process provides unique opportunities regarding the catalyst preparation and activation and at the same time creates several challenges with respect to the thermal energy. The rapid heating allows for a fast *in situ* preparation and deposition of the catalyst without the need for a pre-treatment in an inert environment. As CNT growth depends largely on process conditions and in particular temperature, a well-defined temperature is essential. However, the nature of the laser-assisted process prevents the direct control on temperature at the growth site.

The objective of this thesis was to investigate and optimize carbon nanotube growth using a laser-assisted chemical vapor deposition process. Structural quality and morphological properties of the resulting CNT growth were analyzed by Scanning Electron Microscopy and Raman spectroscopy. For application purposes a reproducible method to grow CNTs is essential and in order to qualitatively assess and compare results, the ability to know temperatures involved during the growth is crucial. The optimization of the process relies on the thorough investigation of a broad range of experimental conditions. In particular, it is essential to know the precise process gas composition at the growth site to be able to draw conclusions from the results.

We demonstrated an integrated approach on investigating and optimizing laser-assisted CNT growth. A closed-loop control mechanism was developed to enhance controllability and reproducibility of the process. The feedback control relies on a direct measurement of emitted thermal radiation. This radiation is used as a first approximation of the average temperature at the growth site. The reflected laser intensity is monitored as well, and provides information about the CNT growth dynamics. From open-loop experiments we identified several stages of CNT growth and linked those to the reflection signal. Increased substrate absorptivity as a result of CNT growth resulted in overheating, further demonstrating the necessity of a closed-loop control. A detailed thermal model was developed, including temperature dependent properties for the materials involved in the process. This model enables the qualitative comparison of the results, linking growth temperature to structural quality and geometry of the CNT growth.

To further optimize the process, we developed a dedicated miniaturized reaction chamber. The investigation of growth kinetics relies on a precise knowledge of the gas composition at the growth site, which the reaction chamber provides using a forced laminar flow over the substrate. For this chamber another thermal model was developed to investigate the temperatures involved during the CNT synthesis. The thermal model combines heat and flow simulations to a maximum deviation of substrate temperature of about 13%. The size of the chamber greatly improved the process time as well.

Using the dynamically changing reflected laser intensity signal, combined with SEM analysis, we have developed a method to measure *in situ* the average CNT growth rate. This information is essential to study growth kinetics of the process. Using the dedicated reaction chamber, we have investigated the influence of the different process gases over a wide range of partial pressures and temperatures. From these results, we were able to propose several growth

regimes. The proposed regimes are characterized by a unique rate-limiting step, which is determined by chemical rate equations and each have a specific apparent activation energy, ranging from 0.3 - 0.8 eV. CNTs grown in the *surface diffusion-limited* regime generally have the highest quality, while the *dissociation-limited* regime results in the longest vertically aligned forest. The reaction order of ethylene is found to be 1, in accordance with derived rate equations. The two other growth regimes are the *mass diffusion-limited* regime and the *adsorption-limited* regime. These regimes originated from a varying carrier gas (argon) flow rate, resulting either in an undersupply of carbon (mass diffusion-limited) or the shielding of the catalyst by a too high argon concentration (adsorption-limited). The influence of hydrogen was found to mainly determine the catalyst reduction and activation properties during the start of the process.

Using the unique properties of the laser-assisted CNT growth method, in particular the possibility of localized and rapid heating, a number of application perspectives have been presented, demonstrating the possibilities for future technologies and applications.

6.2 Outlook

Catalytic CVD growth of carbon nanotubes is still far from fully comprehended, especially the underlying catalytic mechanisms remain poorly understood. Although the work described in this thesis significantly contributes to the general understanding of those mechanisms and in particular on LACVD growth, several follow-up questions remain.

The catalytic nanoparticles have not been studied intensively in this thesis, although the catalyst remains an important parameter that co-determines the resulting CNT growth. Detailed investigation and careful selecting of the catalyst type and material could result in more specific tuning of and control over the CNT properties. A similar argument holds for the process gases used in this study. An expansion of the study would also have to cover the investigation of different process gases, such as acetylene, ethanol and methane, as well as the influence of trace amounts of water and oxygen, recently emerged as essential in the growth of ultra-long nanotubes.^[191,192] The preventing of the termination of CNT growth, as a result of the addition of those gases could also be studied in detail in combination with LACVD, further enhancing the direct local growth of CNTs. As this thesis clearly shows, the specific gas-catalyst combination ultimately determines CNT growth kinetics and as such is responsible for the structural, morphological and geometrical properties of the CNTs. A detailed and systematic study of more and different gas-catalyst combinations is therefore crucial for further optimization and understanding of the catalytic growth of CNTs.

Fortunately, the methodology and technological achievements described in this thesis offer a framework for succeeding studies. The approach described could effortlessly be used to investigate the kinetics of other gas-catalyst combinations. On top of that, the technique could even be expanded beyond CNT growth, simply by using different gases and catalysts. For instance, combinations of gold nanoparticles with silane gas could be used to locally grow silicon nanowires.

Bibliography

- [1] Y. van de Burgt, *Laser-assisted growth of carbon nanotubes - a review*, submitted (2014).
- [2] M. Haluška, Y. Bellouard, Y. van de Burgt, and A. Dietzel, *In situ monitoring of single-wall carbon nanotube laser assisted growth*, *Nanotechnology* **21** (2010), no. 7, 075602.
- [3] Y. van de Burgt, Y. Bellouard, R. Mandamparambil, M. Haluska, and A. Dietzel, *Closed-loop control of laser assisted chemical vapor deposition growth of carbon nanotubes*, *Journal of Applied Physics* **112** (2012), no. 3, 034904–034904–8.
- [4] Y. van de Burgt, Y. Bellouard, W. van Loon, and R. Mandamparambil, *Miniaturized reaction chamber for optimized laser-assisted carbon nanotube growth*, *Journal of Laser Micro Nanoengineering* (2014).
- [5] Y. van de Burgt, Y. Bellouard, and R. Mandamparambil, *Kinetics of laser-assisted carbon nanotube growth*, *Physical Chemistry Chemical Physics* **16** (2014), no. 11, 5162–5173.
- [6] Y. van de Burgt, A. Champion, and Y. Bellouard, *In-situ localized carbon nanotube growth inside partially sealed enclosures*, *AIP Advances* **3** (2013), no. 9, 092119.
- [7] Y. van de Burgt, Y. Bellouard, R. Mandamparambil, and A. Dietzel, *Closed-loop control of a laser assisted carbon nanotube growth process for interconnects in flexible electronics*, *MRS Online Proceedings Library* **1365** (2011).
- [8] M. R. Falvo, G. J. Clary, R. M. Taylor, V. Chi, F. P. Brooks, S. Washburn, and R. Superfine, *Bending and buckling of carbon nanotubes under large strain*, *Nature* **389** (1997), no. 6651, 582–584 (en).
- [9] R. S. Lee, H. J. Kim, J. E. Fischer, A. Thess, and R. E. Smalley, *Conductivity enhancement in single-walled carbon nanotube bundles doped with k and br* , *Nature* **388** (1997), no. 6639, 255–257 (en).
- [10] P. G. Collins and P. Avouris, *Nanotubes for electronics.*, *Scientific American* **283** (2000), no. 6, 62–69.
- [11] E. T. Thostenson, Z. Ren, and T.-W. Chou, *Advances in the science and technology of carbon nanotubes and their composites: a review*, *Composites Science and Technology* **61** (2001), no. 13, 1899–1912.

- [12] R. H. Baughman, A. A. Zakhidov, and W. A. De Heer, *Carbon nanotubes—the route toward applications*, *Science* **297** (2002), no. 5582, 787–792 (en).
- [13] J. Robertson, *Realistic applications of CNTs*, *Materials Today* **7** (2004), no. 10, 46–52.
- [14] S. J. Tans, A. R. M. Verschueren, and C. Dekker, *Room-temperature transistor based on a single carbon nanotube*, *Nature* **393** (1998), no. 6680, 49–52 (en).
- [15] R. Martel, T. Schmidt, H. R. Shea, T. Hertel, and P. Avouris, *Single- and multi-wall carbon nanotube field-effect transistors*, *Applied Physics Letters* **73** (1998), no. 17, 2447–2449.
- [16] A. Javey, J. Guo, Q. Wang, M. Lundstrom, and H. Dai, *Ballistic carbon nanotube field-effect transistors*, *Nature* **424** (2003), no. 6949, 654–657 (en).
- [17] H. Park, A. Afzali, S.-J. Han, G. S. Tulevski, A. D. Franklin, J. Tersoff, J. B. Hannon, and W. Haensch, *High-density integration of carbon nanotubes via chemical self-assembly*, *Nature Nanotechnology* (2012) (en).
- [18] W. A. d. Heer, A. Chatelain, and D. Ugarte, *A carbon nanotube field-emission electron source*, *Science* **270** (1995), no. 5239, 1179–1180, ArticleType: research-article / Full publication date: Nov. 17, 1995 / Copyright © 1995 American Association for the Advancement of Science.
- [19] S. Fan, M. G. Chapline, N. R. Franklin, T. W. Tombler, A. M. Cassell, and H. Dai, *Self-oriented regular arrays of carbon nanotubes and their field emission properties*, *Science* **283** (1999), no. 5401, 512–514 (en).
- [20] W. I. Milne, K. B. K. Teo, G. a. J. Amaratunga, P. Legagneux, L. Gangloff, J.-P. Schnell, V. Semet, V. T. Binh, and O. Groening, *Carbon nanotubes as field emission sources*, *Journal of Materials Chemistry* **14** (2004), no. 6, 933–943 (en).
- [21] W. B. Choi, D. S. Chung, J. H. Kang, H. Y. Kim, Y. W. Jin, I. T. Han, Y. H. Lee, J. E. Jung, N. S. Lee, G. S. Park, and J. M. Kim, *Fully sealed, high-brightness carbon-nanotube field-emission display*, *Applied Physics Letters* **75** (1999), no. 20, 3129–3131.
- [22] J. Kong, N. R. Franklin, C. Zhou, M. G. Chapline, S. Peng, K. Cho, and H. Dai, *Nanotube molecular wires as chemical sensors*, *Science* **287** (2000), no. 5453, 622–625 (en).
- [23] A. Modi, N. Koratkar, E. Lass, B. Wei, and P. M. Ajayan, *Miniaturized gas ionization sensors using carbon nanotubes*, *Nature* **424** (2003), no. 6945, 171–174 (en).
- [24] T. Y. Tsai, C. Y. Lee, N. H. Tai, and W. H. Tuan, *Transfer of patterned vertically aligned carbon nanotubes onto plastic substrates for flexible electronics and field emission devices*, *Applied Physics Letters* **95** (2009), no. 1, 013107.
- [25] A. Srivastava, O. N. Srivastava, S. Talapatra, R. Vajtai, and P. M. Ajayan, *Carbon nanotube filters*, *Nature Materials* **3** (2004), no. 9, 610–614 (en).

- [26] J. K. Holt, H. G. Park, Y. Wang, M. Stadermann, A. B. Artyukhin, C. P. Grigoropoulos, A. Noy, and O. Bakajin, *Fast mass transport through sub-2-nanometer carbon nanotubes*, *Science* **312** (2006), no. 5776, 1034–1037 (en), PMID: 16709781.
- [27] T. Guan and M. Yao, *Use of carbon nanotube filter in removing bioaerosols*, *Journal of Aerosol Science* **41** (2010), no. 6, 611–620.
- [28] A. Naeemi and J. D. Meindl, *Carbon nanotube interconnects*, *Annual Review of Materials Research* **39** (2009), no. 1, 255–275.
- [29] H. Dai, J. H. Hafner, A. G. Rinzler, D. T. Colbert, and R. E. Smalley, *Nanotubes as nanoprobe in scanning probe microscopy*, *Nature* **384** (1996), no. 6605, 147–150.
- [30] M. W. Rowell, M. A. Topinka, M. D. McGehee, H.-J. Prall, G. Dennler, N. S. Sariciftci, L. Hu, and G. Gruner, *Organic solar cells with carbon nanotube network electrodes*, *Applied Physics Letters* **88** (2006), no. 23, 233506–233506–3.
- [31] M. M. Shulaker, G. Hills, N. Patil, H. Wei, H.-Y. Chen, H.-S. P. Wong, and S. Mitra, *Carbon nanotube computer*, *Nature* **501** (2013), no. 7468, 526–530 (en).
- [32] S. Iijima, *Helical microtubules of graphitic carbon*, *Nature* **354** (1991), no. 6348, 56–58 (en).
- [33] P. L. Walker, J. F. Rakszawski, and G. R. Imperial, *Carbon mixture over iron catalysts. II. rates of carbon formation*, *J. Phys. Chem.* **63** (1959), no. 2, 140–149.
- [34] P. Tesner, E. Robinovich, I. Rafalkes, and E. Arefieva, *Formation of carbon fibers from acetylene*, *Carbon* **8** (1970), no. 4, 435–442.
- [35] R. Baker, M. Barber, P. Harris, F. Feates, and R. Waite, *Nucleation and growth of carbon deposits from the nickel catalyzed decomposition of acetylene*, *Journal of Catalysis* **26** (1972), no. 1, 51–62.
- [36] A. Oberlin, M. Endo, and T. Koyama, *Filamentous growth of carbon through benzene decomposition*, *Journal of Crystal Growth* **32** (1976), no. 3, 335–349.
- [37] D. S. Bethune, C. H. Klang, M. S. d. Vries, G. Gorman, R. Savoy, J. Vazquez, and R. Beyers, *Cobalt-catalysed growth of carbon nanotubes with single-atomic-layer walls*, *Nature* **363** (1993), no. 6430, 605–607 (en).
- [38] T. Guo, P. Nikolaev, A. G. Rinzler, D. Tomanek, D. T. Colbert, and R. E. Smalley, *Self-assembly of tubular fullerenes*, *J. Phys. Chem.* **99** (1995), no. 27, 10694–10697.
- [39] T. Guo, P. Nikolaev, A. Thess, D. Colbert, and R. Smalley, *Catalytic growth of single-walled nanotubes by laser vaporization*, *Chemical Physics Letters* **243** (1995), no. 1–2, 49–54.
- [40] A. A. Puzos, H. Schittenhelm, X. Fan, M. J. Lance, L. F. Allard, and D. B. Geohegan, *Investigations of single-wall carbon nanotube growth by time-restricted laser vaporization*, *Physical Review B* **65** (2002), no. 24, 245425.

- [41] A.-C. Dupuis, *The catalyst in the CCVD of carbon nanotubes—a review*, Progress in Materials Science **50** (2005), no. 8, 929 – 961.
- [42] M. Kumar and Y. Ando, *Chemical vapor deposition of carbon nanotubes: A review on growth mechanism and mass production*, Journal of Nanoscience and Nanotechnology **10** (2010), no. 6, 3739–3758.
- [43] M. José-Yacamán, M. Miki-Yoshida, L. Rendón, and J. G. Santiesteban, *Catalytic growth of carbon microtubules with fullerene structure*, Applied Physics Letters **62** (1993), no. 6, 657–659.
- [44] W. Z. Li, S. S. Xie, L. X. Qian, B. H. Chang, B. S. Zou, W. Y. Zhou, R. A. Zhao, and G. Wang, *Large-scale synthesis of aligned carbon nanotubes*, Science **274** (1996), no. 5293, 1701–1703 (en).
- [45] Y. C. Choi, Y. M. Shin, Y. H. Lee, B. S. Lee, G.-S. Park, W. B. Choi, N. S. Lee, and J. M. Kim, *Controlling the diameter, growth rate, and density of vertically aligned carbon nanotubes synthesized by microwave plasma-enhanced chemical vapor deposition*, Applied Physics Letters **76** (2000), no. 17, 2367–2369.
- [46] Y. Li, W. Kim, Y. Zhang, M. Rolandi, D. Wang, and H. Dai, *Growth of single-walled carbon nanotubes from discrete catalytic nanoparticles of various sizes*, J. Phys. Chem. B **105** (2001), no. 46, 11424–11431.
- [47] E. Kukovitsky, S. L'vov, N. Sainov, V. Shustov, and L. Chernozatonskii, *Correlation between metal catalyst particle size and carbon nanotube growth*, Chemical Physics Letters **355** (2002), no. 5–6, 497–503.
- [48] Y. Y. Wei, G. Eres, V. I. Merkulov, and D. H. Lowndes, *Effect of catalyst film thickness on carbon nanotube growth by selective area chemical vapor deposition*, Applied Physics Letters **78** (2001), no. 10, 1394–1396.
- [49] S. Hofmann, M. Cantoro, B. Kleinsorge, C. Casiraghi, A. Parvez, J. Robertson, and C. Ducati, *Effects of catalyst film thickness on plasma-enhanced carbon nanotube growth*, Journal of Applied Physics **98** (2005), no. 3, 034308.
- [50] Z. P. Huang, J. W. Xu, Z. F. Ren, J. H. Wang, M. P. Siegal, and P. N. Provencio, *Growth of highly oriented carbon nanotubes by plasma-enhanced hot filament chemical vapor deposition*, Applied Physics Letters **73** (1998), no. 26, 3845–3847.
- [51] M. Meyyappan, *A review of plasma enhanced chemical vapour deposition of carbon nanotubes*, Journal of Physics D: Applied Physics **42** (2009), no. 21, 213001.
- [52] D. Narducci, L. Toselli, and P. Milani, *Modeling of aerosol-assisted chemical vapor co-deposition of NiO and carbon nanotubes*, Le Journal de Physique IV **09** (1999), no. PR8, Pr8–741–Pr8–747.
- [53] K. Hernadi, A. Fonseca, J. Nagy, D. Bernaerts, and A. Lucas, *Fe-catalyzed carbon nanotube formation*, Carbon **34** (1996), no. 10, 1249–1257.

- [54] D. Venegoni, P. Serp, R. Feurer, Y. Kihn, C. Vahlas, and P. Kalck, *Parametric study for the growth of carbon nanotubes by catalytic chemical vapor deposition in a fluidized bed reactor*, *Carbon* **40** (2002), no. 10, 1799–1807.
- [55] H. Kanzow, A. Schmalz, and A. Ding, *Laser-assisted production of multi-walled carbon nanotubes from acetylene*, *Chemical Physics Letters* **295** (1998), no. 5–6, 525–530.
- [56] N. Grobert, M. Terrones, S. Trasobares, K. Kordatos, H. Terrones, J. Olivares, J. Zhang, P. Redlich, W. Hsu, C. Reeves, D. Wallis, Y. Zhu, J. Hare, A. Pidduck, H. Kroto, and D. Walton, *A novel route to aligned nanotubes and nanofibres using laser-patterned catalytic substrates*, *Applied Physics A: Materials Science & Processing* **70** (2000), no. 2, 175–183.
- [57] M. H. Rummeli, C. Kramberger, M. Löffler, M. Kalbác, H.-W. Hübers, A. Grüneis, A. Barreiro, D. Grimm, P. Ayala, T. Gemming, F. Schäffel, L. Dunsch, B. Büchner, and T. Pichler, *Synthesis of single wall carbon nanotubes with invariant diameters using a modified laser assisted chemical vapour deposition route*, *Nanotechnology* **17** (2006), no. 21, 5469–5473.
- [58] M. Löffler, M. H. Rummeli, C. Kramberger, E. Borowiak-Palen, R. Klingeler, T. Gemming, B. Büchner, and T. Pichler, *On the formation of single-walled carbon nanotubes in pulsed-laser-assisted chemical vapor deposition*, *Chem. Mater.* **20** (2007), no. 1, 128–134.
- [59] K. Maehashi, Y. Ohno, K. Inoue, and K. Matsumoto, *Chirality selection of single-walled carbon nanotubes by laser resonance chirality selection method*, *Applied Physics Letters* **85** (2004), no. 6, 858–860.
- [60] K. Sakai, S. Doi, N. Iwata, H. Yajima, and H. Yamamoto, *Growth position and chirality control of single-walled carbon nanotubes*, *Icice Transactions on Electronics* **E94C** (2011), no. 12, 1861–1866 (English), WOS:000298305000011.
- [61] M. Mahjouri-Samani, Y. S. Zhou, W. Xiong, Y. Gao, M. Mitchell, and Y. F. Lu, *Laser induced selective removal of metallic carbon nanotubes*, *Nanotechnology* **20** (2009), no. 49, 495202.
- [62] J.-P. Tessonier and D. S. Su, *Recent progress on the growth mechanism of carbon nanotubes: A review*, *ChemSusChem* **4** (2011), no. 7, 824–847 (en).
- [63] K. Zimmer, R. Böhme, and B. Rauschenbach, *Local growth of aligned carbon nanotubes at surface sites irradiated by pulsed laser*, *Physica E: Low-dimensional Systems and Nanostructures* **40** (2008), no. 7, 2223–2226.
- [64] J. Kong, H. T. Soh, A. M. Cassell, C. F. Quate, and H. Dai, *Synthesis of individual single-walled carbon nanotubes on patterned silicon wafers*, *Nature* **395** (1998), no. 6705, 878–881 (en).
- [65] K. B. K. Teo, M. Chhowalla, G. A. J. Amaratunga, W. I. Milne, D. G. Hasko, G. Pirio, P. Legagneux, F. Wyczisk, and D. Pribat, *Uniform patterned growth of carbon nanotubes without surface carbon*, *Applied Physics Letters* **79** (2001), no. 10, 1534–1536.

- [66] S. Hofmann, M. Cantoro, M. Kaempgen, D.-J. Kang, V. Golovko, H. Li, Z. Yang, J. Geng, W. Huck, B. Johnson, S. Roth, and J. Robertson, *Catalyst patterning methods for surface-bound chemical vapor deposition of carbon nanotubes*, Applied Physics A: Materials Science & Processing **81** (2005), no. 8, 1559–1567.
- [67] F. Xu, X. Liu, and S. D. Tse, *Synthesis of carbon nanotubes on metal alloy substrates with voltage bias in methane inverse diffusion flames*, Carbon **44** (2006), no. 3, 570–577.
- [68] O. Englander, D. Christensen, and L. Lin, *Local synthesis of silicon nanowires and carbon nanotubes on microbridges*, Applied Physics Letters **82** (2003), no. 26, 4797–4799.
- [69] S. Dittmer, O. Nerushev, and E. Campbell, *Low ambient temperature CVD growth of carbon nanotubes*, Applied Physics A: Materials Science & Processing **84** (2006), no. 3, 243–246.
- [70] D. S. Engstrøm, N. L. Rupesinghe, K. B. K. Teo, W. I. Milne, and P. Bøggild, *Vertically aligned CNT growth on a microfabricated silicon heater with integrated temperature control—determination of the activation energy from a continuous thermal gradient*, Journal of Micromechanics and Microengineering **21** (2011), no. 1, 015004.
- [71] T. Xu, J. Miao, H. Li, and Z. Wang, *Local synthesis of aligned carbon nanotube bundle arrays by using integrated micro-heaters for interconnect applications*, Nanotechnology **20** (2009), no. 29, 295303.
- [72] M. S. Haque, K. B. K. Teo, N. L. Rupesinghe, S. Z. Ali, I. Haneef, S. Maeng, J. Park, F. Udrea, and W. I. Milne, *On-chip deposition of carbon nanotubes using CMOS microhotplates*, Nanotechnology **19** (2008), no. 2, 025607.
- [73] B. D. Sosnowchik and L. Lin, *Rapid synthesis of carbon nanotubes via inductive heating*, Applied Physics Letters **89** (2006), no. 19, 193112–193112–3.
- [74] B. D. Sosnowchik, L. Lin, and O. Englander, *Localized heating induced chemical vapor deposition for one-dimensional nanostructure synthesis*, Journal of Applied Physics **107** (2010), no. 5, 051101–051101–14.
- [75] D. Bäuerle, *Laser processing and chemistry*, Springer, August 2011 (en).
- [76] O. Conde and A. Silvestre, *Laser-assisted deposition of thin films from photoexcited vapour phases*, Applied Physics A: Materials Science & Processing **79** (2004), no. 3, 489–497.
- [77] T. F. Deutsch, D. J. Ehrlich, and R. M. Osgood, *Laser photodeposition of metal films with microscopic features*, Applied Physics Letters **35** (1979), no. 2, 175–177.
- [78] D. Bäuerle, *Laser chemical processing: an overview to the 30th anniversary*, Applied Physics A: Materials Science & Processing **101** (2010), no. 2, 447–459.
- [79] G. Leyendecker, D. Bäuerle, P. Geittner, and H. Lydtin, *Laser induced chemical vapor deposition of carbon*, Applied Physics Letters **39** (1981), no. 11, 921–923.

- [80] W. Kräuter, D. Bäuerle, and F. Fimberger, *Laser induced chemical vapor deposition of ni by decomposition of ni(CO)₄*, Applied Physics A: Materials Science & Processing **31** (1983), no. 1, 13–18.
- [81] M. S. Dresselhaus and P. C. Eklund, *Phonons in carbon nanotubes*, Advances in Physics **49** (2000), no. 6, 705–814.
- [82] M. Dresselhaus, G. Dresselhaus, R. Saito, and A. Jorio, *Raman spectroscopy of carbon nanotubes*, Physics Reports **409** (2005), no. 2, 47 – 99.
- [83] R. Alexandrescu, A. Crunteanu, R. E. Morjan, I. Morjan, F. Rohmund, L. K. L. Falk, G. Ledoux, and F. Huisken, *Synthesis of carbon nanotubes by CO₂-laser-assisted chemical vapour deposition*, Infrared Physics & Technology **44** (2003), no. 1, 43–50.
- [84] F. Rohmund, R.-E. Morjan, G. Ledoux, F. Huisken, and R. Alexandrescu, *Carbon nanotube films grown by laser-assisted chemical vapor deposition*, Journal of Vacuum Science & Technology B: Microelectronics and Nanometer Structures **20** (2002), no. 3, 802.
- [85] V. Jourdain and C. Bichara, *Current understanding of the growth of carbon nanotubes in catalytic chemical vapour deposition*, Carbon **58** (2013), 2–39.
- [86] Z. Chen, Y. Wei, C. Luo, K. Jiang, L. Zhang, Q. Li, S. Fan, and J. Gao, *Laser direct writing carbon nanotube arrays on transparent substrates*, Applied Physics Letters **90** (2007), no. 13, 133108–133108–3.
- [87] J. Park, M. Jeong, and S. Jeong, *Direct writing of carbon nanotube patterns by laser-induced chemical vapor deposition on a transparent substrate*, Applied Surface Science **225** (2009), 4526 – 4530.
- [88] M. C. D. Bock, R. Denk, C. T. Wirth, P. Goldberg-Oppenheimer, S. Hofmann, and J. J. Baumberg, *Optical feedback mechanisms in laser induced growth of carbon nanotube forests*, Applied Physics Letters **100** (2012), no. 1, 013112–013112–3.
- [89] S. Bondi, W. Lackey, R. Johnson, X. Wang, and Z. Wang, *Laser assisted chemical vapor deposition synthesis of carbon nanotubes and their characterization*, Carbon **44** (2006), no. 8, 1393–1403.
- [90] R. Longtin, L.-P. Carignan, C. Fauteux, D. Therriault, and J. Pegna, *Selective area synthesis of aligned carbon nanofibers by laser-assisted catalytic chemical vapor deposition*, Diamond and Related Materials **16** (2007), no. 8, 1541–1549.
- [91] R. Longtin, C. Fauteux, L.-P. Carignan, D. Therriault, and J. Pegna, *Laser-assisted synthesis of carbon nanofibers: From arrays to thin films and coatings*, Surface and Coatings Technology **202** (2008), no. 12, 2661–2669.
- [92] J. Shi, Y. F. Lu, H. Wang, K. J. Yi, Y. S. Lin, R. Zhang, and S. H. Liou, *Synthesis of suspended carbon nanotubes on silicon inverse-opal structures by laser-assisted chemical vapour deposition*, Nanotechnology **17** (2006), no. 15, 3822–3826.

- [93] S. Pisana, M. Cantoro, A. Parvez, S. Hofmann, A. Ferrari, and J. Robertson, *The role of precursor gases on the surface restructuring of catalyst films during carbon nanotube growth*, *Physica E: Low-dimensional Systems and Nanostructures* **37** (2007), no. 1–2, 1–5.
- [94] G. D. Nessim, A. J. Hart, J. S. Kim, D. Acquaviva, J. Oh, C. D. Morgan, M. Seita, J. S. Leib, and C. V. Thompson, *Tuning of vertically-aligned carbon nanotube diameter and areal density through catalyst pre-treatment*, *Nano Lett.* **8** (2008), no. 11, 3587–3593.
- [95] G. D. Nessim, M. Seita, D. L. Plata, K. P. O'Brien, A. John Hart, E. R. Meshot, C. M. Reddy, P. M. Gschwend, and C. V. Thompson, *Precursor gas chemistry determines the crystallinity of carbon nanotubes synthesized at low temperature*, *Carbon* **49** (2011), no. 3, 804–810.
- [96] I. Morjan, I. Soare, R. Alexandrescu, R.-E. Morjan, L. Gavrilă-Florescu, G. Prodan, I. Sandu, E. Popovici, F. Dumitrache, I. Voicu, and M. Scarisoreanu, *Carbon nanotubes growth from C₂H₂ and C₂H₄/NH₃ by catalytic LCVD on supported iron-carbon nanocomposites*, *Physica E: Low-dimensional Systems and Nanostructures* **37** (2007), no. 1–2, 26–33.
- [97] I. Morjan, I. Soare, R. Alexandrescu, L. Gavrilă-Florescu, R.-E. Morjan, G. Prodan, C. Fleaca, I. Sandu, I. Voicu, F. Dumitrache, and E. Popovici, *Carbon nanotubes grown by catalytic CO₂ laser-induced chemical vapor deposition on core-shell Fe/C composite nanoparticles*, *Infrared Physics & Technology* **51** (2008), no. 3, 186–197.
- [98] C. J. Lee and J. Park, *Growth model for bamboolike structured carbon nanotubes synthesized using thermal chemical vapor deposition*, *The Journal of Physical Chemistry B* **105** (2001), no. 12, 2365–2368.
- [99] K. Kwok and W. K. Chiu, *Growth of carbon nanotubes by open-air laser-induced chemical vapor deposition*, *Carbon* **43** (2005), no. 2, 437 – 446.
- [100] S. Corthals, J. Van Noyen, J. Geboers, T. Vosch, D. Liang, X. Ke, J. Hofkens, G. Van Tendeloo, P. Jacobs, and B. Sels, *The beneficial effect of CO₂ in the low temperature synthesis of high quality carbon nanofibers and thin multiwalled carbon nanotubes from CH₄ over ni catalysts*, *Carbon* **50** (2012), no. 2, 372–384.
- [101] Y. Fujiwara, K. Maehashi, Y. Ohno, K. Inoue, and K. Matsumoto, *Position-controlled growth of single-walled carbon nanotubes by laser-irradiated chemical vapor deposition*, *Japanese Journal of Applied Physics* **44** (2005), 1581–1584.
- [102] K. Kasuya, K. Nagato, Y. Jin, H. Morii, T. Ooi, and M. Nakao, *Rapid and localized synthesis of single-walled carbon nanotubes on flat surface by laser-assisted chemical vapor deposition*, *Japanese Journal of Applied Physics* **46** (2007), L333–L335.
- [103] J. B. Park, S. Jeong, M. Jeong, S. Lim, I. Lee, and Y. Lee, *The rapid growth of vertically aligned carbon nanotubes using laser heating*, *Nanotechnology* **20** (2009), 185604.
- [104] J. B. Park, S. H. Jeong, and M. S. Jeong, *Position-controlled synthesis of single-walled carbon nanotubes on a transparent substrate by laser-induced chemical vapor deposition*, *Applied Surface Science* **257** (2010), no. 2, 641–649.

- [105] S. Shang, D. Wellburn, E. Fearon, S. Yan, S. Edwardson, G. Dearden, and K. Watkins, *Laser assisted direct write process with novel beam profiles*, *Optics and Lasers in Engineering* **51** (2013), no. 5, 527–532.
- [106] S. Chiashi, M. Kohno, Y. Takata, and S. Maruyama, *Localized synthesis of single-walled carbon nanotubes on silicon substrates by a laser heating catalytic CVD*, *Journal of Physics: Conference Series* **59** (2007), 155–158.
- [107] J. Shi, Y. F. Lu, K. J. Yi, Y. S. Lin, S. H. Liou, J. B. Hou, and X. W. Wang, *Direct synthesis of single-walled carbon nanotubes bridging metal electrodes by laser-assisted chemical vapor deposition*, *Applied Physics Letters* **89** (2006), no. 8, 083105–083105–3.
- [108] M. Haluška, Y. Bellouard, and A. Dietzel, *Time dependent growth of vertically aligned carbon nanotube forest using a laser activated catalytical CVD method, time dependent growth of vertically aligned carbon nanotube forest using a laser activated catalytical CVD method*, *physica status solidi (b)* **245**, **245** (2008), no. 10, 10, 1927, 1927–1930, 1930 (en, en).
- [109] Z. Liu, D. Styers-Barnett, A. Puretzky, C. Rouleau, D. Yuan, I. Ivanov, K. Xiao, J. Liu, and D. Geohegan, *Pulsed laser CVD investigations of single-wall carbon nanotube growth dynamics*, *Applied Physics A: Materials Science & Processing* **93** (2008), 987–993, 10.1007/s00339-008-4804-8.
- [110] T. Uchida and Y. Yoshida, *Development of a laser-assisted chemical vapor deposition system for the growth of carbon nanotubes*, *Journal of Laser Micro Nanoengineering* **6** (2011), no. 3, 214–219 (English), WOS:000300355900008.
- [111] D. L. Jeanmaire and R. P. Van Duyne, *Surface raman spectroelectrochemistry: Part i. heterocyclic, aromatic, and aliphatic amines adsorbed on the anodized silver electrode*, *Journal of Electroanalytical Chemistry and Interfacial Electrochemistry* **84** (1977), no. 1, 1–20.
- [112] L. Cao, D. N. Barsic, A. R. Guichard, and M. L. Brongersma, *Plasmon-assisted local temperature control to pattern individual semiconductor nanowires and carbon nanotubes*, *Nano Letters* **7** (2007), no. 11, 3523–3527.
- [113] W. H. Hung, I.-K. Hsu, A. Bushmaker, R. Kumar, J. Theiss, and S. B. Cronin, *Laser directed growth of carbon-based nanostructures by plasmon resonant chemical vapor deposition*, *Nano Letters* **8** (2008), no. 10, 3278–3282.
- [114] G. D. Nessim, *Properties, synthesis, and growth mechanisms of carbon nanotubes with special focus on thermal chemical vapor deposition*, *Nanoscale* **2** (2010), no. 8, 1306–1323 (en).
- [115] C. J. Lee, S. C. Lyu, Y. R. Cho, J. H. Lee, and K. I. Cho, *Diameter-controlled growth of carbon nanotubes using thermal chemical vapor deposition*, *Chemical Physics Letters* **341** (2001), no. 3-4, 245 – 249.
- [116] W. Xiong, Y. S. Zhou, M. Mahjouri-Samani, W. Q. Yang, K. J. Yi, X. N. He, S. H. Liou, and Y. F. Lu, *Self-aligned growth of single-walled carbon nanotubes using optical near-field effects*, *Nanotechnology* **20** (2009), no. 2, 025601.

- [117] M. Mahjouri-Samani, Y. S. Zhou, W. Xiong, Y. Gao, M. Mitchell, L. Jiang, and Y. F. Lu, *Diameter modulation by fast temperature control in laser-assisted chemical vapor deposition of single-walled carbon nanotubes*, *Nanotechnology* **21** (2010), no. 39, 395601.
- [118] M. Balkanski, R. F. Wallis, and E. Haro, *Anharmonic effects in light scattering due to optical phonons in silicon*, *Physical Review B* **28** (1983), no. 4, 1928–1934.
- [119] S. Chiashi, Y. Murakami, Y. Miyauchi, and S. Maruyama, *Temperature dependence of raman scattering from single-walled carbon nanotubes: Undefined radial breathing mode peaks at high temperatures*, *Japanese Journal of Applied Physics* **47** (2008), no. 4, 2010–2015.
- [120] M. C. LeMieux, M. Roberts, S. Barman, Y. W. Jin, J. M. Kim, and Z. Bao, *Self-sorted, aligned nanotube networks for thin-film transistors*, *Science* **321** (2008), no. 5885, 101–104 (en).
- [121] M. Ullmann, S. K. Friedlander, and A. Schmidt-Ott, *Nanoparticle formation by laser ablation*, *Journal of Nanoparticle Research* **4** (2002), no. 6, 499–509.
- [122] F. Dumitrache, I. Morjan, R. Alexandrescu, R. Morjan, I. Voicu, I. Sandu, I. Soare, M. Ploscaru, C. Fleaca, V. Ciupina, G. Prodan, B. Rand, R. Brydson, and A. Woodward, *Nearly monodispersed carbon coated iron nanoparticles for the catalytic growth of nanotubes/nanofibres*, *Diamond and Related Materials* **13** (2004), no. 2, 362–370.
- [123] Y. Avigal and R. Kalish, *Growth of aligned carbon nanotubes by biasing during growth*, *Applied Physics Letters* **78** (2001), no. 16, 2291–2293.
- [124] Y. Zhang, A. Chang, J. Cao, Q. Wang, W. Kim, Y. Li, N. Morris, E. Yenilmez, J. Kong, and H. Dai, *Electric-field-directed growth of aligned single-walled carbon nanotubes*, *Applied Physics Letters* **79** (2001), no. 19, 3155–3157.
- [125] S. Huang, X. Cai, and J. Liu, *Growth of millimeter-long and horizontally aligned single-walled carbon nanotubes on flat substrates*, *Journal of the American Chemical Society* **125** (2003), no. 19, 5636–5637.
- [126] M. Hofmann, D. Nezich, A. R. , and J. Kong, *In-situ sample rotation as a tool to understand chemical vapor deposition growth of long aligned carbon nanotubes*, *Nano Letters* **8** (2008), no. 12, 4122–4127.
- [127] Y. S. Zhou, W. Xiong, J. Park, M. Qian, M. Mahjouri-Samani, Y. Gao, L. Jiang, and Y. Lu, *Laser-assisted nanofabrication of carbon nanostructures*, *Journal of Laser Applications* **24** (2012), no. 4, 042007–042007–19.
- [128] W. Ruan, Z. Wang, J. Li, K. Jiang, and L. Liu, *Synthesis of carbon nanotubes on suspending microstructures by rapid local laser heating*, *Ieee Sensors Journal* **11** (2011), no. 12, 3424–3425 (English), WOS:000301878500031.
- [129] E. R. Meshot, D. L. Plata, S. Tawfick, Y. Zhang, E. A. Verploegen, and A. J. Hart, *Engineering vertically aligned carbon nanotube growth by decoupled thermal treatment of precursor and catalyst*, *ACS Nano* **3** (2009), no. 9, 2477–2486.

- [130] J. B. In, C. P. Grigoropoulos, A. A. Chernov, and A. Noy, *Growth kinetics of vertically aligned carbon nanotube arrays in clean oxygen-free conditions*, ACS Nano **5** (2011), no. 12, 9602–9610.
- [131] D. B. Geohegan, A. A. Puzos, I. N. Ivanov, S. Jesse, G. Eres, and J. Y. Howe, *In situ growth rate measurements and length control during chemical vapor deposition of vertically aligned multiwall carbon nanotubes*, Applied Physics Letters **83** (2003), no. 9, 1851–1853.
- [132] A. Puzos, D. Geohegan, S. Jesse, I. Ivanov, and G. Eres, *In situ measurements and modeling of carbon nanotube array growth kinetics during chemical vapor deposition*, Applied Physics A: Materials Science & Processing **81** (2005), no. 2, 223–240.
- [133] S. Linderoth, S. Mørup, and M. D. Bentzon, *Oxidation of nanometer-sized iron particles*, Journal of Materials Science **30** (1995), no. 12, 3142–3148.
- [134] Z.-P. Yang, L. Ci, J. A. Bur, S.-Y. Lin, and P. M. Ajayan, *Experimental observation of an extremely dark material made by a low-density nanotube array*, Nano Letters **8** (2008), no. 2, 446–451.
- [135] A. C. Ferrari, *Raman spectroscopy of graphene and graphite: Disorder, electron–phonon coupling, doping and nonadiabatic effects*, Solid State Communications **143** (2007), no. 1–2, 47–57.
- [136] A. Loiseau, X. Blase, J.-C. Charlier, P. Gadelle, C. Journet, C. Laurent, and A. Peigney, *Synthesis methods and growth mechanisms*, Understanding Carbon Nanotubes (A. Loiseau, P. Launois, P. Petit, S. Roche, and J.-P. Salvetat, eds.), Lecture Notes in Physics, no. 677, Springer Berlin Heidelberg, January 2006, pp. 49–130.
- [137] H.-C. Wu, C.-T. Hong, H.-T. Chiu, and Y.-Y. Li, *Continuous synthesis of carbon spheres by a non-catalyst vertical chemical vapor deposition*, Diamond and Related Materials **18** (2009), no. 4, 601–605.
- [138] C. L. Yaws and W. Braker, *Matheson gas data book*, McGraw-Hill Professional, June 2001 (en).
- [139] S. W. Churchill and H. H. Chu, *Correlating equations for laminar and turbulent free convection from a vertical plate*, International Journal of Heat and Mass Transfer **18** (1975), no. 11, 1323–1329.
- [140] O. A. Nerushev, S. Dittmar, R.-E. Morjan, F. Rohmund, and E. E. B. Campbell, *Particle size dependence and model for iron-catalyzed growth of carbon nanotubes by thermal chemical vapor deposition*, Journal of Applied Physics **93** (2003), no. 7, 4185–4190.
- [141] A. Moisala, A. G. Nasibulin, and E. I. Kauppinen, *The role of metal nanoparticles in the catalytic production of single-walled carbon nanotubes*, Journal of Physics: Condensed Matter **15** (2003), no. 42, 3011 – 3035.
- [142] M. V. C. Sastri, R. P. Viswanath, and B. Viswanathan, *Studies on the reduction of iron oxide with hydrogen*, International Journal of Hydrogen Energy **7** (1982), no. 12, 951–955.

- [143] A. Pineau, N. Kanari, and I. Gaballah, *Kinetics of reduction of iron oxides by H_2 : Part i: Low temperature reduction of hematite*, *Thermochimica Acta* **447** (2006), no. 1, 89–100.
- [144] C. Mattevi, C. T. Wirth, S. Hofmann, R. Blume, M. Cantoro, C. Ducati, C. Cepek, A. Knop-Gericke, S. Milne, C. Castellarin-Cudia, S. Dolafi, A. Goldoni, R. Schloegl, and J. Robertson, *In-situ x-ray photoelectron spectroscopy study of Catalyst-Support interactions and growth of carbon nanotube forests*, *J. Phys. Chem. C* **112** (2008), no. 32, 12207–12213.
- [145] P. B. Amama, C. L. Pint, S. M. Kim, L. McJilton, K. G. Eyink, E. A. Stach, R. H. Hauge, and B. Maruyama, *Influence of alumina type on the evolution and activity of alumina-supported Fe catalysts in single-walled carbon nanotube carpet growth*, *ACS Nano* **4** (2010), no. 2, 895–904, PMID: 20131855.
- [146] H. Sato, Y. Hori, K. Hata, K. Seko, H. Nakahara, and Y. Saito, *Effect of catalyst oxidation on the growth of carbon nanotubes by thermal chemical vapor deposition*, *Journal of Applied Physics* **100** (2006), no. 10, 104321–104321–6.
- [147] A. Jorio, R. Saito, J. H. Hafner, C. M. Lieber, M. Hunter, T. McClure, G. Dresselhaus, and M. S. Dresselhaus, *Structural (n, m) determination of isolated single-wall carbon nanotubes by resonant raman scattering*, *Physical Review Letters* **86** (2001), no. 6, 1118–1121.
- [148] C. T. Wirth, C. Zhang, G. Zhong, S. Hofmann, and J. Robertson, *Diffusion- and reaction-limited growth of carbon nanotube forests*, *ACS Nano* **3** (2009), no. 11, 3560–3566.
- [149] R. Xiang, Z. Yang, Q. Zhang, G. Luo, W. Qian, F. Wei, M. Kadowaki, E. Einarsson, and S. Maruyama, *Growth deceleration of vertically aligned carbon nanotube arrays: Catalyst deactivation or feedstock diffusion controlled?*, *The Journal of Physical Chemistry C* **112** (2008), no. 13, 4892–4896.
- [150] I. Lebedeva, A. Knizhnik, A. Gavrikov, A. Baranov, B. Potapkin, S. Aceto, P.-A. Bui, C. Eastman, U. Grossner, D. Smith, and T. Sommerer, *First-principles based kinetic modeling of effect of hydrogen on growth of carbon nanotubes*, *Carbon* **49** (2011), no. 7, 2508–2521.
- [151] S. Hofmann, G. Csányi, A. C. Ferrari, M. C. Payne, and J. Robertson, *Surface diffusion: The low activation energy path for nanotube growth*, *Physical Review Letters* **95** (2005), no. 3, 036101.
- [152] K. Liu, K. Jiang, C. Feng, Z. Chen, and S. Fan, *A growth mark method for studying growth mechanism of carbon nanotube arrays*, *Carbon* **43** (2005), no. 14, 2850–2856.
- [153] S. L. Pirard, S. Douven, C. Bossuot, G. Heyen, and J.-P. Pirard, *A kinetic study of multi-walled carbon nanotube synthesis by catalytic chemical vapor deposition using a Fe-Co/Al₂O₃ catalyst*, *Carbon* **45** (2007), no. 6, 1167–1175.

- [154] L. Zhu, D. W. Hess, and C.-P. Wong, *Monitoring carbon nanotube growth by formation of nanotube stacks and investigation of the diffusion-controlled kinetics*, *The Journal of Physical Chemistry B* **110** (2006), no. 11, 5445–5449.
- [155] G. Zhong, T. Iwasaki, J. Robertson, and H. Kawarada, *Growth kinetics of 0.5 cm vertically aligned single-walled carbon nanotubes*, *The Journal of Physical Chemistry B* **111** (2007), no. 8, 1907–1910.
- [156] I. Chorkendorff and J. W. Niemantsverdriet, *Concepts of modern catalysis and kinetics*, Wiley-VCH Verlag GmbH & Co. KGaA, October 2007 (en).
- [157] L. X. Zheng, M. J. O'Connell, S. K. Doorn, X. Z. Liao, Y. H. Zhao, E. A. Akhadow, M. A. Hoffbauer, B. J. Roop, Q. X. Jia, R. C. Dye, D. E. Peterson, S. M. Huang, J. Liu, and Y. T. Zhu, *Ultralong single-wall carbon nanotubes*, *Nature Materials* **3** (2004), no. 10, 673–676 (en).
- [158] A. A. Puretzky, D. B. Geohegan, X. Fan, and S. J. Pennycook, *In situ imaging and spectroscopy of single-wall carbon nanotube synthesis by laser vaporization*, *Appl. Phys. Lett.* **76** (2000), no. 2, 182 – 184.
- [159] R. Baker, P. Harris, R. Thomas, and R. Waite, *Formation of filamentous carbon from iron, cobalt and chromium catalyzed decomposition of acetylene*, *Journal of Catalysis* **30** (1973), no. 1, 86–95.
- [160] M. Chhowalla, K. B. K. Teo, C. Ducati, N. L. Rupesinghe, G. A. J. Amaratunga, A. C. Ferrari, D. Roy, J. Robertson, and W. I. Milne, *Growth process conditions of vertically aligned carbon nanotubes using plasma enhanced chemical vapor deposition*, *Journal of Applied Physics* **90** (2001), no. 10, 5308–5317.
- [161] Y. T. Lee, J. Park, Y. S. Choi, H. Ryu, and H. J. Lee, *Temperature-dependent growth of vertically aligned carbon nanotubes in the range 800-1100 c*, *The Journal of Physical Chemistry B* **106** (2002), no. 31, 7614–7618.
- [162] C. Ducati, I. Alexandrou, M. Chhowalla, G. A. J. Amaratunga, and J. Robertson, *Temperature selective growth of carbon nanotubes by chemical vapor deposition*, *Journal of Applied Physics* **92** (2002), no. 6, 3299–3303.
- [163] S. Hofmann, C. Ducati, J. Robertson, and B. Kleinsorge, *Low-temperature growth of carbon nanotubes by plasma-enhanced chemical vapor deposition*, *Applied Physics Letters* **83** (2003), no. 1, 135–137.
- [164] Y. T. Lee, N. S. Kim, J. Park, J. B. Han, Y. S. Choi, H. Ryu, and H. J. Lee, *Temperature-dependent growth of carbon nanotubes by pyrolysis of ferrocene and acetylene in the range between 700 and 1000 c*, *Chemical Physics Letters* **372** (2003), no. 5–6, 853–859.
- [165] O. A. Louchev, T. Laude, Y. Sato, and H. Kanda, *Diffusion-controlled kinetics of carbon nanotube forest growth by chemical vapor deposition*, *The Journal of Chemical Physics* **118** (2003), no. 16, 7622–7634.

- [166] K.-E. Kim, K.-J. Kim, W. S. Jung, S. Y. Bae, J. Park, J. Choi, and J. Choo, *Investigation on the temperature-dependent growth rate of carbon nanotubes using chemical vapor deposition of ferrocene and acetylene*, *Chemical Physics Letters* **401** (2005), no. 4–6, 459–464.
- [167] M. J. Bronikowski, *Longer nanotubes at lower temperatures: The influence of effective activation energies on carbon nanotube growth by thermal chemical vapor deposition†*, *The Journal of Physical Chemistry C* **111** (2007), no. 48, 17705–17712.
- [168] L. Zhu, J. Xu, F. Xiao, H. Jiang, D. W. Hess, and C. Wong, *The growth of carbon nanotube stacks in the kinetics-controlled regime*, *Carbon* **45** (2007), no. 2, 344–348.
- [169] E. Einarsson, Y. Murakami, M. Kadowaki, and S. Maruyama, *Growth dynamics of vertically aligned single-walled carbon nanotubes from in situ measurements*, *Carbon* **46** (2008), no. 6, 923–930.
- [170] S. K. Pal, S. Talapatra, S. Kar, L. Ci, R. Vajtai, T. Borca-Tasciuc, L. S. Schadler, and P. M. Ajayan, *Time and temperature dependence of multi-walled carbon nanotube growth on inconel 600*, *Nanotechnology* **19** (2008), no. 4, 045610 (en).
- [171] C.-T. Hsieh, Y.-T. Lin, W.-Y. Chen, and J.-L. Wei, *Parameter setting on growth of carbon nanotubes over transition metal/alumina catalysts in a fluidized bed reactor*, *Powder Technology* **192** (2009), no. 1, 16–22.
- [172] G. D. Nessim, M. Seita, K. P. O'Brien, A. J. Hart, R. K. Bonaparte, R. R. Mitchell, and C. V. Thompson, *Low temperature synthesis of vertically aligned carbon nanotubes with electrical contact to metallic substrates enabled by thermal decomposition of the carbon feedstock*, *Nano Letters* **9** (2009), no. 10, 3398–3405.
- [173] R. Philippe, P. Serp, P. Kalck, Y. Kihn, S. Bordère, D. Plee, P. Gaillard, D. Bernard, and B. Caussat, *Kinetic study of carbon nanotubes synthesis by fluidized bed chemical vapor deposition*, *AIChE Journal* **55** (2009), no. 2, 450–464 (en).
- [174] P. Vinten, J. Lefebvre, and P. Finnie, *Kinetic critical temperature and optimized chemical vapor deposition growth of carbon nanotubes*, *Chemical Physics Letters* **469** (2009), no. 4–6, 293–297.
- [175] J. Robertson, *Heterogeneous catalysis model of growth mechanisms of carbon nanotubes, graphene and silicon nanowires*, *Journal of Materials Chemistry* **22** (2012), no. 37, 19858–19862 (en).
- [176] W. F. Gale and T. C. Totemeier, *Smithells metals reference book*, Butterworth-Heinemann, Oxford, December 2003 (en).
- [177] A. B. Anderson, *Interaction of hydrogen, carbon, ethylene, acetylene, and alkyl fragments with iron surfaces. catalytic hydrogenation, dehydrogenation, carbon bond breakage, and hydrogen mobility*, *Journal of the American Chemical Society* **99** (1977), no. 3, 696–707.
- [178] R. Sharma, E. Moore, P. Rez, and M. M. J. Treacy, *Site-specific fabrication of fe particles for carbon nanotube growth*, *Nano Letters* **9** (2009), no. 2, 689–694.

- [179] K. Yang and R. Yang, *The accelerating and retarding effects of hydrogen on carbon deposition on metal surfaces*, Carbon **24** (1986), no. 6, 687–693.
- [180] Y. Nishiyama and Y. Tamai, *Effect of hydrogen on carbon deposition catalyzed by copper-nickel alloys*, Journal of Catalysis **45** (1976), no. 1, 1–5.
- [181] S. McCaldin, M. Bououdina, D. Grant, and G. Walker, *The effect of processing conditions on carbon nanostructures formed on an iron-based catalyst*, Carbon **44** (2006), no. 11, 2273–2280.
- [182] Z. Yu, D. Chen, B. Tøtdal, T. Zhao, Y. Dai, W. Yuan, and A. Holmen, *Catalytic engineering of carbon nanotube production*, Applied Catalysis A: General **279** (2005), no. 1–2, 223–233.
- [183] M. Pérez-Cabero, E. Romeo, C. Royo, A. Monzón, A. Guerrero-Ruiz, and I. Rodríguez-Ramos, *Growing mechanism of CNTs: a kinetic approach*, Journal of Catalysis **224** (2004), no. 1, 197–205.
- [184] G. D. Chen, F. Fachin, M. Fernandez-Suarez, B. L. Wardle, and M. Toner, *Nanoporous elements in microfluidics for multiscale manipulation of bioparticles*, Small **7** (2011), no. 8, 1061–1067 (en).
- [185] G. D. Chen, F. Fachin, E. Colombini, B. L. Wardle, and M. Toner, *Nanoporous microelement arrays for particle interception in microfluidic cell separation*, Lab on a Chip **12** (2012), no. 17, 3159–3167 (en).
- [186] A. Sepúlveda, F. Fachin, R. G. d. Villoria, B. Wardle, J. Viana, A. Pontes, and L. Rocha, *Nanocomposite flexible pressure sensor for biomedical applications*, Procedia Engineering **25** (2011), 140–143.
- [187] Y. Bellouard, A. Said, M. Dugan, and P. Bado, *Fabrication of high-aspect ratio, microfluidic channels and tunnels using femtosecond laser pulses and chemical etching*, Optics Express **12** (2004), no. 10, 2120–2129.
- [188] C. B. Schaffer, J. F. García, and E. Mazur, *Bulk heating of transparent materials using a high-repetition-rate femtosecond laser*, Applied Physics A **76** (2003), no. 3, 351–354 (en).
- [189] J. B. Park, W. Xiong, Y. Gao, M. Qian, Z. Q. Xie, M. Mitchell, Y. S. Zhou, G. H. Han, L. Jiang, and Y. F. Lu, *Fast growth of graphene patterns by laser direct writing*, Applied Physics Letters **98** (2011), no. 12, 123109.
- [190] J. B. Park, W. Xiong, Z. Q. Xie, Y. Gao, M. Qian, M. Mitchell, M. Mahjouri-Samani, Y. S. Zhou, L. Jiang, and Y. F. Lu, *Transparent interconnections formed by rapid single-step fabrication of graphene patterns*, Applied Physics Letters **99** (2011), no. 5, 053103.
- [191] P. B. Amama, C. L. Pint, L. McJilton, S. M. Kim, E. A. Stach, P. T. Murray, R. H. Hauge, and B. Maruyama, *Role of water in super growth of single-walled carbon nanotube carpets*, Nano Letters **9** (2009), no. 1, 44–49.

- [192] G. Zhang, D. Mann, L. Zhang, A. Javey, Y. Li, E. Yenilmez, Q. Wang, J. P. McVittie, Y. Nishi, J. Gibbons, and H. Dai, *Ultra-high-yield growth of vertical single-walled carbon nanotubes: Hidden roles of hydrogen and oxygen*, Proceedings of the National Academy of Sciences of the United States of America **102** (2005), no. 45, 6141 – 16145.

List of publications

Refereed Journal Publications

- 2010 M. Haluška, Y. Bellouard, Y. van de Burgt and A. Dietzel, *In situ monitoring of single-wall carbon nanotube laser assisted growth*, Nanotechnology 21, 075602 (2010).
- 2012 Y. van de Burgt, Y. Bellouard, R. Mandamparambil, M. Haluška, and A. Dietzel, *Closed-loop control of laser assisted chemical vapor deposition growth of carbon nanotubes*, Journal of Applied Physics 112, 034904-034904-8 (2012).
- 2013 Y. van de Burgt, A. Champion and Y. Bellouard, *In-situ localized carbon nanotube growth inside partially sealed enclosures*, AIP Advances 3, 092119 (2013).
- 2014 Y. van de Burgt, Y. Bellouard and R. Mandamparambil, *Kinetics of Laser-Assisted Carbon Nanotube Growth*, Physical Chemistry Chemical Physics 16, 5162-5173 (2014).
- 2014 Y. van de Burgt, Y. Bellouard, W. van Loon and R. Mandamparambil, *Miniaturized Reaction Chamber for Optimized Laser-Assisted Carbon Nanotube Growth*, accepted for publication in Journal of Laser Micro / Nanoengineering (2014).
- 2014 Y. van de Burgt, *Laser-assisted growth of carbon nanotubes - a review*, submitted (2014).

Conference Proceedings

- 2011 Y. van de Burgt, Y. Bellouard, R. Mandamparambil and A. Dietzel, *Closed-loop Control of a Laser Assisted Carbon Nanotube Growth Process for Interconnects in Flexible Electronics.*, MRS Online Proceedings Library 1365, (2011).
- 2013 Y. van de Burgt, Y. Bellouard, W. van Loon and R. Mandamparambil, *Miniaturized Reaction Chamber for Optimized Laser-Assisted Carbon Nanotube Growth*, Proceedings of LPM (Niigata), Japan Laser Processing Society (JLPS), (2013).
- 2014 Y. van de Burgt and Y. Bellouard, *Laser-assisted growth of carbon nanotubes on laser-patterned substrates and inside sealed micro-channels*, SPIE Conference Proceedings, (2014).

Samenvatting

Koolstof nanobuisjes of *carbon nanotubes* zijn een speciale vorm van pure koolstof opgerold tot een buisje met een diameter in de orde van grootte van een nanometer (1 miljoenste millimeter). Door deze speciale vorm bezitten ze bijzondere eigenschappen en zijn er legio technologische toepassingen te bedenken zoals in sensoren, transistors en in de elektronica-, display- en zonnecellen-industrie. Omdat de uiteindelijke eigenschappen van de buisjes voor een groot gedeelte afhangen van de specifieke geometrie en vorm van de buisjes is het van belang hierop een zo groot mogelijke invloed te kunnen uitoefenen. Chemisch opdampen of *chemical vapor deposition* heeft zich de afgelopen jaren ontwikkeld als de productiemethode met een hoge mate van beheersing van de eigenschappen van de koolstof nanobuisjes. Deze methode maakt gebruik van een substraat met een katalysator, in dit geval een dunne laag ijzer, thermische energie en een koolstofhoudend gas, om op een gecontroleerde manier nanobuisjes te groeien.

Sommige toepassingen vereisen dat de koolstof nanobuisjes lokaal worden geproduceerd of *gegroeid* en dit is niet mogelijk met de conventionele methode van chemisch opdampen. Groei van koolstof nanobuisjes met behulp van een laser (zoals de titel van dit proefschrift: *laser-assisted growth of carbon nanotubes*) is een veelbelovende techniek om dit mogelijk te maken. Bij deze techniek wordt de warmte, als energiebron nodig voor de groei, geleverd door een laserstraal. Het lastige aan deze techniek is echter dat het vrij moeilijk is om precies te weten wat er op het substraat gebeurt onder invloed van die laser. Het meten van de temperatuur bijvoorbeeld is erg ingewikkeld.

In dit proefschrift wordt deze lasergeleide techniek onderzocht en geoptimaliseerd. Het proces wordt continu gemeten door middel van verschillende sensoren, waaronder een thermische straling-sensor die gebruikt wordt om de temperatuur te bepalen, en een reflectie-sensor die inzicht geeft in groeikarakteristieken en groeikinetic. Het proces wordt geregeld door een regelsysteem dat oververhitting voorkomt en tegelijk zorgt voor een verbetering van de reproduceerbaarheid.

Om de beheersing van de groei en eigenschappen van de nanobuisjes nog verder te vergroten is een mini reactiekamer ontwikkeld. Deze reactiekamer heeft namelijk als voordeel dat de stroming van het gas over het substraat laminair is en dat de samenstelling van dit gas beter bekend is. Tevens heeft de relatief kleine inhoud van de reactiekamer als gevolg dat er sneller experimenten gedaan kunnen worden. Hierdoor is het mogelijk om een groot aantal verschillende experimentele condities, zoals de verhouding tussen de gassen, de temperatuur en het gas-debiet, te onderzoeken. Dit onderzoek heeft geresulteerd in de ontdekking van verschillende *groeigebieden* voor verschillende groeicondities. Deze gebieden hebben allemaal hun eigen karakteristieken en resulteren in specifieke structurele eigenschappen van de nanobuisjes.

De op deze lasertechniek gebaseerde manier om koolstof nanobuisjes te maken, biedt een

aantal toepassingsperspectieven. Zo wordt in dit proefschrift getoond dat de nanobuisjes in een flexibele polymeer laag kunnen worden opgenomen, met als eventuele toepassing elektrische connecties in flexibele elektronica (denk aan oprolbare elektronica). Ook de directe groei van nanobuisjes in een microkanaal wordt gedemonstreerd, waarin ze bijvoorbeeld dienst kunnen doen als filters of sensoren in *lab-on-a-chip* toepassingen. Als laatste wordt een aantal unieke groeimethoden gedemonstreerd waaronder het produceren van *banen* van nanobuisjes door, tijdens het groeiproces, de gehele reactiekamer te bewegen ten opzichte van de laser.

Samenvattend draagt dit proefschrift niet alleen bij aan het begrijpen en optimaliseren van lasergeleide groei van koolstof nanobuisjes, maar levert het ook nieuwe inzichten in de algemene groeikinetiek en potentiële toepassingen van de nanobuisjes. Door de speciale eigenschappen van dit nieuwe materiaal levert het unieke mogelijkheden op om allerlei toepassingen en bestaande technieken zuiniger, sneller, goedkoper, sterker en milieuvriendelijker te maken. In de toekomst zullen al deze eigenschappen steeds belangrijker worden en het fundamentele onderzoek naar dit soort unieke materialen, zoals onder andere beschreven in dit proefschrift, is daarom van groot belang om deze beloftes waar te kunnen maken.

Dankwoord / Acknowledgements

In dit laatste gedeelte van mijn proefschrift wil ik graag een aantal mensen bedanken voor alle hulp die ik heb mogen ontvangen in de afgelopen jaren. Zoals kennelijk ieder promotieonderzoek struikelblokken kent, liep ook mijn onderzoek af en toe stroef. Geen of nauwelijks resultaten, blauwe schermen tijdens de experimenten, een kapotte laser en talloze foutmeldingen tijdens computersimulaties hebben de nodige invloed gehad op het hele traject en brachten mij soms ook aan het twijfelen. Daarom ben ik iedereen die mij in welk opzicht dan ook door de afgelopen 4,5 jaar heeft heen geholpen erg dankbaar.

First and foremost I want to thank Yves Bellouard, who, as my daily supervisor, was always available for new ideas and inspiring discussions as well as keeping track of the work still to be done, marking milestones and providing me with the right amount of trust and confidence to finish the work in time. Yves, without you I would not have been able to get where I am today and for that I want to express my deepest gratitude. I always felt more than welcome and at ease in your presence. Our discussions often deviated far from the topic at hand and I am confident that I was privileged to get to know you personally quite well. Many thanks for all your advice, suggestions and insights, I sincerely hope that we will maintain this good relation in the future.

Secondly, I want to thank my two promotors Andreas Dietzel and Jaap den Toonder and my external supervisor, Rajesh Mandamparambil. Andreas, thank you for offering me the chance to do this research by hiring me when I completed my Master's degree. I still remember the phone call in which I had to decide whether I would take the position. We worked together for almost 3 years when you decided to go back to Germany and become a professor at the University of Braunschweig, which, at the time, I understood but also regretted. I am very grateful to you for starting this project, for all your help, from my internship in Bangalore, India until today, for the trust you put in me and for the opportunity you provided me to fulfill this goal.

Jaap, bedankt voor het onzelfzuchtig opnemen van de taak als eerste promotor en alles wat daarbij hoort. Als nieuw hoofd van onze vrij gevarieerde groep heb je ook de verantwoording op je genomen om alle bestaande projecten tot een goed einde te begeleiden. Ondanks het feit dat ook mijn onderzoek inhoudelijk gezien redelijk ver van je eigen achtergrond ligt, heb ik veel steun aan je gehad, zowel wat betreft het lezen en corrigeren van mijn artikelen en het proefschrift, als bij de formaliteiten rond de afronding. Het was een groot plezier om met je samen te mogen werken.

I want to thank you Rajesh, for all the helpful "Thursday" discussions, providing me with new insights and ideas, and the freedom you gave me within the Holst Centre project. As long as it was Thursday, your door was always open for a quick chat or a lengthy detailed discussion. And of course I could always pay you a visit at the High Tech Campus.

I am also truly grateful to Alberto Salleo for taking part in my defence-committee, evaluating my dissertation and joining the ceremony all the way from the United States.

Natuurlijk ook veel dank aan de andere leden van de promotiecommissie, Philip de Goey, Erik Bakkers en Anton van Steenhoven voor de tijd en moeite om mijn proefschrift te lezen en te beoordelen. Met name Anton wil ik ontzettend bedanken voor alle hulp tijdens de periode waarin er geen hoofd van de groep was. Jij hebt de groep draaiende gehouden en mij, weliswaar met een iets meer thermische benadering, kritisch in de gaten gehouden en gezorgd dat mijn onderzoek netjes op de rails bleef.

Apart from my supervisors at the university, I am also very grateful to Miro Haluska, currently working at ETH Zurich, for all his help and suggestions during the past 5 years. Miro, you always answered all my questions quickly and thoroughly, even though you must have been always busy yourself. I really enjoyed our time together, both here in Eindhoven as well as in Australia.

Natuurlijk is onderzoek doen niet mogelijk zonder de technische hulp van anderen. Hoewel ik natuurlijk zoveel mogelijk zelf probeerde te doen, is dat lang niet altijd mogelijk geweest. Heel veel dank daarom aan Willy ter Elst voor alle praktische zaken en hulp in het lab, Marc van Maris voor alle hulp en discussies in het Multiscale-lab, Jos Laven voor hulp bij de Raman-microscoop, Henri Fledderus van Holst Centre voor laser gerelateerde zaken en Harrie de Laat en Ruud de Regt van de GTD voor het meedenken en fabriceren van de opstellingen.

Ik heb, in de bijna 6,5 jaar dat ik bij deze dynamische groep hoor, met veel plezier samengewerkt met de groep. Vooral Stijn wil ik bedanken voor alle plezierige jaren in ons 'grote' kantoor, alle discussies over ons werk en vooral ook voor de gesprekken tussendoor die zorgden voor een aangename afleiding. Liesbeth, bedankt dat je altijd voor me klaarstond en meteen alles wist te regelen. Ik heb met erg veel plezier al die jaren met je samengewerkt en vond het heel fijn dat ik zowel mijn frustraties als mijn gelukkige momenten met jou kon delen. Het binnenlopen van jouw kamer zorgde daarom bij mij altijd voor een glimlach.

Thanks to all my other (former) colleagues for a great time, both inside as well as outside the university. Sikko, Johan, Allwyn, Allison, Chuan, Audrey, Tau, Gari, Ben, Nathaniel, Hossein, Giuseppe, Christos, Martijn, Erik, Regina, Arjan, Dirk, David, Victor and all others that I worked with in the past years, thanks for all the inspiring discussions and everything else.

Ook wil ik graag mijn twee Bachelor eindstudenten, Ton en Wouter, bedanken voor de hulp en bijdrage aan mijn onderzoek. Wouter, ontzettend veel dank en waardering voor het ontwerp en de fabricage van de prachtige en functionele reactiekamer, beschreven in dit proefschrift.

Wat is het leven zonder je vrienden en familie? Ik ben ontzettend blij met zo'n grote en fijne vriendengroep en met mijn warme en hechte familie. Iedereen ontzettend bedankt voor alle gesprekken, discussies, vakanties, zomeravonden, feestjes en festivals. In het bijzonder veel dank aan mijn broer Igor en zus Sacha, voor onze fijne band en het feit dat ze altijd voor me klaar staan. Ook Lotus wil ik graag bedanken voor haar altijd luisterend oor en al haar steun en adviezen tijdens mijn promotietraject. Maar natuurlijk ook veel dank aan de rest van mijn familie en vrienden, in het bijzonder Emma, Jelte, Roel en Pieter, voor alle steun,

raadgevingen en afleiding, zodat ik regelmatig even een gezonde afstand kon nemen van mijn werk en met frisse moed weer verder kon gaan. En natuurlijk Berry, bedankt voor je hulp bij het maken van de cover van dit boekje.

Ten slotte wil ik graag mijn ouders, Ger en Hanneke bedanken. Bedankt dat jullie er altijd voor mij zijn geweest. Jullie hebben mij altijd in al mijn, soms lastige, keuzes gesteund en mij geleerd dat alles goed is zolang ik maar mijn best doe. Ik kan oprecht van geluk spreken dat ik zulke fijne, lieve en zorgzame ouders heb, zonder wie ik niet de persoon zou zijn geworden die ik nu ben. Dank jullie wel!

Yoeri

Curriculum vitae

Yoen van de Burgt was born in Huisseling on March 3, 1986. After finishing high school in 2004, he studied Mechanical Engineering at Eindhoven University of Technology. After completing his Bachelors degree in 2007, he received his Master's degree (cum laude) in 2010 in the Micro- and Nano-scale Engineering group of prof. Andreas Dietzel on a project done in collaboration with TNO Holst Centre.

In 2010 he started a PhD in the same group, which became the Microsystems group in 2013, headed by prof. Jaap den Toonder, on the optimization and control of laser-assisted carbon nanotube growth of which the most important results are presented in this dissertation.